University of South Carolina
Scholar Commons

Theses and Dissertations

2015

Fabrication and Characterization of Graphene based Biocompatible Ion-Sensitive Field Effect Transistor (ISFET)

Rina Patel
University of South Carolina

Follow this and additional works at: http://scholarcommons.sc.edu/etd

Part of the Electrical and Computer Engineering Commons

Recommended Citation

Patel, R.(2015). *Fabrication and Characterization of Graphene based Biocompatible Ion-Sensitive Field Effect Transistor (ISFET)*. (Master's thesis). Retrieved from http://scholarcommons.sc.edu/etd/3639

This Open Access Thesis is brought to you for free and open access by Scholar Commons. It has been accepted for inclusion in Theses and Dissertations by an authorized administrator of Scholar Commons. For more information, please contact SCHOLARC@mailbox.sc.edu.

FABRICATION AND CHARACTERIZATION OF GRAPHENE BASED BIOCOMPATIBLE ION-SENSITIVE FIELD EFFECT TRANSISTOR (ISFET)

by

Rina Patel

Bachelor of Engineering
Veer Narmad South Gujarat University, 2009

Submitted in Partial Fulfillment of the Requirements

For the Degree of Master of Science in

Electrical Engineering

College of Engineering and Computing

University of South Carolina

2015

Accepted by:

Goutam Koley, Director of Thesis

MVS Chandrashekhar, Reader

Lacy Ford, Senior Vice Provost and Dean of Graduate Studies

© Copyright by Rina Patel, 2015
All Rights Reserved.

DEDICATION

Dedicated to my adored spouse Haresh, my Parents and my family for their endless care, encouragement and whole hearted support.

ACKNOWLEDGEMENTS

Graduate study as a Master student was an intriguing and priceless learning knowledge for me. As a matter of first importance, I want to acknowledge my scholastic advisor, Prof. Goutam Koley, for offering me this opportunity to study in the interdisciplinary exploration range of Graphene based devices. In the previous 2 years of my graduate study life, Prof. Koley has been giving me perpetual help and direction. Notwithstanding his incalculable exertion in numerous hours of dialog with me on every day exploration work, I particularly admire his assistance for preparing me to have a receptive outlook towards at first sudden examination results and further improve my capacity of discriminating intuition when confronting "certifiable" issues included in hands-on test. Under his impact, I have a superior seeing in circumstances and related obligations as a future building proficient in this data and innovation time.

Here, I might want to likewise recognize my council part, Dr. Chandrashekhar for his direction. I might want to say thanks to Dr. Walsh, additionally as our exploration coconspirator from School of Medicine at USC, for giving me the exceptionally fascinating examination subject of biocompatible sensor advancement for living cell and his bolster, direction and consolation in regular exploration work.I might likewise want to recognize Prof. Richard A. Webb, who liberally conceded me the entrance to their clean room office for device fabrication and characterization. I am likewise appreciative to Prof. Christopher T. Williams and Clemson research group for permitting me to utilize their Raman spectroscopy for graphene study.

I might want to thank Dr. Yihao Zhu, Ifat Jahangir, Alina Wilson, Dr. Amol Singh and all the colleagues at NESL lab at diverse times. It is my honor to have the chance to work and study together with them and I got innumerable help furthermore motivation from them in regular examination work. Last but not the least, I might want to thank my spouse, my friends Anusha and Bojidha, my parents and my relatives for all that they have accomplished for me to succeed for the duration of my life. Thank and admire all their affection and backing at whatever point I am up or down in life.

ABSTRACT

Graphene, a two-dimensional material with a high surface to volume ratio, has drawn extensive research enthusiasm for applications in the field of electronic sensors. The special material properties that make graphene a highly promising material include its biocompatibility, very high mobility, low 1/f and thermal noise, modulation of carrier concentration and fermi level by electrical, optical, and chemical means. To exploit these properties for practical applications a large area high quality graphene, transferred on appropriate substrates, is required. In this work, high quality single monolayer graphene (determined from Raman spectroscopy) has been synthesized by chemical vapor deposition (CVD) technique for bio-sensing applications utilizing methane and hydrogen as precursor gases.

In this work, small channel graphene field effect transistors (GFETs) were fabricated utilizing monolayer or few layer high quality transferred graphene, and electrical, voltage bias stressing and temperature dependent characterizations have been performed. The electrical characterization, carried out in a back-gated field effect transistor configuration, yielded mobility as high as 1000 $cm^2V^{-1}s^{-1}$.

Additionally, a novel bio-compatible device called Ion sensitive field effect transistor (ISFET) was fabricated using the CVD grown graphene. Graphene ISFET senses the ions efflux from solutions using graphene as the active layer (conducting channel). The graphene ISFETs were encapsulated using bio-compatible epoxy except the active layer (graphene) region to perform highly sensitivity solution based

measurements. The ISFET devices were used to perform real-time Potassium (K^+) efflux measurement from ion concentration change in electrolyte solution. The ion concentration change is transduced into an electrical (current) signal due to surface potential change in graphene. In this work, an extensive study of the I-V and C-V characteristics of the graphene ISFET in an electrolyte solution with different K^+ concentration has been performed and superior performance of the graphene ISFET has been demonstrated.

During development and testing of the graphene ISFET, we also discovered that the epoxy utilized for the sensor encapsulation has a significant impact on the electric transport properties of graphene including conductivity, carrier concentration and field-effect mobility. N-type doping impact of the epoxy on graphene has been demonstrated through systematic experiments, which is promising as a new method for surface doping of graphene.

TABLE OF CONTENTS

DEDICATION…… iii

ACKNOWLEDGEMENTS iv

ABSTRACT………… vi

LIST OF TABLES x

LIST OF FIGURES xi

CHAPTER 1 INTRODUCTION 1

1.1 WHAT IS GRAPHENE? 2

1.2 THERMAL PROPERTIES OF GRAPHENE 3

1.3 MECHANICAL PROPERTIES OF GRAPHENE 3

1.4 OPTICAL PROPERTIES OF GRAPHENE 4

1.5 ELECTRONIC PROPERTIES OF GRAPHENE 4

1.6 APPLICATIONS AND TRENDS 7

1.7 OUTLINE OF THE THESIS 9

CHAPTER 2 GRAPHENE GROWTH 11

2.1 MICROMECHANICAL CLEAVAGE AND ULTRASONICATION 11

2.2 EPITAXIAL GROWTH OF GRAPHENE 12

2.3 REDUCED GRAPHENE OXIDE 14

2.4 CHEMICAL VAPOR DEPOSITION GROWTH OF GRAPHENE 15

2.5 GROWTH ON CU FOIL 19

2.6 RAMAN CHARACTERIZATION OF GRAPHENE 22

2.7 UNIFORMITY OF GRAPHENE 25

CHAPTER 3 GFET DEVICE FABRICATION AND CHARACTERIZATION 27

3.1 GRAPHENE TRANSFER 27

3.2 BACK-GATED FET BASED DEVICE FABRICATION 29
3.3 RAMAN CHARACTERIZATION OF BACK GATED GRAPHENE DEVICES 32
3.4 MOBILITY OF BACK GATED GRAPHENE DEVICES 35
3.5 BIAS STRESSING EFFECT ON GRAPHENE BASED DEVICES 38
3.6 TEMPERATURE EFFECT ON GRAPHENE DEVICES 40
CHAPTER 4 DESIGN, FABRICATION AND CHARACTERIZATION OF GRAPHENE BASED ION-SENSITIVE FIELD EFFECT TRANSISTOR (ISFET)................................. 44
4.1 INTRODUCTION 44
4.2 SI BASED ISFET AND ITS LIMITATION 45
4.3 GRAPHENE AS AN ALTERNATIVE FOR ISFET.. 47
4.4 GRAPHENE BASED ISFET SENSING MECHANISM 49
4.5 DEVICE FABRICATION AND ENCAPSULATION USING EPOXY............................. 50
4.6 I-V CHARACTERISTICS OF GRAPHENE ISFET 52
4.7 C-V CHARACTERISTICS OF GRAPHENE ISFET 54
4.8 DOPING EFFECT OF EPOXY ON ISFET.. 57
4.9 ISFET ENCAPSULATION USING PHOTORESIST 62
CHAPTER 5 CONCLUSION.. 64
5.1 SUMMARY.. 64
REFERENCES.. 67
APPENDIX A : DEVICE FABRICATION PROCESS FLOW 77

LIST OF TABLES

Table 1.1 Electronic and Material Properties of single layer graphene 8

Table 4.1 Electric transport parameters of graphene under the influence of epoxy......... 61

LIST OF FIGURES

Figure 1.1 (a) Schematic representation of single planner hexagon consisting of 6 C atoms connected to each other by sp^2 bonding with C-C bond length of 1.42 Å. (b) Periodic repetition of hexagonal unit resulting in 2-dimensional honeycomb structure of graphene. 1

Figure 1.2 Graphene unique properties [24]. 2

Figure 1.3 Graphene as a building block of various forms of sp2 carbon materials such as fullerene, carbon nanotube, and graphite [2]................................. 5

Figure 1.4 (a) Parabolic bands in most semiconductors (b) Intrinsic graphene is a semi-metal or zero-gap semiconductor where E-k relationship is linear at the Brillouin zone corners.. 6

Figure 1.5 Various applications of graphene using different properties of graphene .. 8

Figure 1.6 Future trend of graphene as surveyed in year 2013 9

Figure 2.1 The small size (10s of μm) chunks of graphene obtained by exfoliation method showing poor contrast for monolayer graphene and better contrast for bilayer graphene [39]. 12

Figure 2.2 (a) STM image of the graphene film formed on a carbon-face semi-insulating SiC substrate showing 1.2 and 1.4 nm steps in the basal plane of the SiC substrate. (b) Atomic resolution STM image of graphene showing triangular sublattice of carbon atoms [46]. 13

Figure 2.3 (a) Chemical structure of graphene oxide. There are carboxylic and carbonyl groups at the edges but are not shown for clarity. (b) AFM image of exfoliated 1 nm thick graphene oxide sheets [48]. 14

Figure 2.4 The generalized CVD growth of graphene on top of a metal catalyst. The steps involved are: reactant transport, activation, transport of reactant thought boundary layer, reactant adsorption on the surface, dissolution and bulk diffusion, chemical reaction, surface migration, film growth, desorption, transport of product through boundary layer, and transport by forced convection [49]. 16

Figure 2.5 **(a)**The CVD graphene growth system with Pressure, temperature and MFC controls (b) Cu foil after graphene growth on quartz boat shown in enlarged image 18

Figure 2.6 (a) The graphene growth mechanism on copper foils [50]. (b) The graphene growth by surface adsorption as revealed by use of C13 and C12 isotopes of carbon [51]........ 19

Figure 2.7 Series of steps involved in growing monolayer graphene on Cu foils. The optimized process parameter is shown in the schematic plot. 20

Figure 2.8 **(**a)Optical Image of Copper film before CVD process. (b) Optical image of Graphene on Copper film after CVD process 21

Figure 2.9 (a) The basic physics of Raman scattering involving ground state vibrational levels and virtual states. Infrared absorption is also shown for comaparison. (b) LabRAM Raman Spectrometer from Horiba used in this work. (c) The ray diagram of Raman spectrum set-up consisting of Laser, notch filters, lenses, grating and CCD detector [53]........ 22

Figure 2.10 (a) Raman spectra of various sp2 carbon based system showing ability to distinguish them based upon intensity, shape and with of D, G G’ or 2D peaks using one simple scan of Raman spectrum [54]. (b) Using the shape of 2D band it is possible to distinguish graphene from graphite and also determine the numbers of monolayers by fitting different Lorentzians to the band [54]. 24

Figure 2.11 (a) Raman spectra of two samples of graphene as-grown on Cu foils by CVD growth technique with optimized parameters. The 2D FWHM of 32.95 and 38.69 is indicative of monolayer graphene. (b) Graphene grown Copper foil after graphene growth 26

Figure 3.1 Processing steps for graphene transfer on any desirable substrate. 28

Figure 3.2 Device processing steps for fabrication of graphene Field effect transistor (GFET) 30

Figure 3.3 Graphene at bottom fabrication process flow.at end Optical image of graphene FET showing 246 μm long and 2300 μm wide graphene channel on top of 300 nm SiO_2 substrate. 31

Figure 3.4 Graphene on Top fabrication process flow 32

Figure 3.5 Raman characterization showing D,G and 2D peak on Graphene on top back gated device fabrication........ 33

Figure 3.6 Raman characterization showing D,G and 2D peak on Graphene on top back gated device fabrication........ 34

Figure 3.7 Raman spectra taken at 6 different locations on a back gated GFET 35

Figure 3.8 Family of curves for graphene FET showing increase in I_{ds} with more negative V_{bg} indicating p-type behavior 36

Figure 3.9 I_{ds}-V_{bg} transfer characteristics of the GFET with Dirac point at 45 V, indicating p-type behavior of graphene transferred on SiO_2. 37

Figure 3.10 The schematics of Vth shift of GFETs under positive bias stressing. ΔVth is defined back-gate voltage V_{bg} shift at a constant I_{ds} [67]. 39

Figure 3.11 GFET device mounted on Hot Plate for Ids-Vbg for temperature study and real time measurement 41

Figure 3.12 Ids–Vbg measurement of GFET from Room temperature to 120 ◦C without stress. As temperature increases to 120 °C, the air ambient (O_2, H_2O, etc.) [70] will cause graphene hole doping effect, which can be seen that the Dirac point shifts to right. 41

Figure 3.13 (a) Current between drain and source (Ids) Vs time profile with temperature increase for 1st Sample. (b) Current between drain and source (Ids) Vs time profile with temperature increase for 2nd Sample. 42

Figure 3.14 GFET device mounted on Hot plate for I-V and real time measurement. 43

Figure 4.1 Illustration of ion channels in a cell membrane for Na+/K+ adopted from Wikipedia 44

Figure 4.2 (a) General device structure of an n-channel Si based ISFET sensor. (b) Electrical biasing scheme for the sensor operation.................................. 46

Figure 4.3 Florescent image of H9C1 cardiac muscle cells growing on graphene thin film CVD synthesized in our lab. 48

Figure 4.4 (a) Schematics of the proposed structure of the graphene based (ISFET) including its bias configuration used in the electrical measurements. The ion sensor is inserted in an electrolyte solution insulated by Epoxy in operating condition. (b) Cross section of graphene based ISFET showing an electrical double layer forming at the graphene/solution interface.[91] 49

Figure 4.5 Fabrication process flow of the graphene based ISFET, which consist of Graphene transfer, shadow mask/photolithography followed by metal deposition using DC sputtering/E-beam evaporation. Final optical image of graphene based ion sensor electrodes encapsulated using biocompatible epoxy. 51

Figure 4.6 Schematic diagram of the experimental setup for sensor electrical (I-V and C-V) characterization 52

Figure 4.7 (a) I-V characteristics of an epoxy coated graphene ISFET in DI water with different K^+ ion concentration. In the measurement, V_{ds} was set to be constant 0.5 V and V_{tg} (solution-gated voltage) was swept from 0 to 0.3 V via a Ag/AgCl reference electrode (Bioanalytical System, Inc.) immersed in the solution. (b) Drain-source current I_{ds} as a function of K^+ ion concentration, at V_{tg} = 0.05 V. 53

Figure 4.8 (a) Device C-V characteristics in DI water with different KCl concentration. (b) Measured capacitance as a function of K^+ ion concentration, at V_{tg} = 0.6 Volts. 54

Figure 4.9 (a) Time dependent capacitance measurements with varying K+ concentration from 0 μM to 1 mM in DI water. Two measurement cycles were performed with different steps in K+ concentration change. (b): Sensor response to 5 uM KCl (red curve) along with a control test without KCl (blue curve). 55

Figure 4.10 Schematic diagram of a graphene ISFET under C-V characterization in KCl electrolyte together with the equivalent electrical circuit describing its operation [92]-[93]. In the circuit, C_{EDL1} and C_{EDL2} represent electrical double layer capacitance formed at reference electrode (RE)/electrolyte and graphene/electrolyte interfaces, respectively. R_{BULK} and R_{gr} correspond to the electrical resistance of bulk salt solution and graphene thin film, respectively. 56

Figure 4.11 (a) Optical image of an epoxy coated graphene ISFET with H9C1 cardiac muscle cells directly plated and cultured on its active sensing area in red box. (b) Enlarge view of the active sensing area defined by the epoxy. (c) Florescent image of the H9C1 cells growing on the graphene thin film .. 57

Figure 4.12 (a) Electrical biasing scheme of a back gate configured graphene ISFET. (b) Device transfer characteristics before epoxy applied (C) Device transfer characteristics after epoxy applied 59

Figure 4.13 (a): Optical image of the device setup for the epoxy effect study. A droplet of uncured epoxy was deposited on the graphene 2~3 mm away from the conducting channel of a back gated graphene FET. (b): Time dependent current change upon epoxy deposition. Inset shows the device I-V characteristics taken at different time instants. (c) Real time current measurement from point A epoxy applied and till it was cured. 60

Figure 4.14 Optical image of an array of three ISFETs fabricated on a single graphene film. Photoresist, S1811 was used to passivate the drain/source electrodes. The channel L ~ 0.45 mm and W ~ 2 mm were defined by standard photolithography. 63

CHAPTER 1

INTRODUCTION

Carbon is considered as the fundamental building blocks of all life forms on earth. It is chemically very versatile and forms larger variety of compounds. Each atoms of carbon can bond with 4 different atoms or molecules. When the carbon atoms link amongst themselves in tetrahedral fashion utilizing sp3 bonding, they form diamond the hardest naturally occurring material with insulating properties, however when they bond with 3 carbon atoms only, in a honeycomb fashion, graphite is formed. It is three dimensional allotrope of carbon with sp^2 hybridization of carbon to carbon bond. Graphite is rich in electrons and conducts along its layers. Graphite became well known after the invention of pencil in 1564. Around that time the mining and production of high purity and soft graphite from Cumbria, England was strictly controlled due to its strategic application as

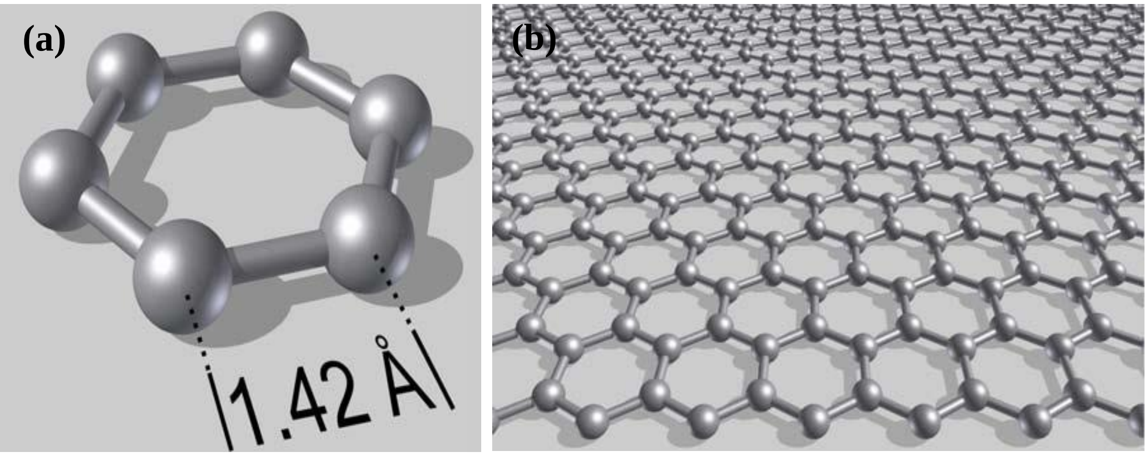

Figure 1.1 (a) Schematic representation of single planner hexagon consisting of 6 C atoms connected to each other by sp^2 bonding with C-C bond length of 1.42 Å. (b) Periodic repetition of hexagonal unit resulting in 2-dimensional honeycomb structure of graphene**.**

refractory lining of canon ball molds. The ability of graphite to write comes from the fact that it made up of individual sheets of carbon which held together by weak Van der waals forces which allows layers to slip under shear force and leave a trace of thinner graphite on the surface. This very ability of slipping also makes them very good lubricants. Since these sheets could slide upon each other they could be separated as very thin graphitic sheet down to single layer as demonstrated on SiO_2 by Novoselov and Geim in 2004 [1].

1.1 What is Graphene?

These individual sheets of carbon, which are constituent of graphite, are made up of planner sp^2 bonded carbon atoms arranged in honeycomb fashion consisting of hexagon of carbon, as in benzene. This hexagon is depicted in **Figure 1.1**(a) with C-C bond length of 1.42 Å. The individual sheet structure as shown in **Figure 1.1** (b) is referred as graphene. While Graphene unique properties such as high conductivity,

Figure 1.2 Graphene unique properties [24].

strength, flexibility, transparency and structural properties shown in **Figure 1.2** and described in detail in next sections.

1.2 Thermal properties of graphene

The thermal conductivity of graphene was recently measured to be between (4.84 ± 0.44) × 10^3 to (5.30 ± 0.48) × 10^3 $Wm^{-1}K^{-1}$ at near-room temperature. These measurements, made by a non-contact optical technique, are in excess of those measured for carbon nanotubes or diamond [31]. In addition, the ballistic thermal conductance of a graphene is shown to give the lower limit of the ballistic thermal conductance, per unit circumference, length of carbon nanotubes [34].

1.3 Mechanical properties of graphene

Graphene also has excellent mechanical properties and is a leading contender for nanoelectromechanical systems (NEMS). To date, graphene appears to be one of the strongest materials ever tested. Measurements have shown that graphene has a breaking strength 200 times greater than breaking strength 200 times greater than steel, with a tensile modulus (stiffness) of 1 TPa (150,000,000 psi)[36]. Using an atomic force microscope (AFM), the spring constant of suspended graphene sheets has been measured. Graphene sheets, held together by van der Waals forces, were suspended over SiO_2 cavities where an AFM tip was probed to test its mechanical properties. Its spring constant was in the range 1–5 N/m and the Young's modulus was 1 TPa, which differs from that of the bulk graphite. These high values make graphene very strong and rigid. These intrinsic properties could lead to using graphene for NEMS applications such as pressure sensors and resonators [27]. Graphene is a flexible material as it can stretch up to 20% to its original size without damaging.

1.4 Optical properties of graphene

The unusual low-energy electronic structure of monolayer graphene provides unique optical properties with an unexpectedly high opacity which allows absorption of ≈ 2.3 % of white light [27]. The property of IR absorption of graphene highest of all known materials with 2.3 % absorption per monolayer (ML) over a broad wavelength range [29].

1.5 Electronic properties of Graphene

Graphene as a true two-dimensional (2D) material possess many amazing properties not seen before in bulk material. **Figure 1.3** captures this description vividly [2]. Its honeycomb structure is the fundamental building block of other allotropes of carbon which can be stacked to form three-dimensional (3D) graphite which is formed by stacking graphene sheets attached by week Van der Waal’s forces, rolled up to form one-dimensional (1D) nanotubes, and wrapped to form zero dimensional (0D) fullerenes. This phenomenal material was thought to be unstable before it was first isolated by Geim et al. [1] in 2004 by a technique called mechanical exfoliation of bulk graphite.

Graphene is a zero-or near-zero-bandgap semiconductor with a linear energy momentum dispersion relation at the Brillouin zone corners. Highly unique electrical, optical, thermal and mechanical properties have been reported for few-layer graphene [1]-[4]. In particular, graphene exhibits remarkably high electron mobility as the charge carriers resemble Dirac fermions, and electron transport in graphene remains ballistic up to 0.3 µm through ambient condition [1]. Other significant properties include carrier-density-dependent conductivity, anomalous quantum Hall effect, and minimum quantum conductivity, plasmonic amplification to name a few [5]-[10]. These unique electrical properties of carriers in graphene stem from its unique band structure, which exhibits

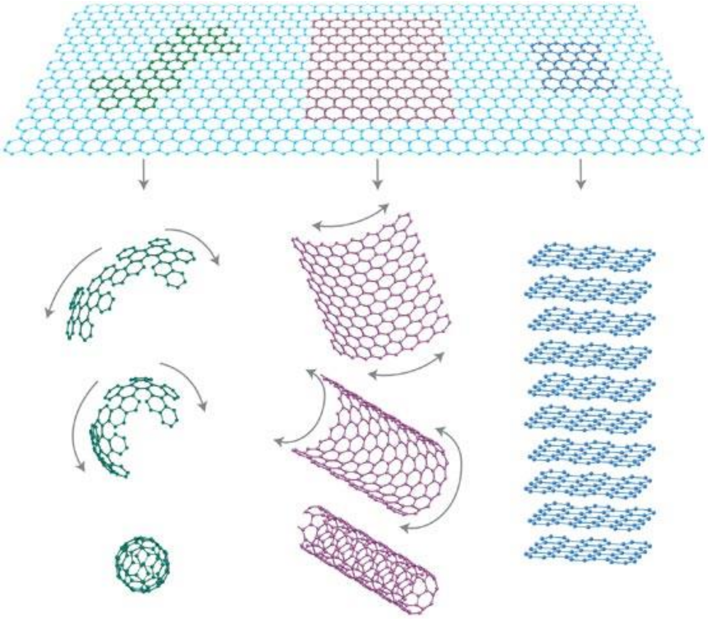

Figure 1.3 Graphene as a building block of various forms of sp2 carbon materials such as fullerene, carbon nanotube, and graphite [2]

conduction and valence bands with near-linear dispersion that touch at the Brillouin zone corners to make it a zero bandgap material. The remarkable mechanical properties in graphene originate from the covalently bonded C-C, the strongest bond in nature, which locks these atoms in place. A suspended single layer of graphene is one of the stiffest known materials characterized by a remarkably high Young's modulus of ~ 1 TPa [10]-[12]. All these properties combined making it a promising material in post Moore's law era, as a single-molecule gas sensor, in optical sensor and devices, in PN-junction diodes. Electronic properties of graphene

1.5.1 Linear E-K relation

Graphene differs from most conventional three-dimensional materials. Intrinsic graphene is a semi-metal or zero-gap semiconductor where E-k relationship is linear at the Brillouin zone corners. Due to this linear dispersion relation at low energies, electrons and holes near these six points, two of which are inequivalent, behave like relativistic massless particles described by the Dirac equation [18]-[19]. Hence, the electrons and holes are called Dirac fermions, and the six corners of the Brillouin zone are called the Dirac points [18]. The equation describing the E-k relation is $E = \hbar v_F K$ where the Fermi velocity $v_F \sim 10^6$ m/s [19].

1.5.2 High electron mobility

Transport measurements show that graphene has a very high electron mobility at room temperature, with reported values in excess of 15,000 $\text{cm}^2\text{V}^{-1}\text{s}^{-1}$ [1]. Additionally, the symmetry of the experimentally measured conductance indicates that the motilities for holes and electrons should be nearly the same [20]. The mobility is nearly independent of temperature between 10 K and 100 K [5], [21]-[22] which implies that the dominant scattering mechanism is defect scattering. Scattering by the acoustic phonons of graphene places intrinsic limits on the room temperature mobility to 200,000 $\text{cm}^2\text{V}^{-1}\text{s}^{-1}$ at a carrier density of 10^{12} cm^{-2} [22]-[23]. However, for graphene on SiO_2 substrates, effects of scattering of electrons by optical phonons of the substrate is larger than

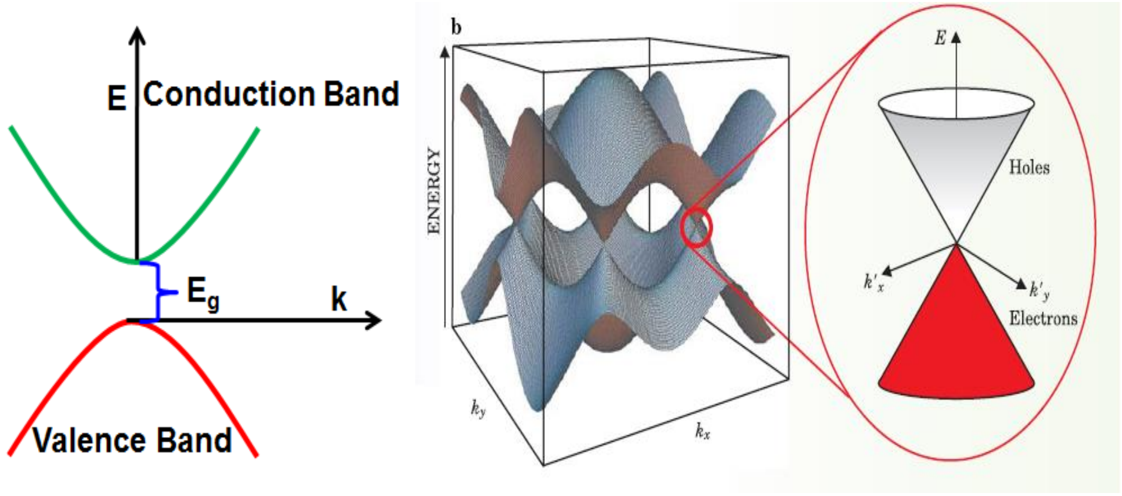

Figure 1.4 (a) Parabolic bands in most semiconductors (b) Intrinsic graphene is a semi-metal or zero-gap semiconductor where E-k relationship is linear at the Brillouin zone corners.

scattering by graphene's own phonons at room temperature which essentially limits the mobility to 40,000 $cm^2\ V^{-1}s^{-1}$ [22].

1.5.3 Minimum conductivity

Despite the zero carrier density near the Dirac points, graphene exhibits a minimum conductivity on the order of $4e^2 / h$. This is possibly due to rippling of the graphene sheet or ionized impurities in the SiO_2 substrate may lead to local puddles of carriers that allow conduction [20]. However, most measurements suggest minimum conductivity depend on impurity concentration [26].

1.5.4 Effects of molecular doping

Recent experiments have probed the influence of chemical dopants on the carrier mobility in graphene [17],[26]. Schedin *et al.* doped graphene with various gaseous species (some acceptors, some donors), and found the initial undoped state of a graphene structure can be recovered by gently heating the graphene in vacuum. They reported that even for chemical dopant concentrations in excess of 10^{12} cm^2 there is no observable change in the carrier mobility [17]. Chen, et al. doped graphene with potassium in ultra high vacuum at low temperature. They found that potassium ions act as expected for charged impurities in graphene [27], and can reduce the mobility 20-fold [17]. The mobility reduction is reversible on heating the graphene to remove the potassium.

1.6 Applications and trends

The combination of various amazing properties as shown in **Figure 1.2** and **Table 1.1** of the graphene enables its application in variety of diverse areas such as terahertz devices, high speed transistors, displays, batteries, ultracapacitors, hydrogen storage, solar cells, membrane for separation of gases, magnetic, charge, strain, and biological

Table 1.1 Electronic and Material Properties of single layer graphene

Mobility	6.5×10^{4} [30]- 10^{6} $\mathrm{Cm^{2}V^{-1}s^{-1}}$ [31]
Thermal conductivity	$(4.84\pm0.44)\times10^{3}$ to $(5.30\pm0.48)\times10^{3}$ $\mathrm{Wm^{-1}K^{-1}}$ [34]
Young's modulus	1.0[36]to (2.4 ± 0.4) TPa[32]
Breaking strength	42 N/m [36]
Breaking strain	25% [36]
Normalized noise spectral density (at f = 10 Hz)	10^{-9} to 10^{-7} $\mathrm{Hz^{-1}}$ [33]
Noise amplitude (μm scale devices)	~10^{-9} to 10^{-7} [33]

sensors, composites etc. to name a few. This list has been ever expanding as new applications come to light by choosing, mixing and matching the properties of graphene alone or with combination with other materials. Due to its amazing properties graphene used for wide range of application. Graphene is strong yet light material which makes it

George Osborne on a visit to the Manchester University lab of Professors Geim and Novoselov

SOLAR PANELS

MIT professors have shown how graphene could be used to make the electrodes in organic solar cells cheaper, lighter and more flexible than in current systems

Graphene is a one-atom thick form, or allotrope, of carbon – other allotropes include diamond and graphite. It is often described as an atomic-scale chicken wire constructed of carbon atoms and their bonds. When graphene sheets are stacked, three million sheets would be needed to create a 1mm thickness. It's been claimed that it is the strongest material known to man, that a clingfilm-thick layer could support an elephant. Despite its strength it can be stretched by 20% without being damaged. It is also an excellent conductor of electricity and the best conductor of heat that has been discovered

AIR TRAVEL

Using graphene would enable aeroplane manufacturers to develop extremely strong yet light components – bringing down weight and therefore reducing fuel costs

MOBILE PHONES

Nokia is exploring the potential uses of graphene in mobile devices. Aside from smaller, more flexible phones, it may allow built-in solar power and transparent electronics

FLEXIBLE SCREENS

Researchers in South Korea have produced a continuous layer of graphene 63cm wide. This has opened up possibilities in electronics, "You could theoretically roll up your iPhone and stick it behind your ear like a pencil," claims one scientist

PROSTHETICS

Aside from allowing for the construction of stronger, more flexible and lighter limbs, its conductivity opens up new possibilities for its use in the electrodes used to turn brain signals into movement

COMPUTER CHIPS

Geim and Novoselov have been working on demonstrating how graphene could replace silicon as the key material in electronic circuits. IBM is one of many electronics firms experimenting with graphene conductors

DNA SEQUENCING

Researchers at British firm Oxford Nanopore, building on discoveries made at Harvard, claim that using graphene could reduce the cost and speed up the process of DNA sequencing

Figure 1.5 Various applications of graphene using different properties of graphene suitable for aviation and space application. Due to its flexibility and transparency it can be used to produce flexible screen, transparent mobile phones and computer chip. As graphene is biocompatible it can be used for DNA sequencing and prostatic application as shown in **Figure 1.5**. This shows major applications of graphene which have already been demonstrated utilizing different properties of graphene. **Figure 1.6** shows Future trend of graphene surveyed in 2013. This chart was prepared after a comprehensive survey of graphene companies and clearly highlights the versatility of graphene. The graphene market expected to reach around 150 million in 2020. In this figure the global graphene market is shown by its application, type, and geography and by its dynamic.

Figure 1.6 Future trend of graphene as surveyed in year 2013

1.7 Outline of the thesis

Despite of being highly promising material for various kind of application such as those shown in **Figure 1.5** graphene still remains a newer material. It completed 10 years of its first isolation in 2014. It therefore offers many challenges to be solved like any other new material system such as nitride semiconductors before it could become a commercial success. One of the major challenge graphene faces is its manufacturability. Growing device quality, large area graphene still remains a challenge for mass production. Two approaches appears promising, namely epitaxial and chemical vapor deposition bases graphene growth. The later growth technique constitute the scope of this thesis and is discussed in chapter 2, which also focuses on Raman spectroscopy as the principle characterization technique of graphene to determine its quality and type and even to determine of the grown material is graphene or not and weather it’s uniform or not. Chapter 3 will be more focused on Transfer process of graphene on to Si/Sio2 from Copper film and fabrication process flow for small channel devices GFET. GFET mobility measurement, Raman characterization and AFM characterization shown further to confirm quality and thickness of graphene. It will lead to annealing effect and bias stressing effect on graphene based thin film transistor.

Chapter 4 will be design and development of biocompatible ion sensitive field effect transistor (ISFET) from graphene, which has been proposed and demonstrated for real-time K^+ efflux measurement from in electrolyte solution. In this work, we have extensively studied the I-V and C-V characteristics of the graphene ISFET in electrolyte solutions with different K^+ concentration and doping effect of epoxy while encapsulating graphene based ISFET.

CHAPTER 2

GRAPHENE GROWTH

There are various routes to synthesis or procure graphene. Each technique comes with their own sets of challenges. Broadly there are four well-recognized methods. These methods include micromechanical cleavage, epitaxial growth, growth by CVD and reducing graphene oxide. Epitaxial and CVD growth methods have evolved to generate large area, good quality graphene. The reduced graphene oxide (RGO) is also capable of large area graphene however the structural quality of graphene remains poor. These growth techniques are surveyed briefly to put CVD based growth in perspective

2.1 Micromechanical cleavage and ultrasonication

In the very beginning, Graphene sheets were obtained by mechanical cleavage or exfoliation of graphite, which consists of loosely bonded parallel layers of graphene [38]. The technique often referred to as a “scotch-tape method,” can provide 2D graphene crystals of high structural and electronic quality up to mm size. Though delicate and time consuming, this is the only technique that can guarantee production of defect free graphene without any contamination. Thus, it is very well suited for basic research and for making proof-of-concept devices, which only requires a small size of graphene with typical dimensions on the order of mm or less. **Figure 2.1** shows a representative optical image of monolayer and bilayer exfoliated graphene on 300 nm thick SiO2 substrate [39]. Instead of exfoliating graphite (typically highly oriented pyrolytic graphite) manually, it is also possible to automate the process by using, for example, ultrasonic cleavage [40].

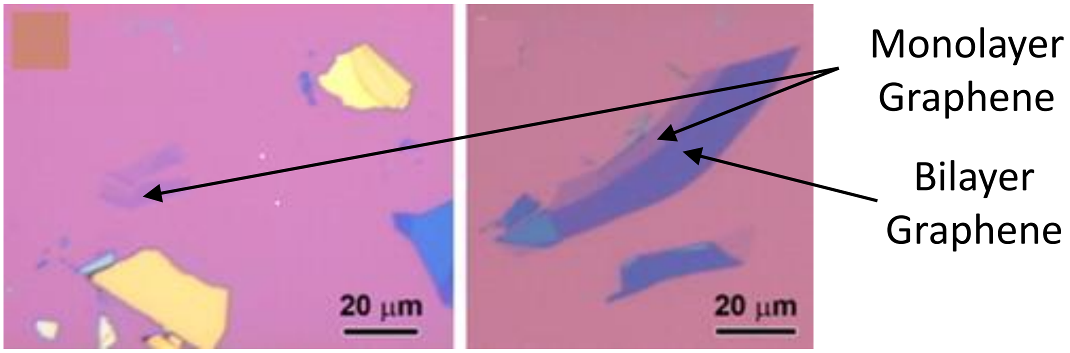

Figure 2.1 The small size (10s of µm) chunks of graphene obtained by exfoliation method showing poor contrast for monolayer graphene and better contrast for bilayer graphene [39].

This leads to stable suspensions of submicron graphene crystallites, which can then be used to make polycrystalline films and composite materials [40]-[41]. Conceptually similar is the ultrasonic cleavage of chemically "loosened" graphite, in which atomic planes are partially detached first by intercalation, making the ultrasonication method more efficient [41]. The ultrasonication method allows production of larger area graphene, although controllability of the process and the structural integrity of graphene are still challenges that need to be addressed.

2.2 Epitaxial growth of graphene

This technique is well established for producing large area graphene of high quality by thermal annealing of SiC wafers [42]-[44]. In this method, which takes advantage of well-established SiC epitaxy, 6-H or 4-H polytype of SiC is heated in the temperature range of 1200 – 1600 ^{o}C in ultra-high vacuum (UHV) of 1×10^{-10} Torr for several minutes. At this high temperature Si leaves the SiC surface owing to its higher vapor pressure than carbon. The remaining C rich surface then rearranges on the growth the SiC substrate surface needs to be cleaned by H_2 etching at 1000 ^{o}C in UHV to hexagonal lattice of SiC to generate single to few-layer graphene [45]. Prior to graphene remove native oxide that is often present. This method results in Graphene growth on both Si and C terminated faces of SiC. Figure 2.2 shows the STM image of graphene grown on semi-insulating C-face SiC [46]. In general, the growth on Si-face is slower and self- limiting, resulting in thinner and better quality graphene (1-3 monolayers), whereas graphene on C-face is usually much thicker (5 – 10 monolayers). The major advantage of this technique is growth of quite uniform, wafer scale and high quality graphene is possible, taking advantage of the precise control of process parameters in a commercial SiC growth chamber. Attempts have also been made to grow graphene on SiC substrate in near atmospheric Ar pressure of 900 mbar and at relatively higher temperature of 1650 ^{o}C with a goal to obtain larger area low defect, mono, bi and tri-layer graphene [47]. One of the disadvantages of this method of graphene synthesis is that it is very difficult to remove or transfer the graphene to another desired substrate, due to the challenges involved in controllably etching SiC. Therefore, processing of graphene devices needs to

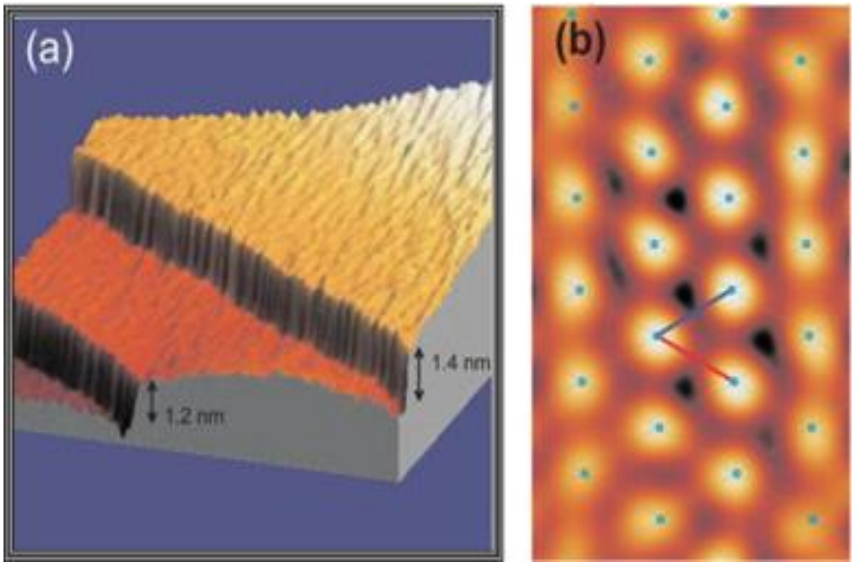

Figure 2.2 (a) STM image of the graphene film formed on a carbon-face semi-insulating SiC substrate showing 1.2 and 1.4 nm steps in the basal plane of the SiC substrate. (b) Atomic resolution STM image of graphene showing triangular sublattice of carbon atoms [46].

be done on the SiC substrate itself. This can be expensive due to the high cost of SiC substrates, and also it does not readily allow the usage of a back gate for realizing transistors, or sensors requiring back-gate modulation.

2.3 Reduced Graphene Oxide

It is chemical route to make graphene from graphite. In this method graphite is oxidized in presence of strong oxidizing agents such as sulphuric acid. A redox reaction takes place in between graphite and oxidizers in which electrons are removed from graphite. The most common method to produce graphite oxide is treating graphite with a mixture of sulphuric acid, sodium nitrate and potassium permanganate. Due to the oxidation process the interplanar spacing between the layers of graphite is increased. The resulting product is graphite oxide. When this graphite oxide is dispersed in solvents like water, graphene oxide results by interaction of water molecules in-between increased separation of interplanar spacing of graphite oxide which helps to separate these layer of Graphene oxide using sonication or stirring. This process causes lots of damage to graphene oxide. The process of reduction of graphene oxide back to individual graphene

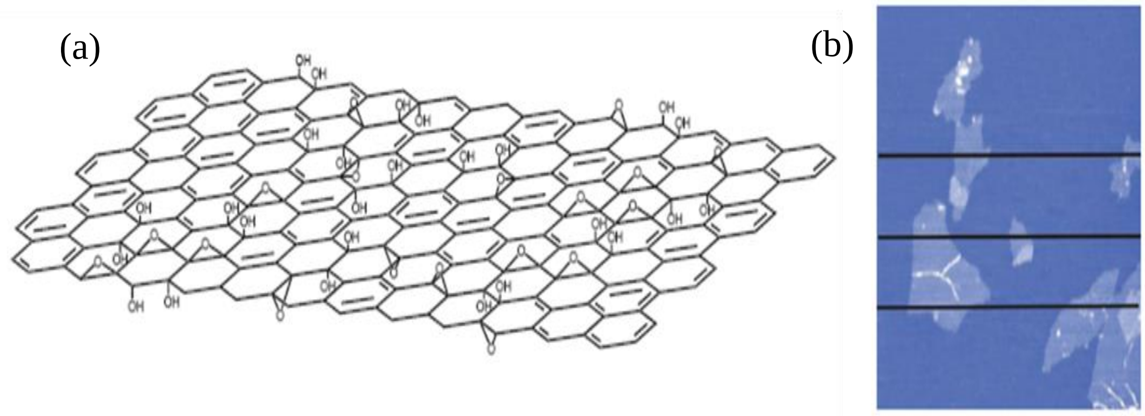

Figure 2.3 (a) Chemical structure of graphene oxide. There are carboxylic and carbonyl groups at the edges but are not shown for clarity. (b) AFM image of exfoliated 1 nm thick graphene oxide sheets [48].

layers introduces even more defects, therefore the resulting product is called reduced graphene oxide (rGO). **Figure 2.3**(a) shows chemical structure of graphene oxide and **Figure 2.3**(b) shows exfoliated graphene oxide [48]. There are various methods of making rGO from graphene oxide such as thermal, chemical and electrochemical means. Some of these techniques can produce very high quality rGO, similar to pristine graphene, but can often be complex or time consuming in nature. The very common technique to make rGO involves, treating GO with hydrazine hydrate at 100 for 24 hours. rGO is ideally suited for large scale industrial application such as energy storage where good quality graphene is not strictly required.

2.4 Chemical Vapor Deposition growth of graphene

Chemical vapor deposition (CVD) involves the activation of gaseous reactants or precursors and the subsequent chemical reaction, followed by the formation of a stable solid deposit over a suitable substrate. The energy for the chemical reaction can be supplied by different sources such as heat, light, or electric discharge as in thermal, laser-assisted, or plasma-assisted CVD respectively. Two types of reactions could be possible for the deposition process namely homogeneous gas-phase reactions, which occur in the gas phase and may results in formation of powders, and heterogeneous chemical reactions which occur on or near a heated surface leading to the formation of powders or films. Though CVD can be used to produce ultrafine powders, but in case of depositing extremely thin graphene films heterogeneous chemical reactions should be favored and homogeneous chemical reactions are avoided during the designed experiments. **Figure 2.4** shows a schematic diagram of a typical CVD process to grow graphene in a tubular furnace [49]. illustrating the generalized steps which involves reactant transport, their activation by thermal means, transport of reactant by gas phase diffusion through a boundary layer, adsorption, chemical reaction, growth, desorption, removal of reaction product etc. The CVD technique of graphene growth has assumed prominence due to its ability to grow large area, monolayer, low defect graphene on inexpensive substrates such as cold rolled, high-purity (99.999%), 25 µm thick Cu foils using inexpensive CVD growth hardware and operational cost. There are host of parameter ranges such as atmospheric pressure to ultra-high vacuum, range of precursor gas ratios, different types of transition metal catalyst as substrate and the range of growth temperature that had been explored to grow graphene by CVD technique. Each of the CVD system, that has reported graphene growth, usually has a window or small range of parameters for most optimized growth which also depends upon the system hardware and its capability. The basic understanding of growth mechanism is needed in order to find suitable parameters

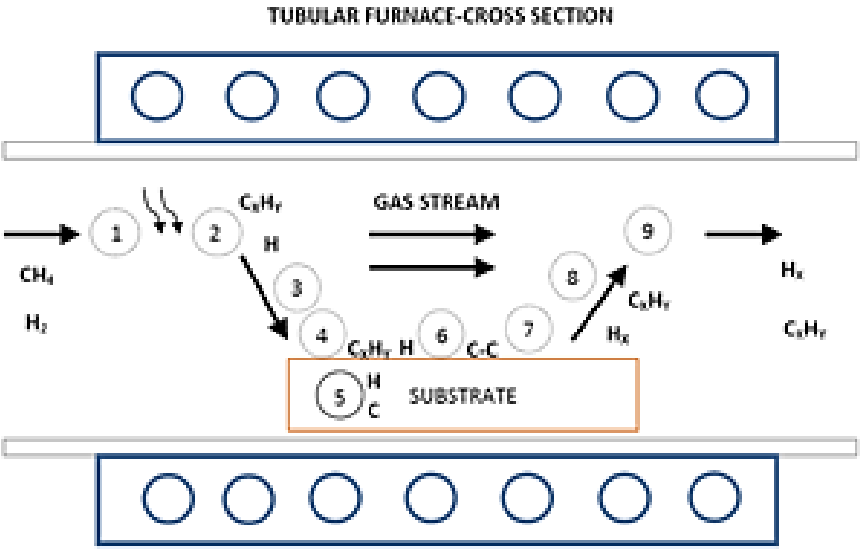

Figure 2.4 The generalized CVD growth of graphene on top of a metal catalyst. The steps involved are: reactant transport, activation, transport of reactant thought boundary layer, reactant adsorption on the surface, dissolution and bulk diffusion, chemical reaction, surface migration, film growth, desorption, transport of product through boundary layer, and transport by forced convection [49].

for optimizing graphene growth with a given hardware. The CVD of large-area, monolayer graphene on transition metal films and foils has been widely explored recently. In spite of the significant progress, CVD-grown graphene remains a polycrystalline film made of micrometer- to millimeter-size domains. It has been reported that, the graphene films grown on Ni foils or films do not yield uniform monolayer graphene. In most cases, a mixture of monolayer and few layers (polygraphene) are obtained. Whereas the use of Cu substrate has proved to be excellent candidate for making large-area, uniform thickness (95%), monolayer graphene due to the low solubility of C in Cu. It was suggested and even demonstrated that the graphene growth on Cu is surface-mediated and self-limiting. In this work the CVD of monolayer graphene was obtained on Cu foil.

2.4.1 Graphene CVD System

A crude CVD reactor was built which involved a round tube furnace, the quartz tube reactor, the precursor gases: CH4, H2, and Ar controlled by flow meters, and a low capacity (up to 9 Torr) DryFast diaphragm pump. The gases tanks were connected by polyethylene tubing. After building CVD systems it was revamped to optimize good quality monolayer graphene growth. The CVD setup consists of the three gas cylinders, each for CH4, H2 and Ar to the corresponding mass flow controllers (MFC) through manual valves and ¼” stainless steel tubing. The stainless steel tubing serves to provide higher conductance path and better leak characteristics as compared to polyethylene tubing. The MFCs were MKS Type 1179A each calibrated for the gas being used. Ar MFC was 1000 sccm range for flow larger amount of Ar and a carrier and diluent gas. H2 and CH4 MFCs were 200 and 50 sccm range for keeping CH4 to H2 ratio low during the growth. The output from MFCs is joined together using a Swagelok Union Cross. One end of the cross is connected to the ¼” quartz delivery tube by a stainless steel bellows. The reaction chamber consists of 1½” diameter wide and 2’ long quartz tube. It is also fitted with ¼” thick compressed BN heat blocker at both the ends. The enclosure is formed by stainless steel end caps with sleeves. The sample or substrate is mounted on a flat quartz boat. The other end of the chamber has one outlet connected to stainless steel tubing with bellows. A barometer and a Pirani gauge (MKS 901P, load lock transducer) are attached downstream to this stainless tubing to monitor the pressure of the system. This tubing then connects to the inlet of a mechanical pump. The mechanical pump is a rotary vane pump from Pfeiffer Vacuum (Model: Duo 10 M) with a capability of 4.5 mTorr ultimate pressure. However the base system pressure remains in the range of 100 mTorr. The outlet of the pump is connected to room exhaust line though a manual valve

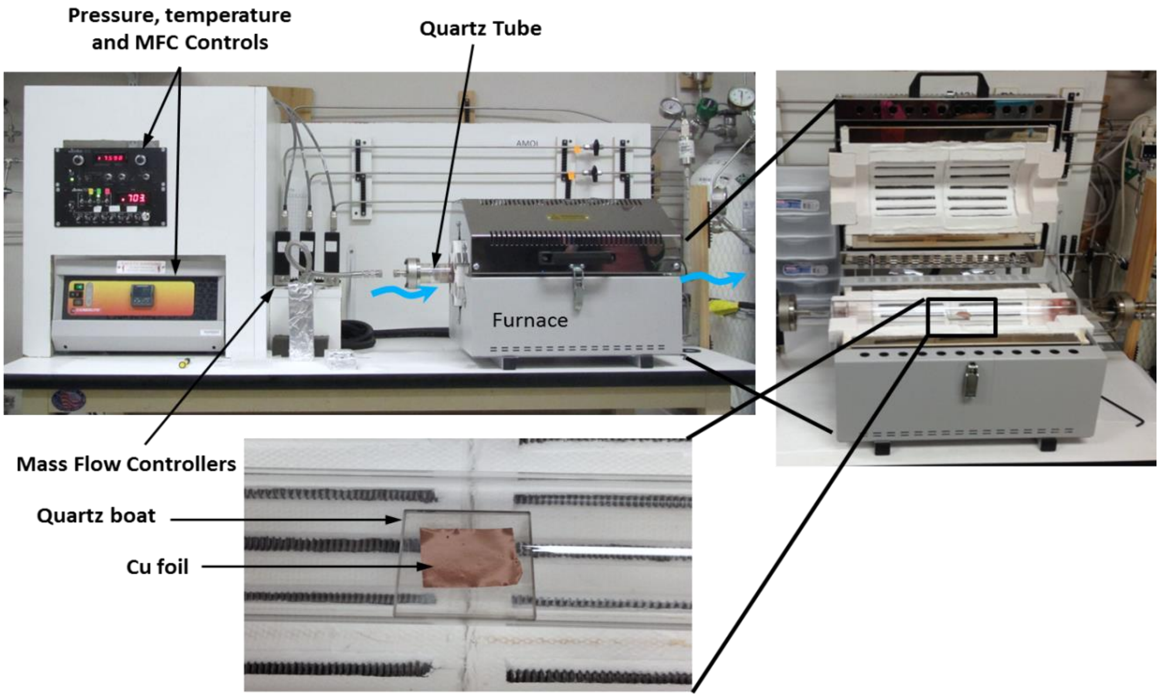

Figure 2.5 (a) The CVD graphene growth system with Pressure, temperature and MFC controls (b) Cu foil after graphene growth on quartz boat shown in enlarged image

which keep the CVD system isolated from exhaust and saves from occasional oil leak of other pumps which are also connected to exhaust. The quartz tube reactor is housed inside a horizontal single zone split tube furnace from Carbolite. This furnace is capable of operating at 1100 °C for prolonged hours and takes about 45 min to reach that temperature. The temperature is controlled by Carbolite 301 controller. Split furnace was chosen to have a faster cooling rate and also to cut-down process time. **Figure 2.5** (a) shows the picture of graphene CVD system in where precursor gas cylinders and mechanical pumps are not in the frame. **Figure 2.5** (b) shows Cu foil after graphene growth The picture shows stainless steel tubing, MFCs, their controller and read-outs, horizontal split-tube furnace and its controller, quartz tube reactor fitted with stainless steel ends caps, pressure gauge and read-out etc.

2.5 Growth on Cu Foil

By virtue of low solubility of C atoms in Cu (< 0.001 atoms % at 1000℃) growing thinner (mono and bi-layer) graphene becomes easier compared to Ni. Here

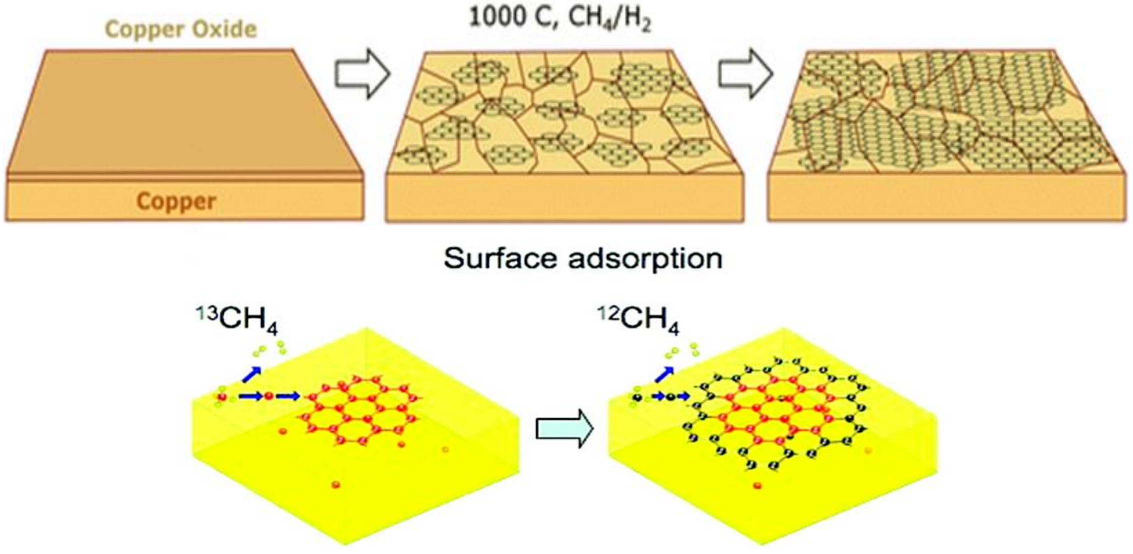

Figure 2.6 (a) The graphene growth mechanism on copper foils [50]. (b) The graphene growth by surface adsorption as revealed by use of C13 and C12 isotopes of carbon [51].

thinner graphene layer is not affected much by cooling rates and CH4 flow rates. The growth mechanism is surface adsorption of C atoms on Cu. At growth temperature say 1000℃ carbon atoms are releases on Cu by dehydrogenation. These released atoms then grow by nucleation and growth as more C atoms are added to the periphery. They keep growing till they become large enough and coalesce to form full coverage of film.**Figure 2.6** (a) show the schematic of this growth mechanism on Cu foils.[50] The use of C13 and C12 isotopes clearly indicates the surface adsorption type growth mechanism owing to low carbon solubility in Cu. This is illustrated in **Figure 2.6** (b) as reported by Li et al [51]. where red colored C13 isotope is delivered to Cu foil at growth temperature by

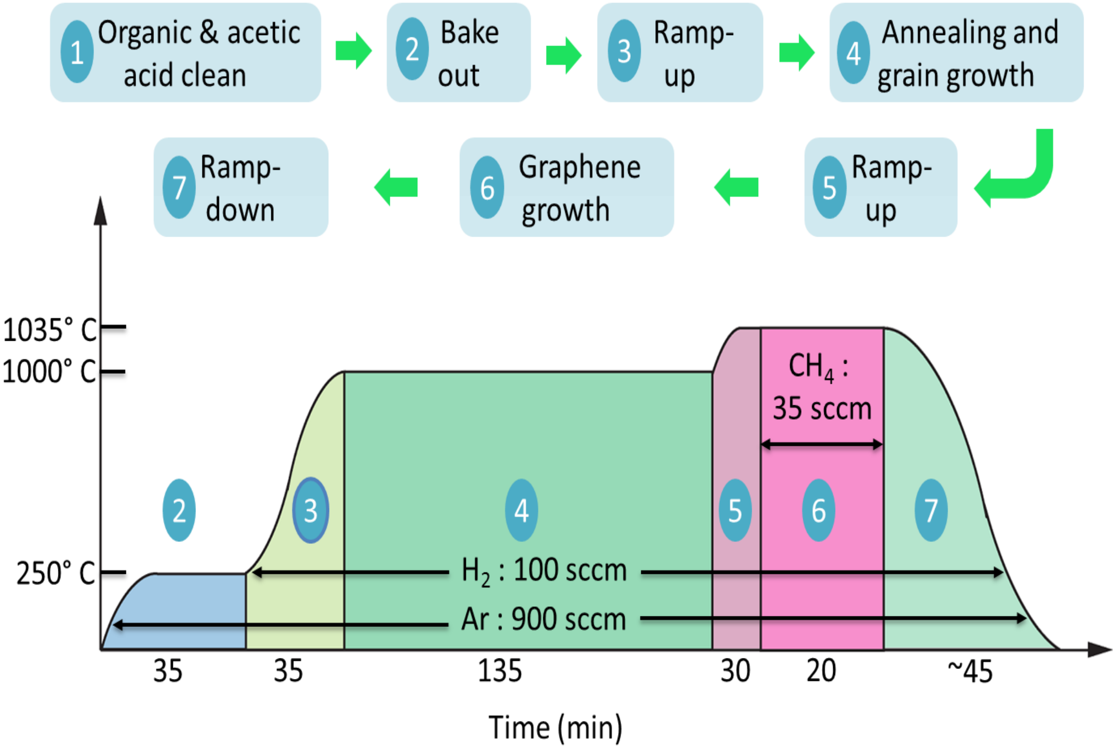

Figure 2.7 Series of steps involved in growing monolayer graphene on Cu foils. The optimized process parameter is shown in the schematic plot.

$^{13}CH_4$ and graphene starts to grow by nucleation and growth. When the gas was switched to 12CH4 the black colored C12 carbon atoms continued the growth by getting embedded to the periphery of the red colored C13 carbon based growing grain. This suggests that C doesn't go in the bulk of Cu foils, therefore it does not segregate out at random places resulting into thicker graphene growth. These conclusion were drawn by Li et al. using Raman mapping and are indicative of the fact that the copper is the material of choice for thin graphene growth. Graphene growth was optimized for Cu as a metal catalyst. The optimization involved a good cleaning procedure for getting rid of copper oxides such as CuO and Cu_2O which are 37 present in cold rolled Cu foils. **Figure 2.7** shows the optimized process parameter and sequence of steps for graphene growth. The Cu foils were first cleaned in acetone and isopropanol and then sonicated in acetic acid to remove oxide. They were loaded in growth chamber under Ar over pressure. The system was evacuated and then Ar was flown at 250℃ for bake out. H2 was flown for 2 hours at

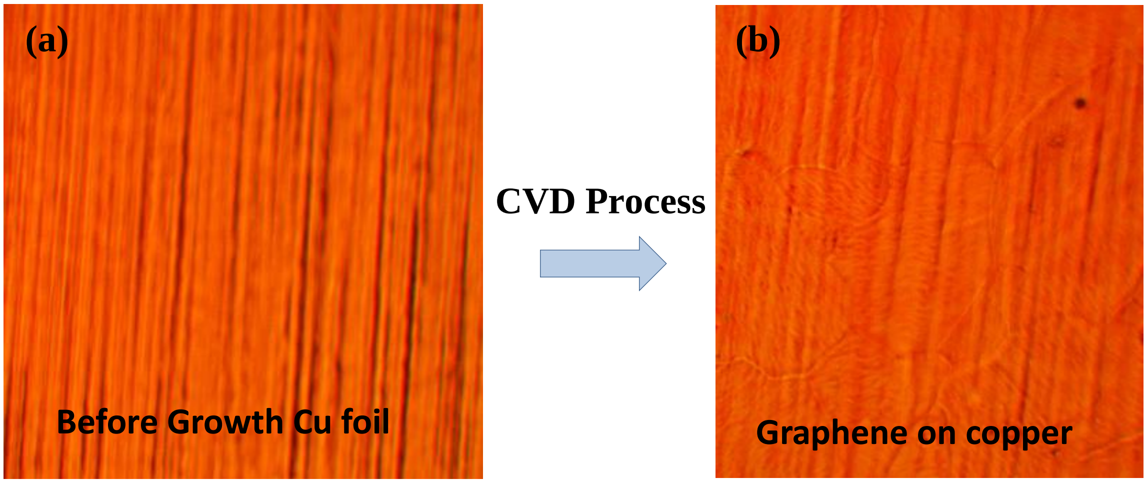

Figure 2.8 **(**a)Optical Image of Copper film before CVD process. (b) Optical image of Graphene on Copper film after CVD process

1000℃ to anneal Cu to increase its crystalline quality and remove any remaining and newly formed oxide. The actual growth was performed at further elevated temperature of 1035℃ in presence of CH4. The forced cooling was done by use of a fan. It takes about 45 minutes to cool down the system to 100℃.

2.6 Raman characterization of Graphene

In order to understand the type and quality of CVD graphene and to device the strategy to improve the CVD, a reliable and quick feedback is very important. In case of graphene Raman spectroscopy provides quick and immediate feedback on as-grown graphene on metal catalyst without any need for sample preparation. In fact Raman spectroscopy was used to determine if the thin film based CVD of graphene is suitable since it will require very large extent of optimization.

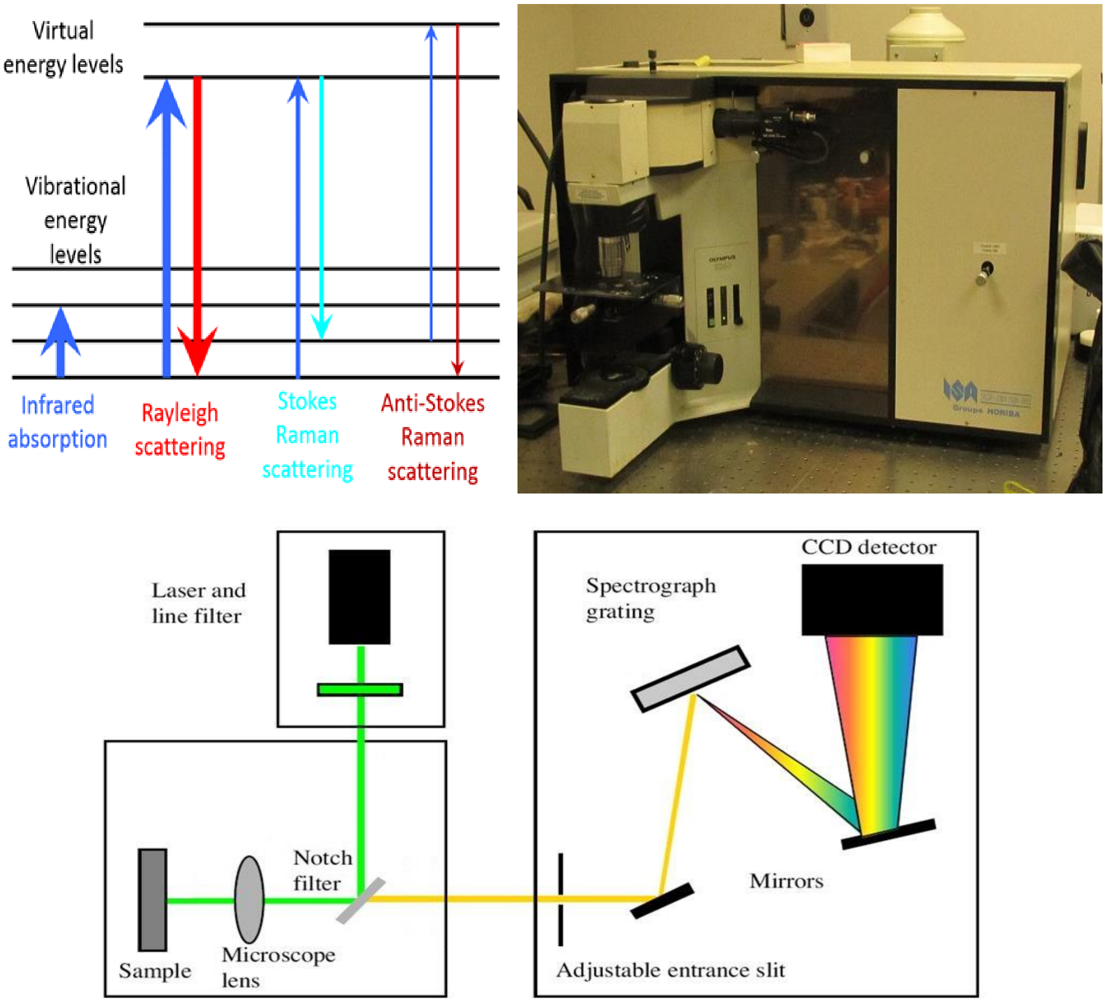

Figure 2.9 (a) The basic physics of Raman scattering involving ground state vibrational levels and virtual states. Infrared absorption is also shown for comaparison. (b) LabRAM Raman Spectrometer from Horiba used in this work. (c) The ray diagram of Raman spectrum set-up consisting of Laser, notch filters, lenses, grating and CCD detector [53].

Raman spectroscopy is based upon vibrational spectrum of a material system. It is becoming increasingly popular in detecting organic, inorganic species and crystallinity of the system. It is sensitive to strain and can detect stress in the semiconductor in very interaction of incident waves to matter results in scattering of waves apart from other small region due to the ability of focusing light beam in very small region. The effects such as absorption or transmission. The scattered waves can be of three types, the predominant Raleigh scattered light which has same wavelength as that of the incident wavelength as seen in **Figure 2.9**(a). The other two types have different wavelength or energy than those of incident photons and are called Raman scattered. These scattered photons interact with optical phonons of the material therefore contain the material information [52]. When incident photons impart energy to the lattice by emitting a phonon, the scattered photon comes out with lower energy or higher wavelength and the process is called as Stoke shifted scattering. On the other hands if a phonon in absorbed in scattering process it is referred as anti-Stoke shifted scattering as seen in **Figure 2.9**(a). Anti-Stoke scattering has lower probability process than Stoke scattering therefore in Raman spectrum Stoke shift is measured. However entire Raman scattering is very low probability process as compared to Raleigh scattering (~1 in 108 parts) therefore a strong monochromatic light source such as laser is a must for obtaining Raman spectrum. **Figure 2.9**(c)[53] shows a simplified schematic of Raman setup consisting of laser source, notch filters to avoid Raleigh scattered photon, grating and CCD detector to measure the spectrum. **Figure 2.9**(b) shows the image of Raman spectrometer setup, LabRAM 1B from Horiba.

The Raman peaks of interest in graphene material lies in the range of 1200 to

3000 cm-1 as shown in Figure 2.10. This spectrum corresponds to a defective graphene to capture all possible peaks in the range of interest since some of the peaks may be absent in good quality graphene. The prominent peaks in the Raman spectra of graphene system are G and G’ or 2D bands occurring at ~1580 cm-1 and ~2700 cm-1 respectively. The

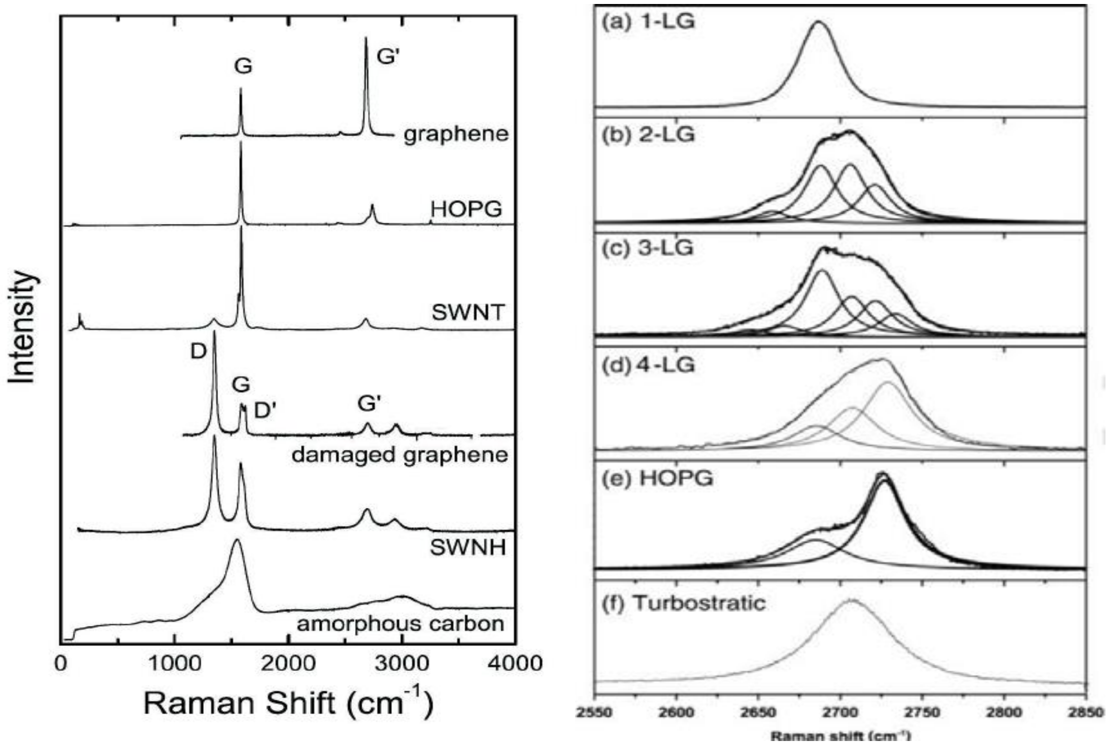

Figure 2.10 (a) Raman spectra of various sp2 carbon based system showing ability to distinguish them based upon intensity, shape and with of D, G G’ or 2D peaks using one simple scan of Raman spectrum [54]. (b) Using the shape of 2D band it is possible to distinguish graphene from graphite and also determine the numbers of monolayers by fitting different Lorentzians to the band [54].

shape, width, position and relative intensities of these bands or peaks helps in distinguishing between graphite, graphene and various other sp^2 based C systems such carbon nanotubes. **Figure 2.10**(a) captures this ability of Raman spectroscopy to distinguish between various carbon based materials very clearly such as amorphous carbon, CNTs, pristine and defective graphene and HOPG.[54] It also helps in determining the number of monolayers present in the sample, based upon shape and width of 2D band, by fitting various different types of Lorentzians as seen in **Figure 2.10**(b).

The D peak as mentioned before corresponds to amount of disorder or defect in graphene material system. Intensity ratio of D and G peaks in graphene (I_D/I_G) helps to quantify the amount of defects and disorder. In general when I_D/I_G is high then the material is considered highly defective. When the ratio of I_D/I_G is less than 0.3 it considered a good quality graphene having lesser density of defects and disorder.

The 2D peak in graphene is the result of double resonance process and is coupled to electron and phonon in graphene dispersion relations. A monolayer exfoliated graphene sample at room temperature exhibits a sharp 2D peak consisting of single Lorentzian feature with a full width at half maximum (FWHM) of ~24 cm^{-1}. The intensity of this peak relative to G peak is very high sometime reaching to 4 time more intense than G peak or $I_{2D}/I_G \sim 4$ [55]. When the ratio of I_{2D}/I_G is around 4 it considered a monolayer to bilayer graphene.

2.7 Uniformity of Graphene

In order to understand the type and quality of CVD graphene quick feedback is very important. In case of graphene Raman spectroscopy provides quick and immediate feedback on as-grown graphene on metal catalyst without any need for sample preparation. In fact Raman spectroscopy was used to determine if the thin film based CVD of graphene is suitable since it will require very large extent of optimization. Raman spectrum of graphene on Cu foils is shown in **Figure 2.11**. It plots the spectra for two different locations on Cu foil. Both the locations show very low defect density as indicated by I_D/I_G value of 0.01 and 0.015. The I_{2D}/I_G value of 2.20 and 1.77 along with

2D FWHM of 32.95 and 38.69 cm^{-1} clearly indicate the presence of monolayer CVD graphene on 25 μm thick foils.

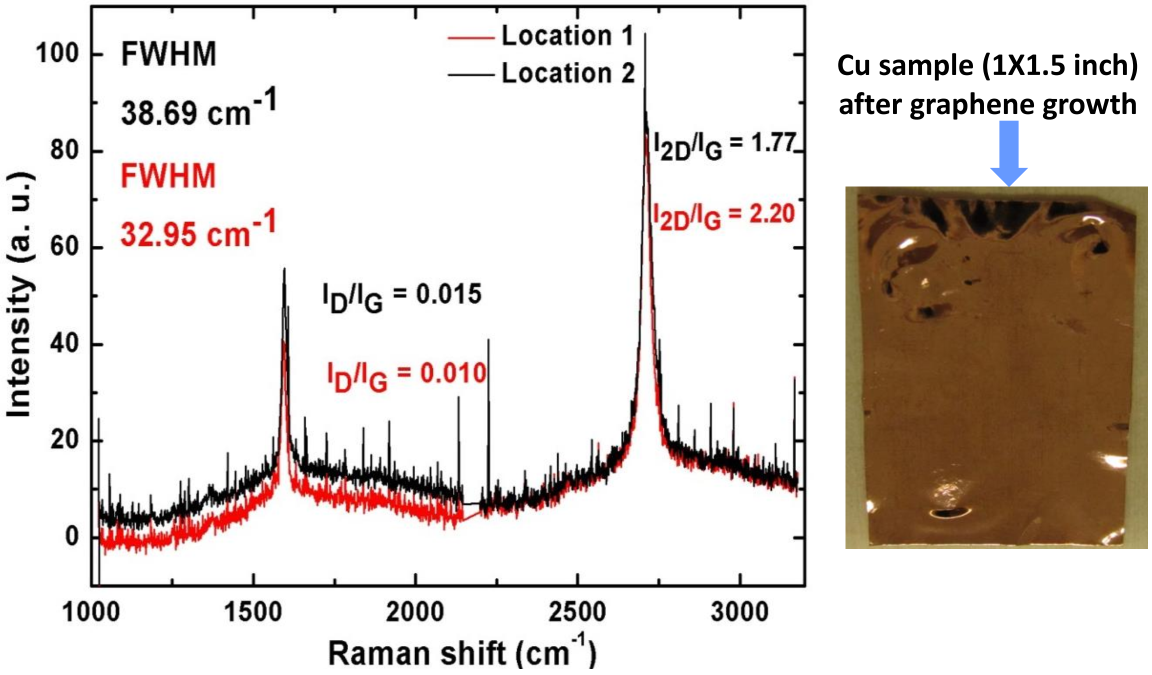

Figure 2.11 (a) Raman spectra of two samples of graphene as-grown on Cu foils by CVD growth technique with optimized parameters. The 2D FWHM of 32.95 and 38.69 is indicative of monolayer graphene. (b) Graphene grown Copper foil after graphene growth

In summary a CVD reactor was set-up to perform graphene grown on transition metal substrates. The reactor was built by assembling different components such as quartz tube chamber, horizontal split furnace, mechanical pump, MFCs and pressure gauges. The optimized process parameter were obtained by understanding growth mechanism and by performing series of growth on different types of substrates and under different growth conditions. The quality of growth was assessed by Raman spectroscopy on as-grown samples. The device fabrication of CVD graphene would require the development of a reliable graphene transfer process on any desirable substrate and also of device processing techniques. The next chapter addresses the processing and different characterization of graphene based devices.

CHAPTER 3
GFET DEVICE FABRICATION AND CHARACTERIZATION

In CVD based graphene growth on transition metal catalyst, the grown graphene cannot be used directly since it sits on top of a metal film or foil. It is required to be transferred on a desired substrate for all possible characterization and device making. The first step in making any CVD graphene device is transfer of graphene on a desirable substrate and followed by fabrication process which described in below sections.

3.1 Graphene Transfer

In our graphene growth on Cu foil it grows on both sides of the foil. In general graphene grown on the bottom side of the foil is of inferior quality as compared to the one gown on the top side. The graphene transfer process therefore entails the following steps as illustrated in **Figure 3.1**The top side graphene is first protected by spin coating of poly methyl methacrylate (PMMA) twice at 3000 rpm for 40 sec. It also provides mechanical strength to graphene in the subsequent processing steps. The PMMA coated sample is loaded upside down in reactive ion etching (RIE) chamber upside down in order to expose the bottom graphene layer. This graphene layer is remover by oxygen plasma which is sustained at 150 W for 180 sec. The sample is then kept in concentrated Cu etchant over night for complete removal of Cu. Both $FeCl_3$ and $(NH_4)_2S_2O_8$ (ammonium persulfate) have been used. This results in graphene/PMMA layer floating in the etchant as seen in Error! Reference source not found.(e).The poor contrast in

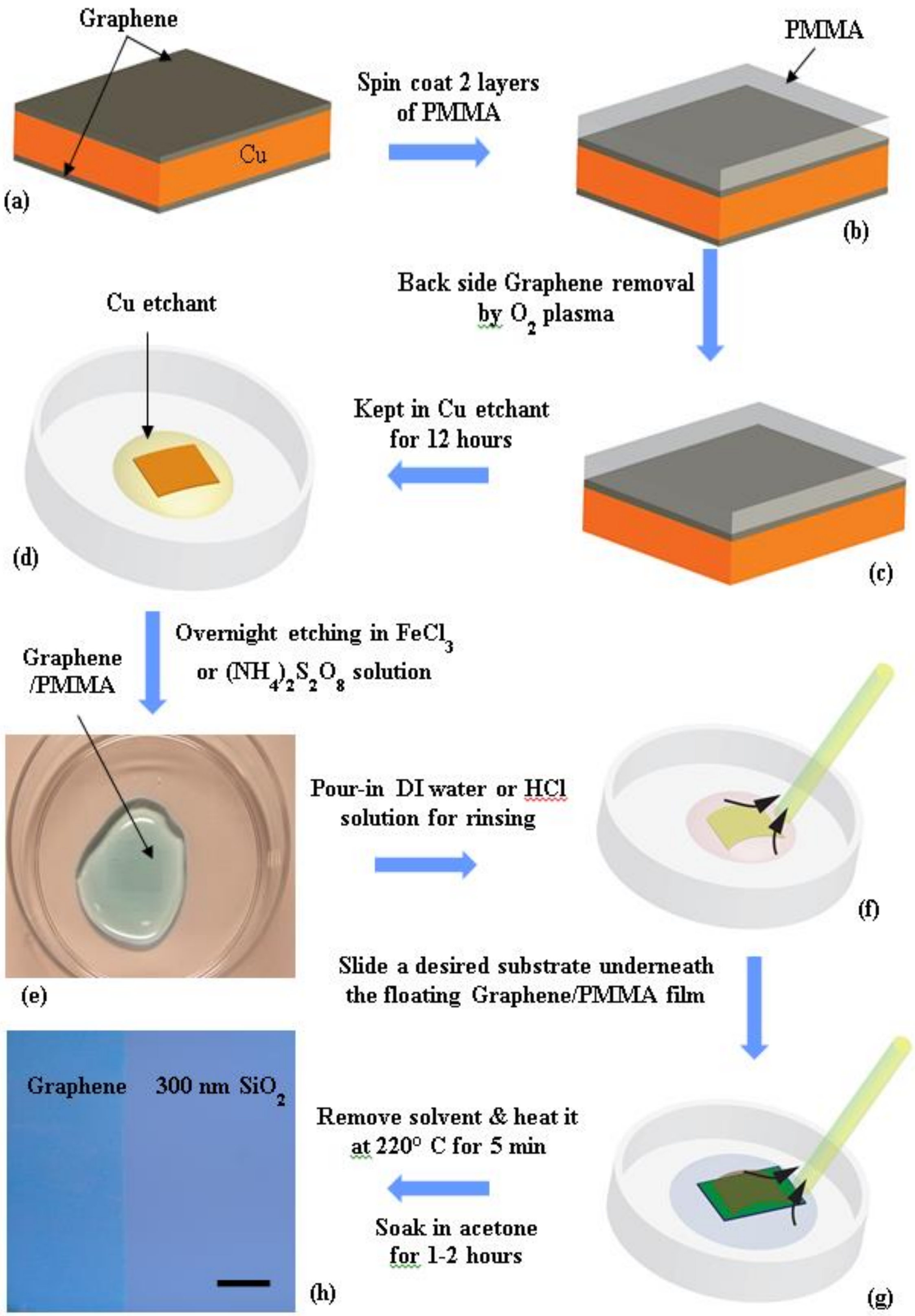

Figure 3.1 Processing steps for graphene transfer on any desirable substrate.

ammonium persulfate solution is the results of monolayer graphene coated with PMMA. The floated graphene is rinses once with HCL and multiple times in deionized water. A desired substrate can then be slid underneath the floating graphene/PMMA as shown in **Figure 3.1**(g). The substrate containing transferred graphene/PMMA is allowed to dry in air and then baked at 220 ˚C above the glass slide. This backing process will allow reflow of PMMA in order to heal the wrinkles in graphene. The sample is then dipped in acetone for 2-3 hours to remove PMMA from top of transferred graphene. This is followed by organic cleaning of the sample in acetone and IPA. One such transferred graphene on 300 nm thick SiO_2 is shown in **Figure 3.1**(h).

3.2 Back-gated FET Based Device Fabrication

For making graphene based back gated FETs we chose 300 nm SiO_2/Si substrate. The Si was to be served as global back-gate therefore had low resistivity in the range of 0.008–0.02 Ω - 50 cm. The graphene was transferred on top of 300 nm SiO2 using process described in previous section 3.1 and as shown in **Figure 3.1**. The graphene with si substrate was spin coated with positive resist S1811 at 4000 rpm for 30 seconds. After spin coating sample photo lithography performed using projector. UV exposed for 8 to 10 second on photoresist to define pattern on resist. The patterns for metal contacts were made in power point to control channel, source and drain scaling parameters. Once exposer process finished sample was developed using MF351 developer. 20 nm of Cr and 80 nm of Au were deposited by DC sputtering or evaporated in e-beam evaporator. The contacts were finally formed using metal lift-off in acetone. Graphene channel is formed on top of 300 nm thick SiO_2 in between Cr/Au source drain electrodes shown in **Figure 3.2**

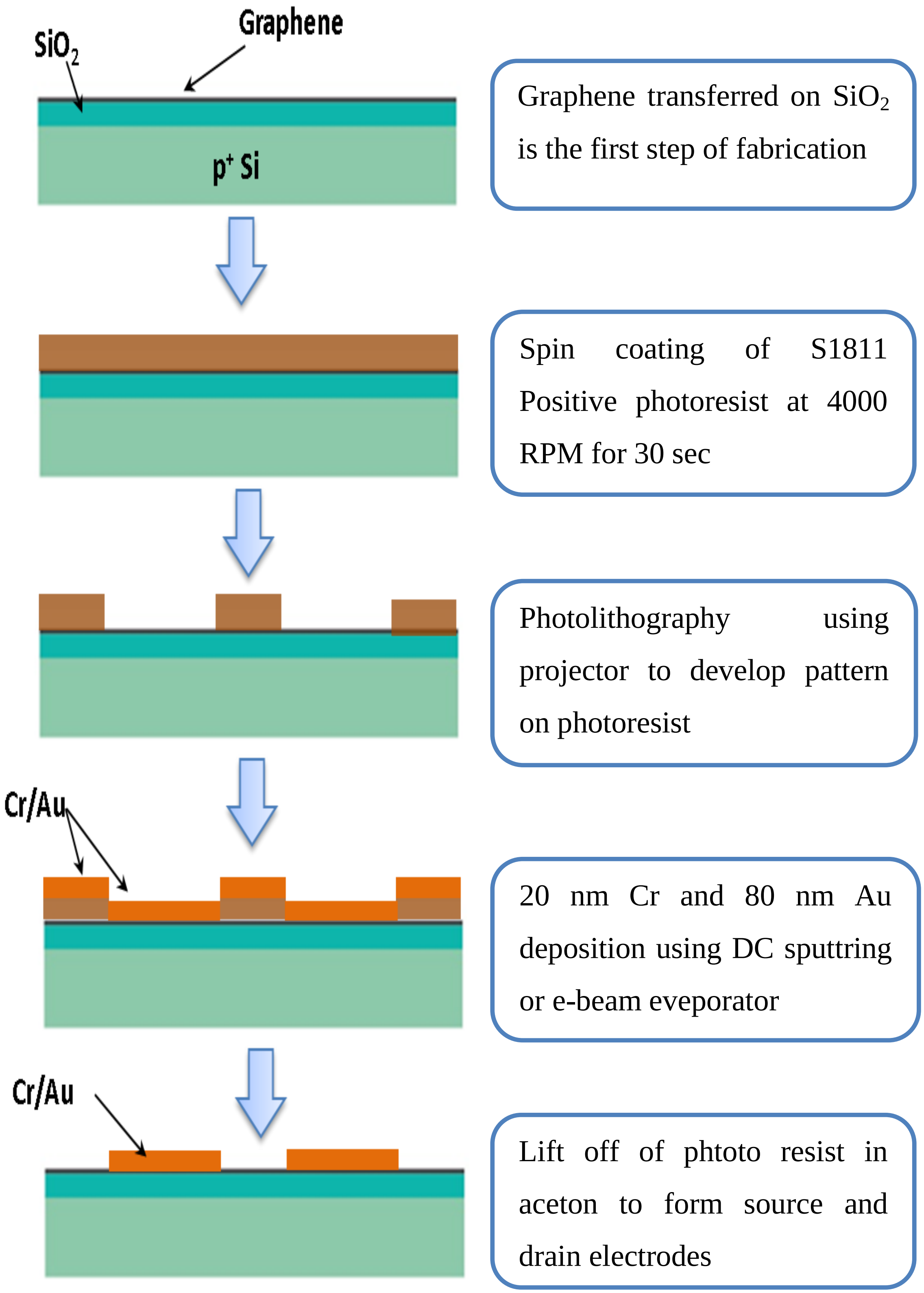

Graphene transferred on SiO_2 is the first step of fabrication

Spin coating of S1811 Positive photoresist at 4000 RPM for 30 sec

Photolithography using projector to develop pattern on photoresist

20 nm Cr and 80 nm Au deposition using DC sputtring or e-beam eveporator

Lift off of phtoto resist in aceton to form source and drain electrodes

Figure 3.2 Device processing steps for fabrication of graphene Field effect transistor (GFET)

3.2.1 Electrodes fabricated on Graphene

As process flow seen in **Figure 3.3**, Graphene transferred on Si/SiO_2 followed by photolithography and metal deposition. As we can see in **Figure 3.3** we observe damage to the contact in lift off process of CVD synthesized graphene. Contact metals were not continuous when metal deposited on graphene. As reported in some literature there are some reason of metal peeling off while lift off like thickness and deposition rate of metal while deposition, metal stress induced because of thickness of metal deposition, PMMA residue left on graphene. To overcome this problem we changed process flow shown in section 3.2.2 and in **Figure 3.4**

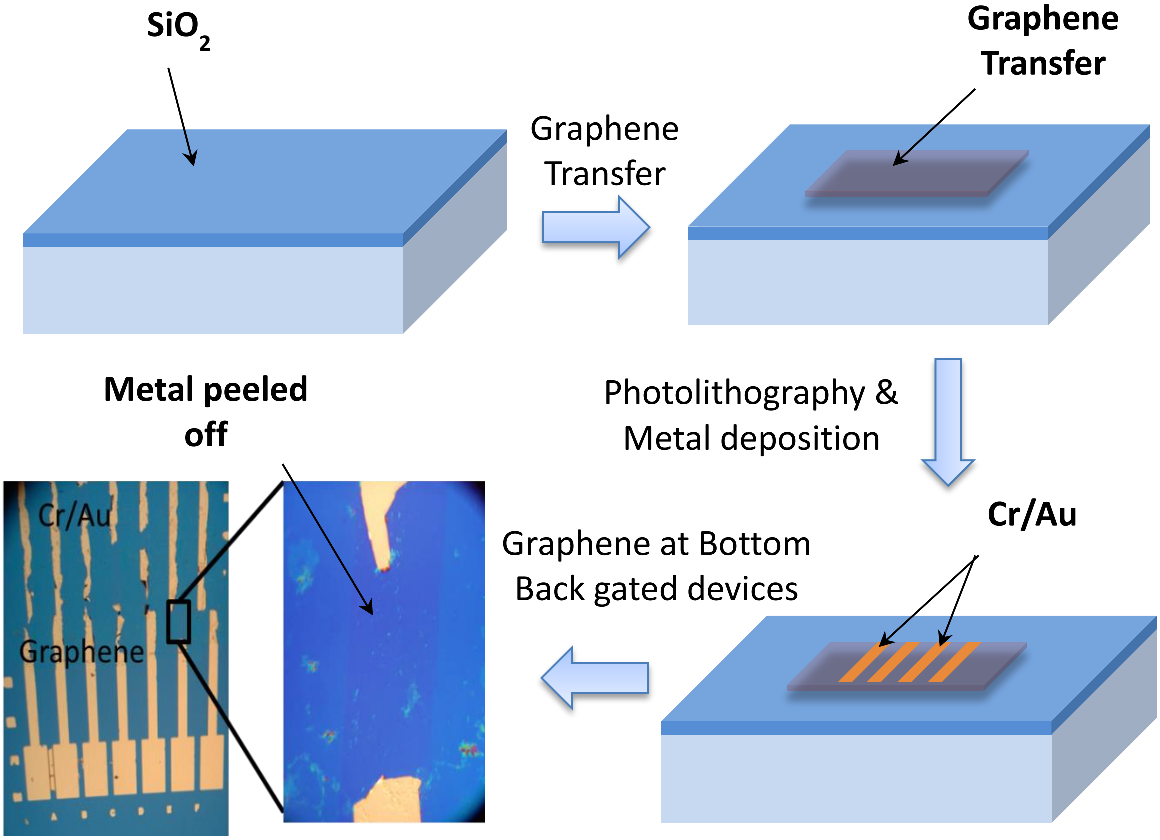

Figure 3.3 Graphene at bottom fabrication process flow.at end Optical image of graphene FET showing 246 μm long and 2300 μm wide graphene channel on top of 300 nm SiO_2 substrate.

3.2.2 Graphene transferred on electrodes

To overcome metal liff of problem discussed in above section we change the process flow for fabricating back gated devices. For device preparation first performed photolithography and metal deposition followed by graphene transfer as shown in figure.

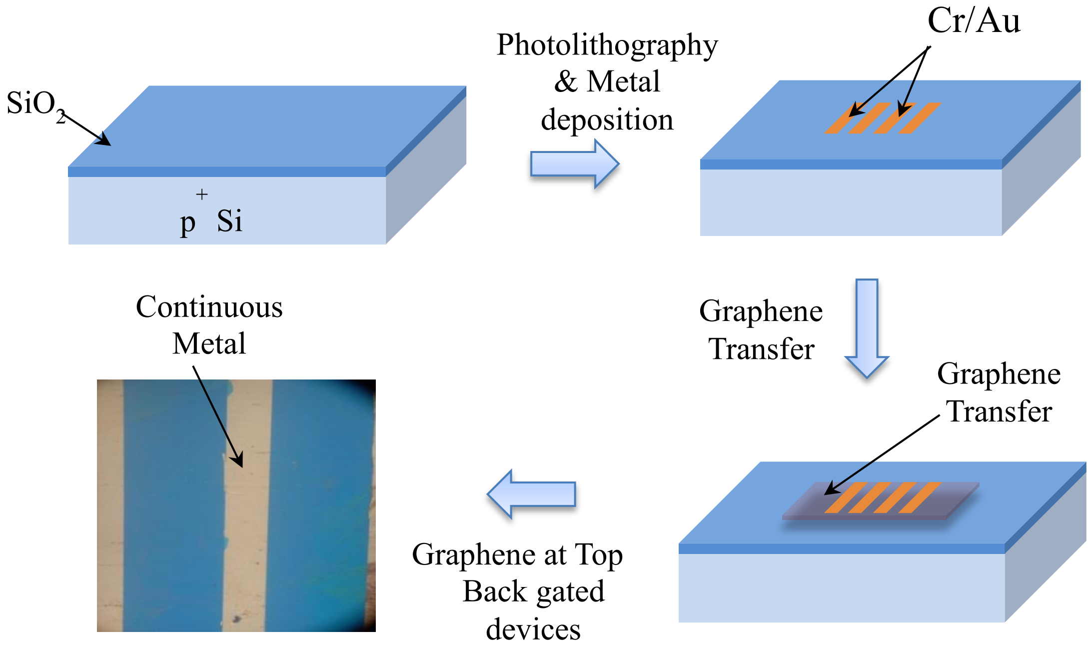

Figure 3.4 Graphene on Top fabrication process flow

As we can see in **Figure 3.4** by using this method after liff off process metal electrode were continuous were graphene was transferred on top of contacts.

3.3 Raman Characterization of Back gated Graphene Devices

The optical property of Graphene is very unique. Even though graphene has just one atomic thickness, it is observable by traditional optical microscope when it is deposited onto the surface of SiO_2 (~300nm)/Si wafer. This is because of the interference phenomenon which occurs from the multiple reflections between graphene and SiO_2 layer. Raman is one of the powerful tools to characterize the optical properties of graphene. It is easy to determine the graphene layer thickness by examining the 2D peak shape and the peak ratio between G and 2D peaks in Raman spectrum. **Figure 3.5** shows the Raman spectra taken using laser excitation wavelength of 514 nm with the prominent G and 2D peaks of graphene occurring at ~1593 cm^{-1} and ~2712 cm^{-1} respectively. This spectrum corresponds to a high quality graphene since the D peak (at 1357 cm-1) which indicates the presence of defective graphene is almost absent. The presence of G peak at 1593 cm^{-1} which is close to the ideal G peak at 1580 cm-1 confirms the presence of carbonaceous material with sp^2 bonding and its intensity is proportional to the thickness of graphene. The other prominent peak 2D is also seen in **Figure 3.5** resulting from a

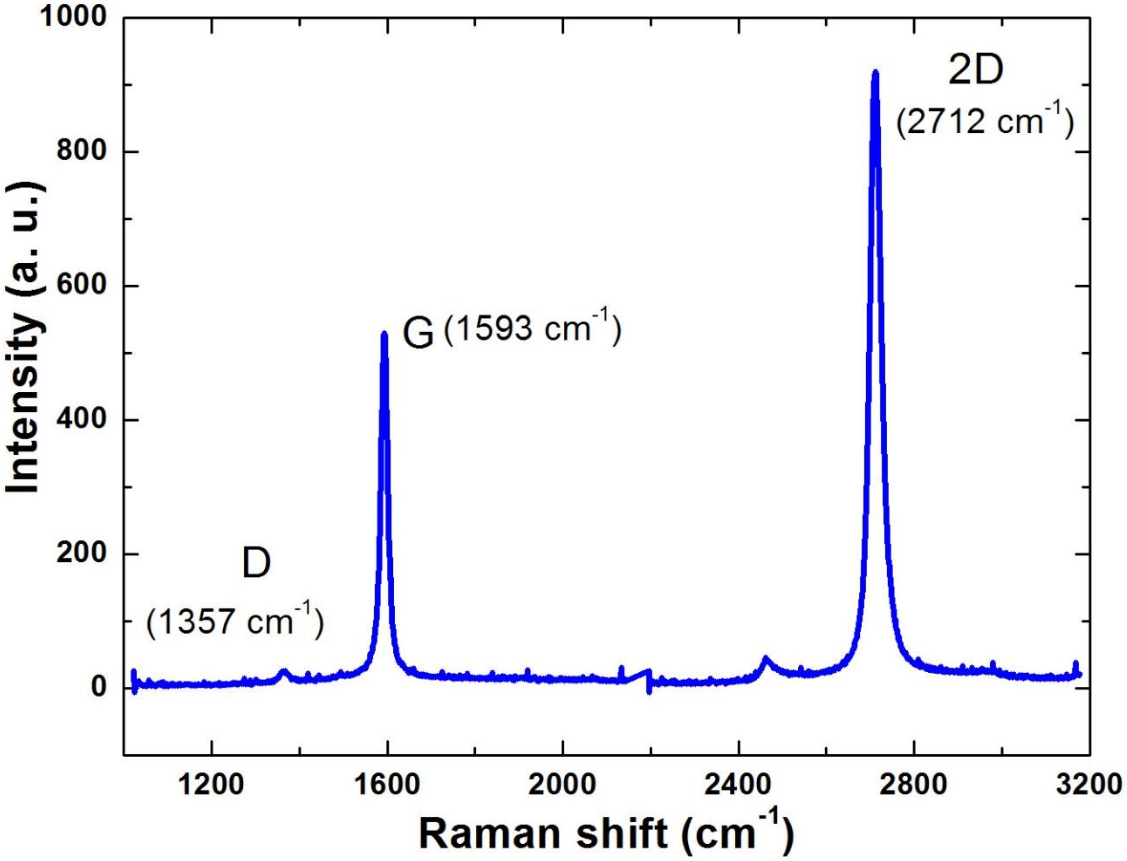

Figure 3.5 Raman characterization showing D,G and 2D peak on Graphene on top back gated device fabrication

second order scattering process that involves double resonance and two iTO phonons near K point.

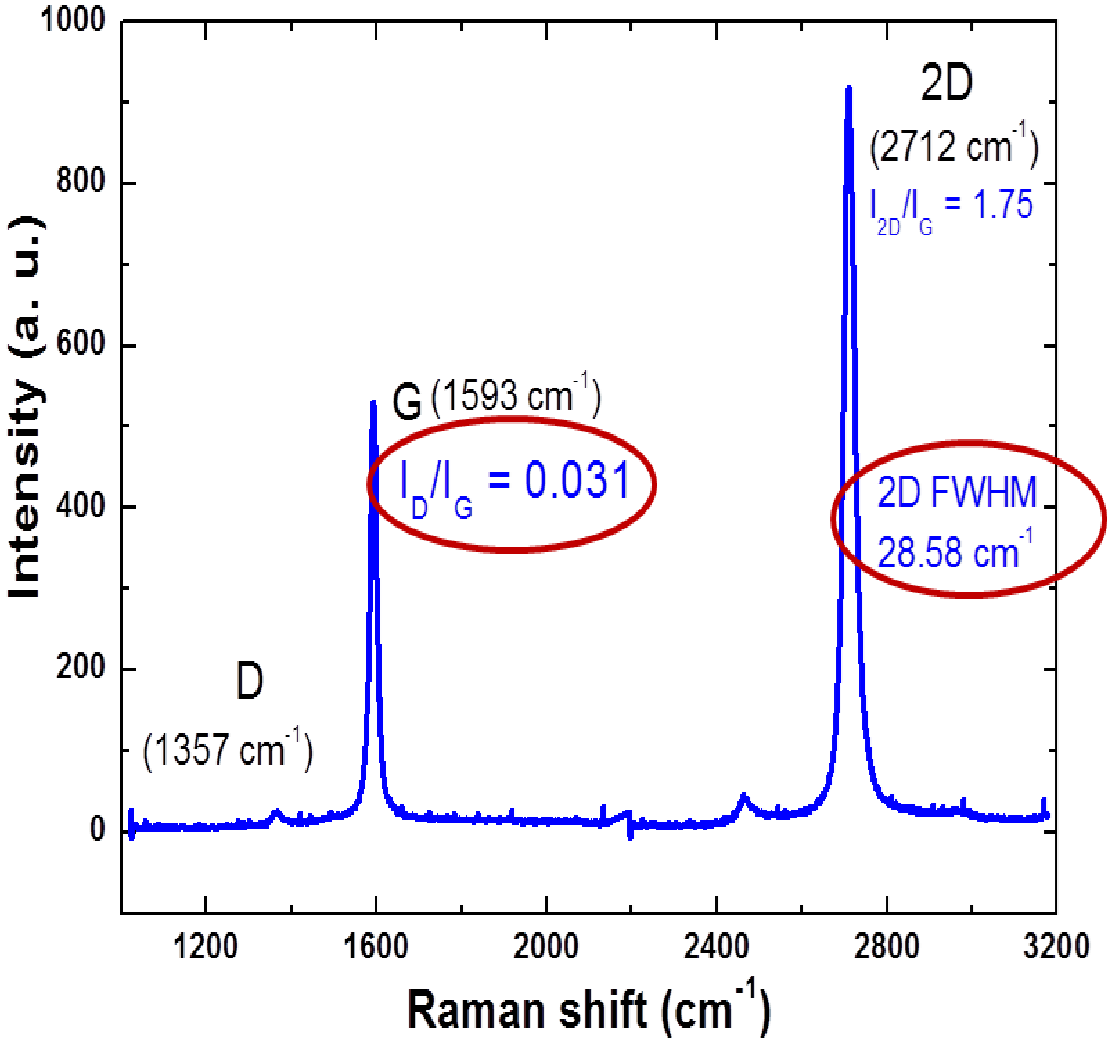

Figure 3.6 Raman characterization showing D,G and 2D peak on Graphene on top back gated device fabrication

The intensity ratio calculated between D and G peaks is about 0.031 as shown in **Figure 3.6**. This confirms the presence of high quality graphene with very less defects and disorder. The ratio between 2D and G peak and the FWHM of 2D peak indicated in **Figure 3.6** confirms the thickness of the graphene to be in the order of monolayer or bilayer.

Figure 3.7shows the Raman spectra taken at 6 different locations on a back gated GFET. The D peak intensity suggests low defect concentration in CVD graphene.

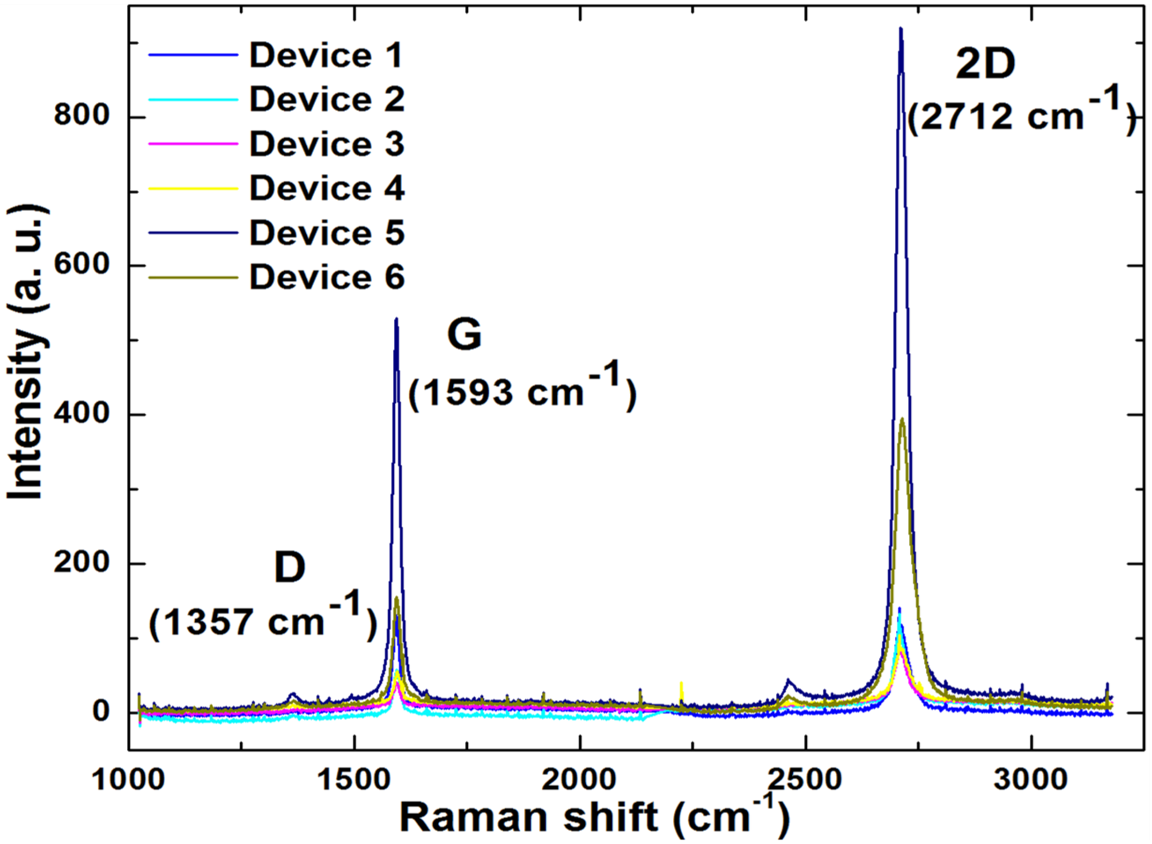

Figure 3.7 Raman spectra taken at 6 different locations on a back gated GFET

However 2D peaks in **Figure 3.7**suggests monolayer to few layer graphene due to 2D FWHM ranging between ~28 to ~41. At location 5 I_D/I_G ration is 0.031, I_{2D}/I_G ration is 1.754 and 2D FWHM is 28.58 cm-1, which indicated presence of monolayer in GFET devices.

3.4 Mobility of Back Gated Graphene Devices

The current-voltage measurements were performed using a Keithley 2612A/ Agilent B2900A Source measurement unit. **Figure 3.8**(a) illustrates the schematic of global back-gated graphene FET and the biasing scheme for the measurement of transistor characteristics. In **Figure 3.8**(b) I_{ds} vs V_{ds} family of curves is shown where back-gate bias Vbg varied from -40 to 0 volt with an increment of ΔV_{bg} of 8V. The V_{ds}

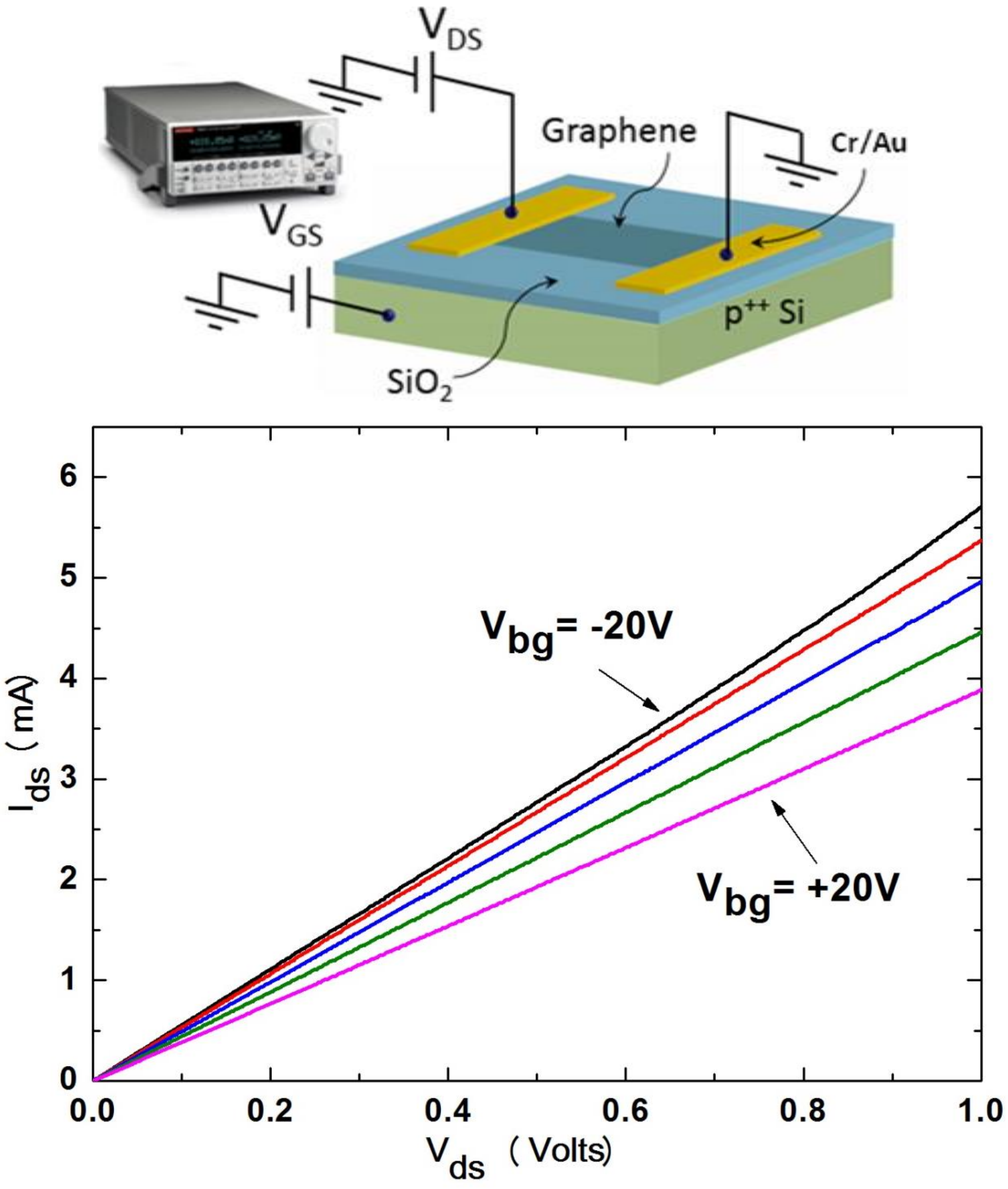

Figure 3.8 Family of curves for graphene FET showing increase in I_{ds} with more negative V_{bg} indicating p-type behavior

was varies from 0 to 1V. This shows p-type behavior of transferred graphene in negative Vbg range. The more accurate picture of carrier types emerges from transfer characteristics of graphene FET from **Figure 3.9** [56] which is also referred as GFET which will be discussed later in the chapter. The I_{ds} vs. V_{bg} plot is ambipolar in nature which is a direct consequence of liner dispersion relation in graphene with zero band gap. The minimum conductivity point in transfer characteristics, also referred as Dirac point, was observed at V_{bg} of 42 V. The positive Dirac point reaffirms that CVD graphene transferred on SiO_2 is p-type in nature. Another important information about material property that can be obtained from transfer characteristics of this device is field-effect mobility, GFET, given by the following expression.

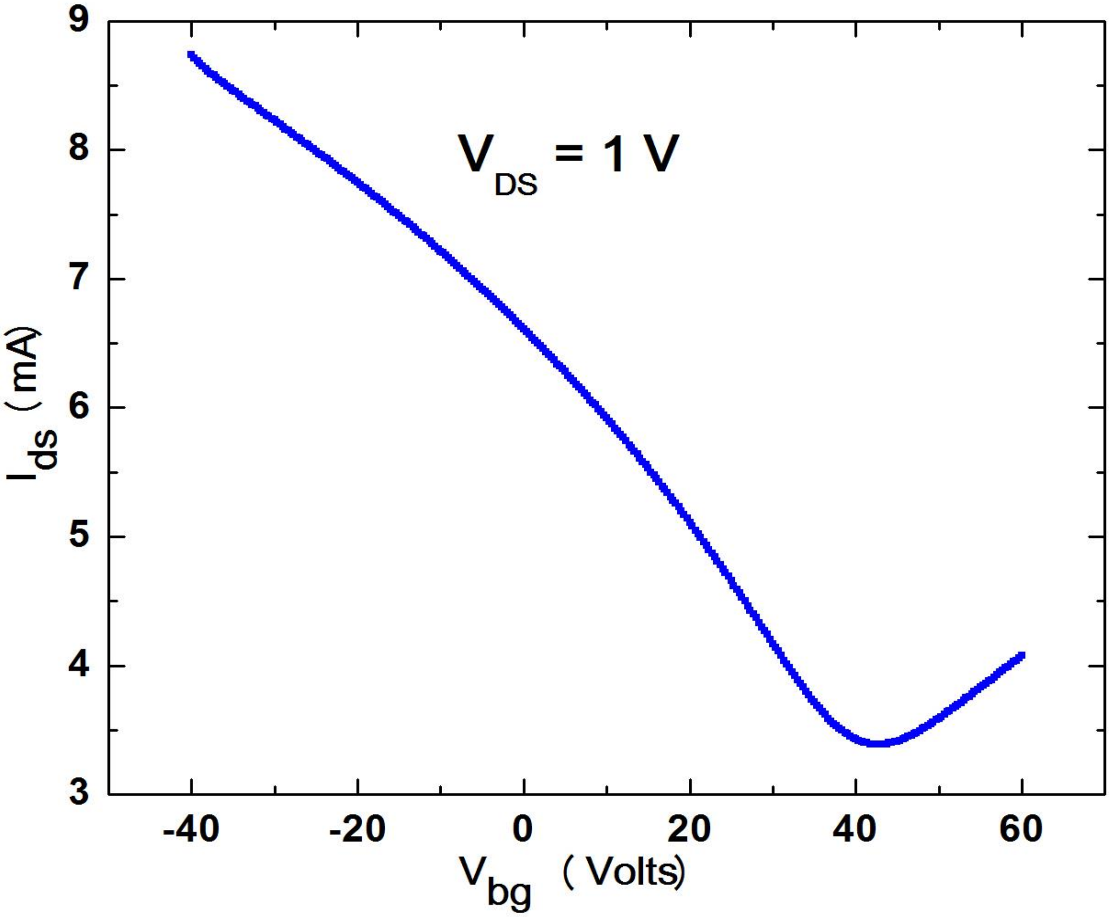

Figure 3.9 I_{ds}-V_{bg} transfer characteristics of the GFET with Dirac point at 45 V, indicating p-type behavior of graphene transferred on SiO_2.

$$\mu_{GFET} = \frac{g_m L}{W C_{ox} V_{ds}} \qquad (3.1)$$

Where gm is transconductance, L is length of graphene channel, W is width of the graphene channel, Cox is the oxide capacitance per unit area. With improvement in the quality of the graphene film we were able to obtain mobility values in the range of 1000 cm^2/Vs on routine basis. We observed variation of mobility at different places on single chip multi-channel devices. These variations may result from already exiting non-uniform defect density in CVD graphene or can be introduced during the processing as well. Our best GFET was calculated as 1000 cm2/Vs.

3.5 Bias stressing Effect on Graphene based devices

Graphene, the one-atom-thick carbon sheet with honeycomb structure, exhibits very high carrier mobility and has great promise as a channel material for future high speed transistor e.g., graphene field effect transistors (GFETs) [57]-[62]. The reliability issues, such as positive bias temperature instability, in conventional metal oxide semiconductor field effect transistors have been studied thoroughly, due to its critical importance to device stability and lifetime evaluation [63]-[66]. However, positive bias-induced Vth instability in single layer and multilayer GFETs has not been studied in depth. In this section, the ΔVth dependence on stressing voltage, under positive bias stress is investigated. The degradation is mainly originated from the electron trapping in bulk SiO_2 or Graphene/SiO_2 interface, and trap generation in bulk SiO_2.

For this study, Graphene were synthesized using CVD process and transferred onto a heavily doped silicon substrate with thermally 300-nm grown SiO_2, which serves as a back-gate dielectric. The number of graphene layers (i.e., single-, double-, and multilayer graphene: SLG, DLG, MLG) were identified by optical microscope and further confirmed by Raman spectroscopy. The photo-resist patterned Cr (20 nm)/Au 70 nm) electrodes were deposited on graphene by electron beam at room temperature, followed by a lift-off process. Graphene channel length (L) and width (W) are ~200 µm and ~1800 µm, respectively. For electrical characterization, both Agilent B2902 and Keithley 2612A source measuring units (SMU) were used. While Bias stressing were performed using a probe station.

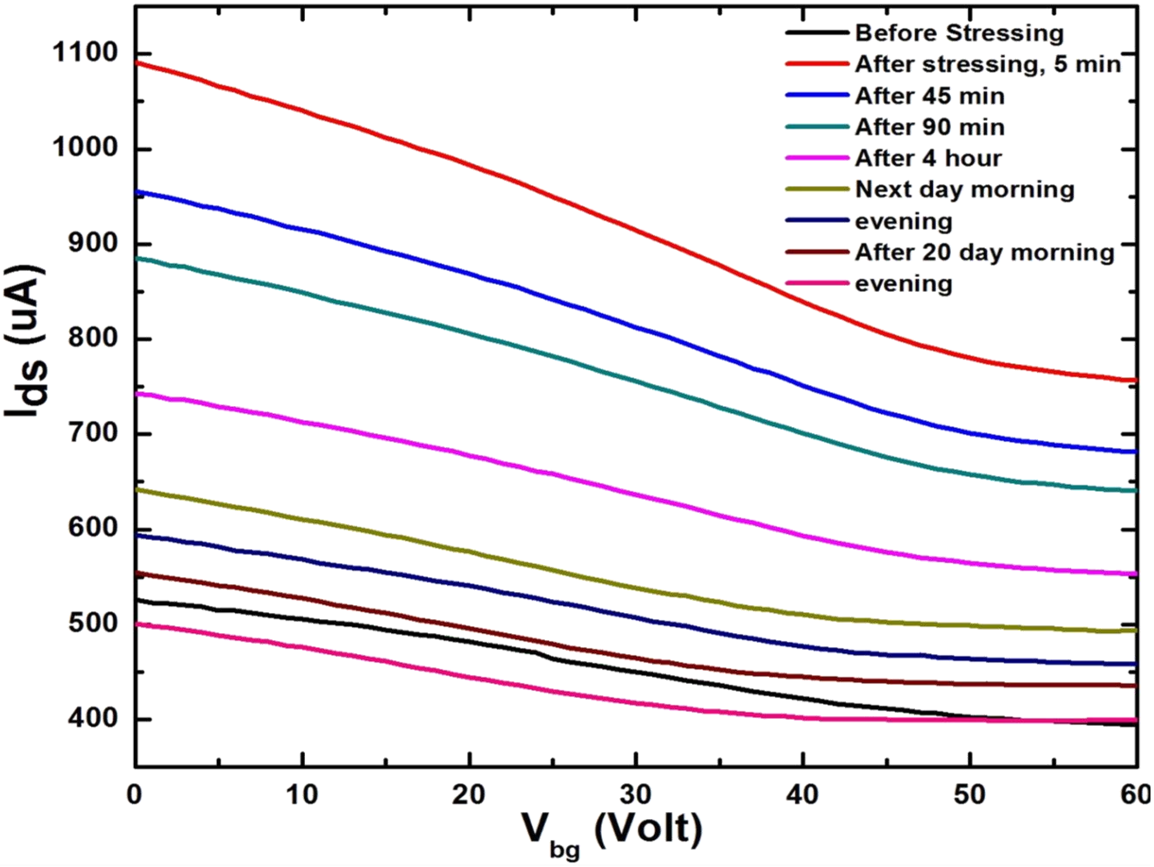

Figure 3.10 The schematics of Vth shift of GFETs under positive bias stressing. ΔVth is defined back-gate voltage V_{bg} shift at constant Ids [67].

Positive bias-induced Vth instability in single- and multilayer graphene field effect transistors (GFETs) with back-gate SiO_2 dielectric. The ΔVth of GFETs increases as stressing time and voltage increases, and tends to saturate after long stressing time. **Figure 3.10** demonstrates the Vth shift of GFETs under the positive bias of 11 Volt between drain and source at room temperature for 1 minute while gate was at 0 volt.

ΔVth is defined as the back-gate voltage Vbg shift at a constant drain current I_{ds} [67], The I_{ds}–V_{bg} curve is observed to shift toward positive voltage with stressing time tstress. Note that there is no degradation caused by measurement itself, as evidenced by the repeatable I_{ds}–V_{bg} sweep has been observed. The positive electric stressing induces the right shift of Vth as shown in figure, while the negative stressing voltage causes Vth left shift has been reported. It is believed that the change of subthreshold slope is an indication of interfacial trap creation [68]. However, from **Figure 3.10**, it can be seen no apparent change in subthreshold slope, and the mobility degradation may be negligible. It is necessary to point out that the ON/OFF ratio of GFETs is small owing to the energy gapless in graphene film. The Vth shift is believed to originate from electron trapping in the bulk SiO_2 or SiO_2/graphene interface and trap generation in bulk SiO_2 under positive bias stressing, since the possible Si-H bonds in bulk oxide may be the source of trap generation centers. The ΔVth of GFETs exhibits the saturation behavior after long stressing time, indicating as well that the trap generation is possibly limited by the number of Si-H bonds.

In summary, positive bias-induced Vth instability in single and multilayer GFETs with back-gate SiO_2 dielectric is investigated. It is observed that the ΔVth increases with power law dependence in the early stage of stressing and gets saturated for long stress time.

3.6 Temperature effect on Graphene devices

In this section, the temperature dependency of diract point ΔVth studied. For fabricating devices same process flow has been used as described in Bias stressing effect. Temperature effect on GFETs was performed on Al wire-bonded devices on hot plate.

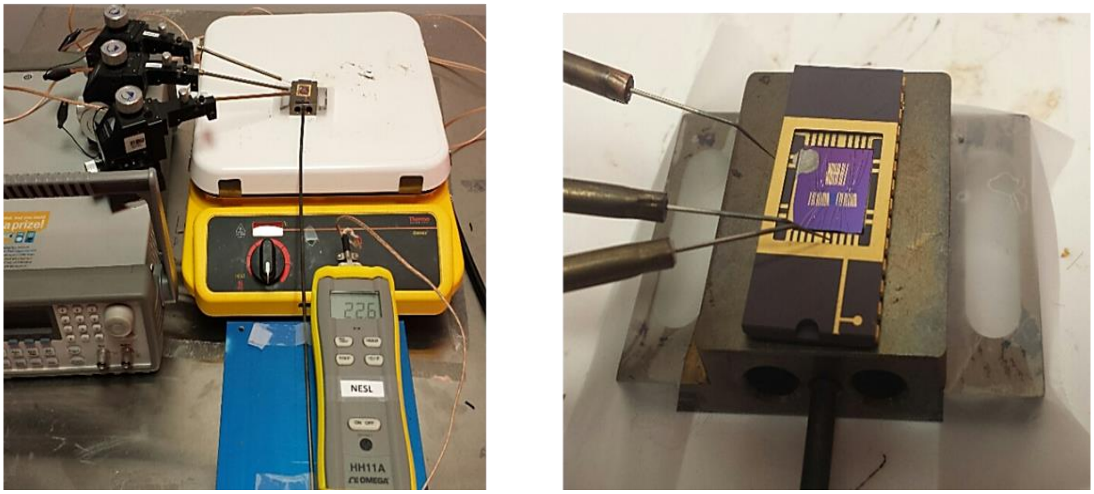

Figure 3.11 GFET device mounted on Hot Plate for Ids-Vbg for temperature study and real time measurement

HH11A omega thermocouple used to measure real time temperature. For electrical characterization, both Agilent B2902 and Keithley 2612A source measuring units (SMU) were used to measure current between drain and source for different Temperature range,

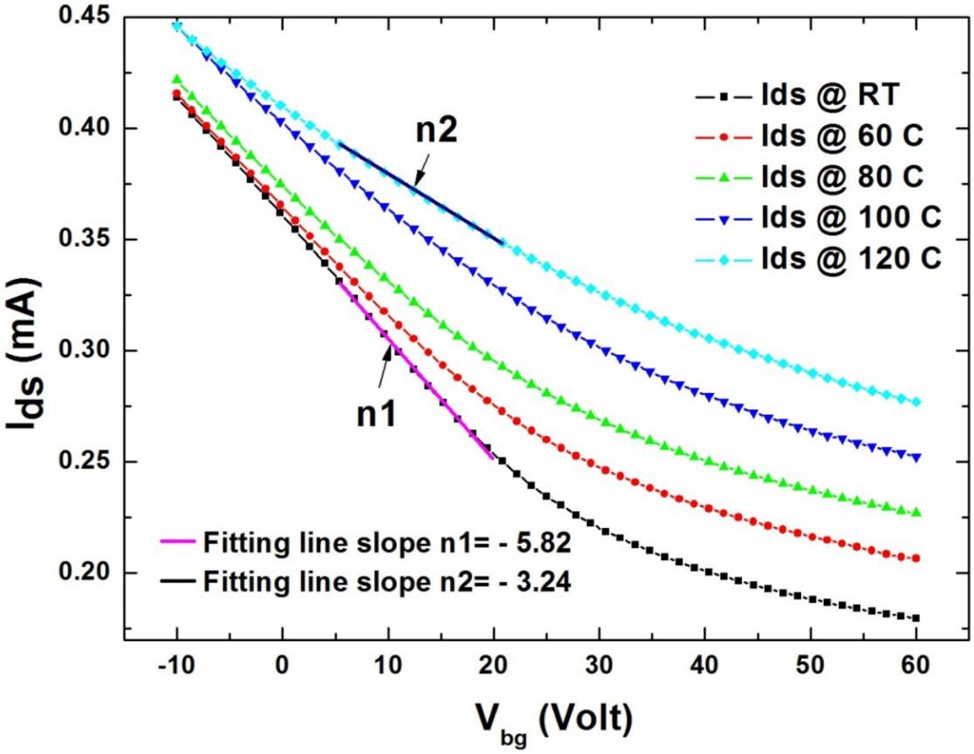

Figure 3.12 Ids–Vbg measurement of GFET from Room temperature to 120 ◦C without stress. As temperature increases to 120 °C, the air ambient (O_2, H_2O, etc.) [70] will cause graphene hole doping effect, which can be seen that the Dirac point shifts to right.

RT to ~120 °C. The image of experiment setup has shown in **Figure 3.11**.The devices were wire bounded and kept on hot plate for temperature experiment while thermocouple used to measure real time temperature for device. The Ids–Vbg measurements of graphene field effect transistor from Room temperature to 120 ◦C without stress shown in **Figure 3.12**. It is observed not only hole doping (Dirac point right shift) occurs but also the mobility degrades when temperature increases. The hole doping at high temperature may enhance the thermal activation for Positive Bias Temperature Instability. The mobility can be extracted by $\mu = |dI_{ds}/dV_{bg}| \times [L/(W\ CgVds)]$. The channel length (L) and width (W) are ∼200 μm and ∼1800 μm, respectively. Applied voltage between darin and source is 0.1 Volt. The temperature study, GFETs device mobility was calculated around ~ 550 $Cm^{-2}V^{-1}S^{-1}$. The carrier mobility (Vth extraction region) is seen to be approximate

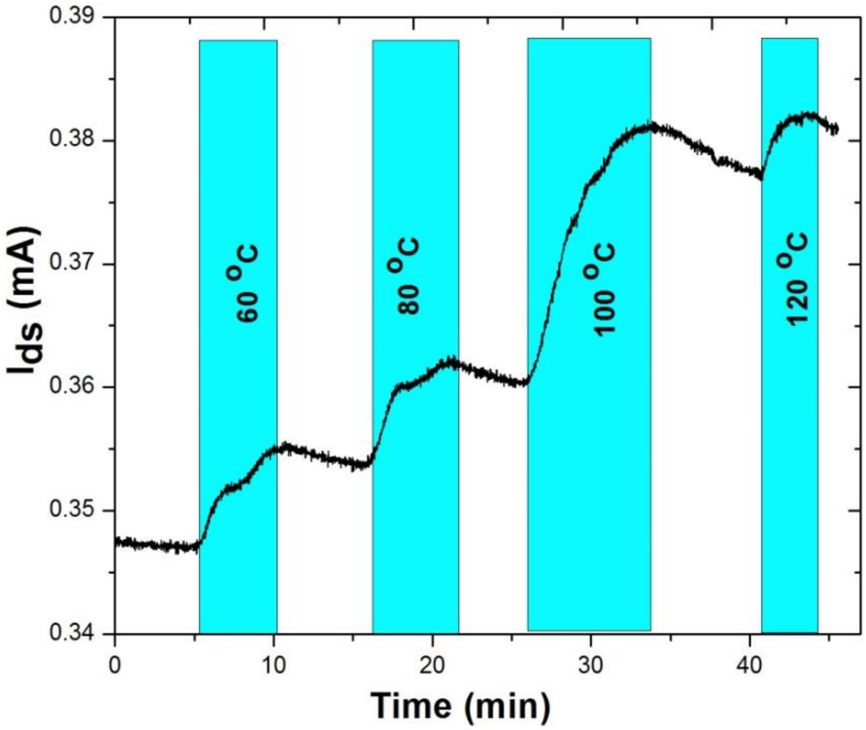

Figure 3.13 (a) Current between drain and source (Ids) Vs time profile with temperature increase for 1st Sample. (b) Current between drain and source (Ids) Vs time profile with temperature increase for 2nd Sample.

n1/n2 (~1.8) times reduction when the temperature is elevated from RT to 120 °C. The mobility reduction at high temperature may be attributed to the thermal driven scattering on intraripple flexural phonons [69].

In summary, Mobility is seen to degrade with temperature increasing. Note that there is no degradation caused by measurement itself, as evidenced by the repeatable Ids–Vbg for for different temperature has been studied and shown in **Figure 3.14**. The degradation is believed to be caused by the trapped electrons in bulk SiO_2 or SiO_2/graphene interface and trap generation in bulk SiO_2. As temperature increases, the carrier mobility decreases, and the ambient doping also results in hole doping in GFETs.

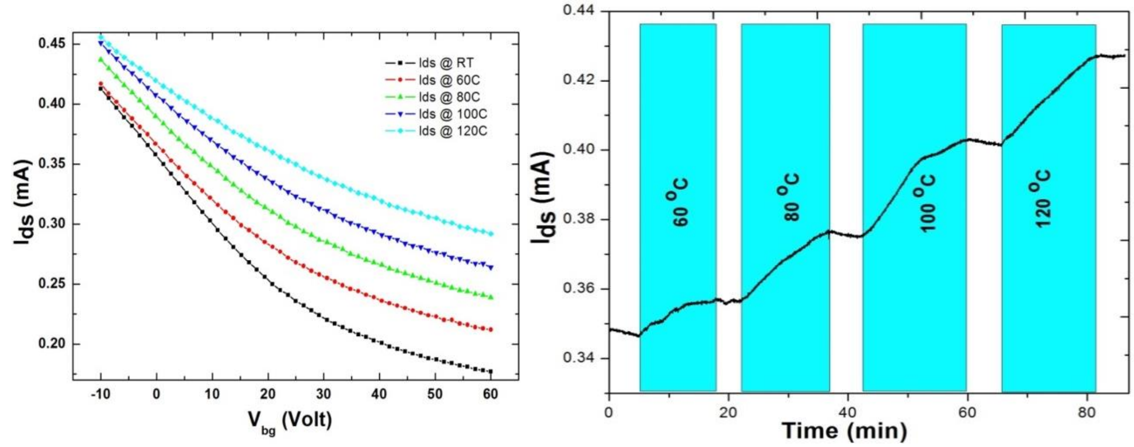

Figure 3.14 GFET device mounted on Hot plate for I-V and real time measurement

CHAPTER 4

DESIGN, FABRICATION AND CHARACTERIZATION OF GRAPHENE BASED ION-SENSITIVE FIELD EFFECT TRANSISTOR (ISFET)

4.1 Introduction

Cell membrane shown in **Figure 4.1**, there are kinds of special proteins that can act as channels responsible for the electrical ion conveyance. These channels are associated in a wide range of extreme conditions such as epilepsy, diabetes, visual impairment, chronic pain, migraines, and Alzheimer's diseases. Thus they have become highly captivating salutary targets for drug revelation in pharmaceutical industry.

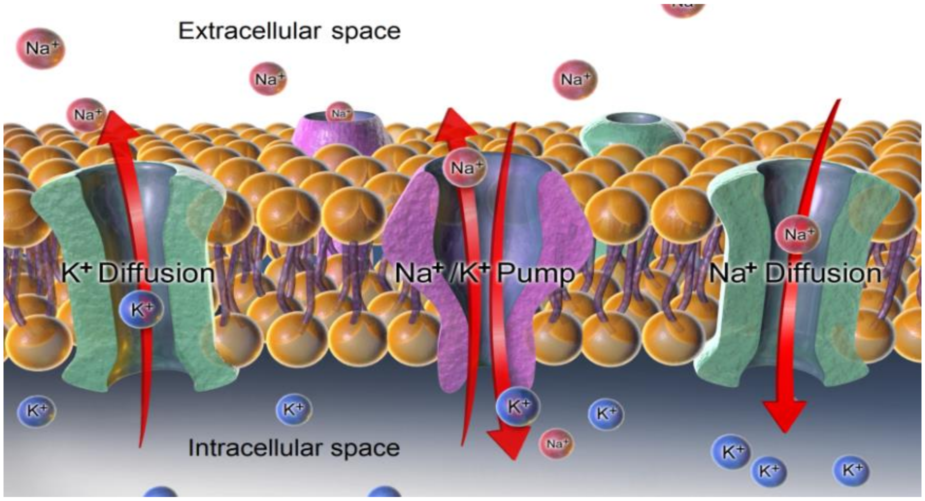

Figure 4.1 Illustration of ion channels in a cell membrane for Na+/K+ adopted from Wikipedia

Over the course of the years, different ion channel screening assays test have been developed including fluorescence, automated patch clamp system, and atomic absorption spectrometry. In any case, instrumentation for the robotized examination of ion channels in essential cells and stem cells is yet inadequate.

Ion sensitive field effect transistor (ISFET) [71] has various qualities making it suitable for building up a novel ion channel screening test. Dissimilar to fluorescent indicators, ISFETs provide a label free direct estimation of ion efflux and are not subject to imaging antiquities. Since the identification can be performed without devouring additional reagent for labeling, it likewise generally increases system's durability. As opposed to atomic absorption spectrometry (AAS), ISFETs can be fabricated for studying a large variety of ion channels and provide real-time acquisition and analysis capability. Its smaller than usual size and large scale integrative capacity also enable us to integrate an array of ISFET sensors on a single chip for simultaneous ion efflux measurement from different cell ion channels. Besides, ISFET based instruments could be utilized for screening primary and stem cells which are not compatible with fluorescence and automated patch clamp systems. In this chapter, we presented the design, fabrication and characterization of a novel graphene based ion sensitive field effect transistor for real-time measuring K+ growth of living cells on graphene to prove biocompatibility of grapahene, epoxy effect of doping on graphene while packaging ISFET device.

4.2 Si based ISFET and its limitation

ISFET, ion sensitive field effect transistor, was first announced in 1970 by Dr. P. Bergveld from Spain [72]. It was initially developed and demonstrated for the measurement of ionic fluxes around a nerve [73] and later evolved into various related devices for other biological sensing applications[74]-[78]. **Figure 4.2**(a) schematically illustrates the simplified device structure of a Silicon based ISFET. Similar to conventional field effect transistors (FETs) [79]-[80], ISFET comprise of three terminals called source, drain and gate. By adjusting the gate voltage (electric field) via a reference electrode, we are able to control the channel conductance that is the current flow from drain to source electrode. For ion detection, the device is normally operated under a fixed electrical bias configuration as shown in **Figure 4.2**(b). A target ion concentration change in electrolyte immediately incites a surface

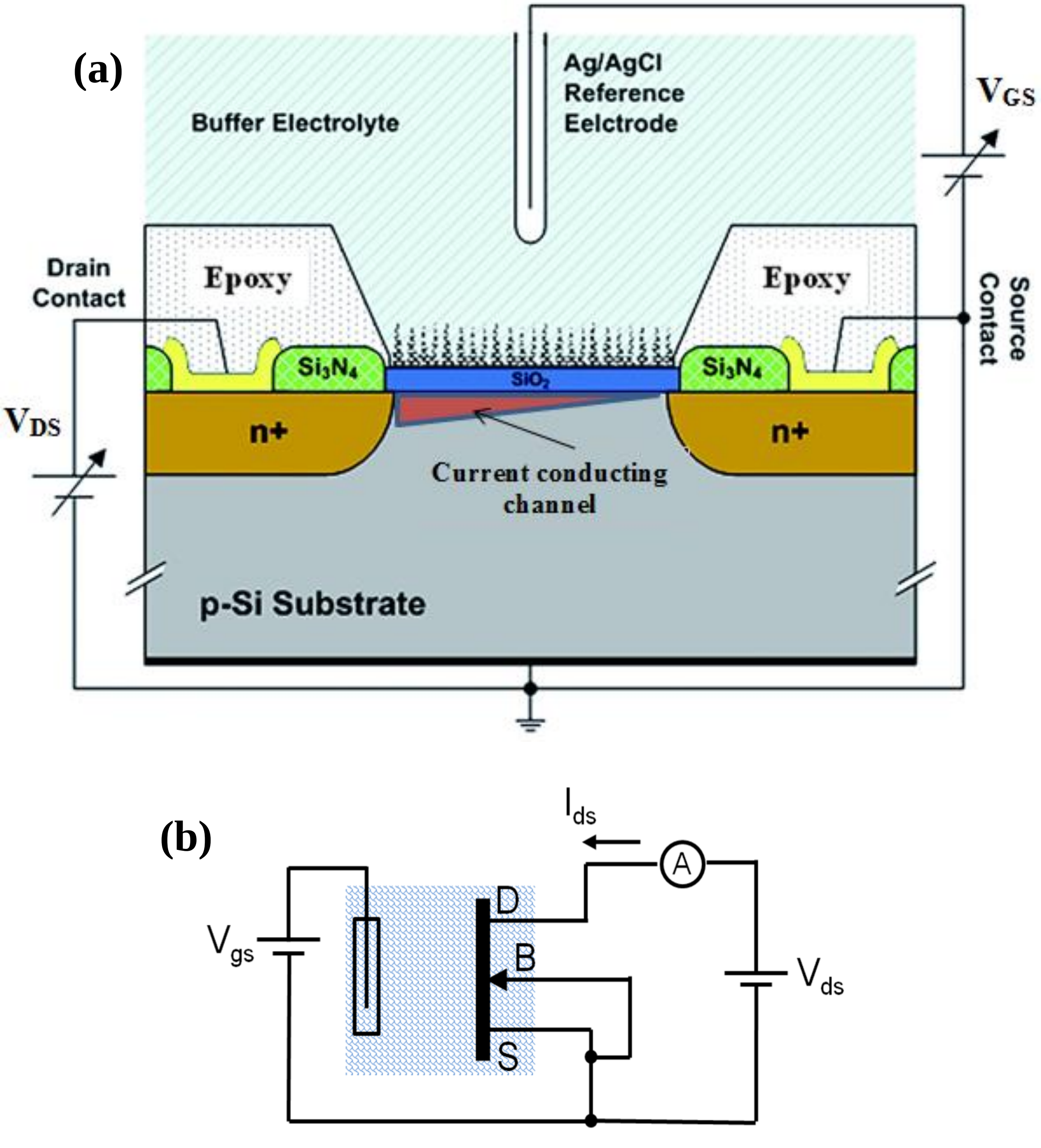

Figure 4.2 (a) General device structure of an n-channel Si based ISFET sensor. (b) Electrical biasing scheme for the sensor operation

potential change at solution/oxide interface, which is further converted and amplified to an output current signal change, in this way accomplishing the ion detection. The ion selectivity of the sensor device is accomplished by incorporating an ion selective membrane (ISM), with either inorganic [81]-[82] or organic nature [83]-[84], into the gate of the FET. The membrane can be either an additional oxide layer deposited on top of the gate dielectric or a polymer membrane drop casted/spin coated using spin coating.

Despite the fact that Si based ISFETs have been well developed and tested, it has its own performance limitations including the relatively low mobility value of Si (~450 cm2/Vs) embraced in the cutting edge ISFET advancement constrains its affectability to ion concentration change and As a result of the poor stability of Si in aqueous solution, ISFET device normally require an extra oxide layer coated on top of the Si. This oxide layer boosts the stability of the device. However, over the time this layer will trap ions in electrolyte that create boisterous interface accordingly debase the sensing signal quality. To beat these impediments, we considered choosing graphene as an alternative material to develop a novel ISFET sensor with better sensor performance explained in detail in section 4.3.

4.3 Graphene as an alternative for ISFET

Graphene has exceptional material properties [86] which are much superior compared to Si with respect to developing sensors for bio-detection applications. The ultrahigh carrier mobility over 10^5 cm^2/ V·s demonstrated for graphene at room temperature [87], is orders of magnitude better than Si (~450 cm^2/ V·s), which is commonly used for bio-electronic applications at present [88]. Higher carrier mobility of an ISFET directly translates to higher sensitivity for ionic detection. In addition, the excellent chemical stability of graphene [89] enables us to use it as a sensing material in direct contact with surrounding harsh biological environment without additional oxide layer like in Si case. A much lower sensing degradation from graphene based ISFET can be expected. Moreover, graphene also exhibit very low thermal and 1/f noise, which indicate better sensing resolution [90]. In terms of biocompatibility, we have confirmed direct cell growth on Graphene synthesized by CVD process in our lab. As showed in the florescent image of **Figure 4.3**, H9C1 cardiac muscle cells were plated and growing well on the thin film of Graphene, indicating very good biocompatibility of graphene. Finally, large scale graphene synthesis can be done inexpensively through chemical vapor deposition using a basic quartz tube furnace, as discussed in section 2.4.1. All these properties are conducive for developing robust, low cost, and highly sensitive biosensors.

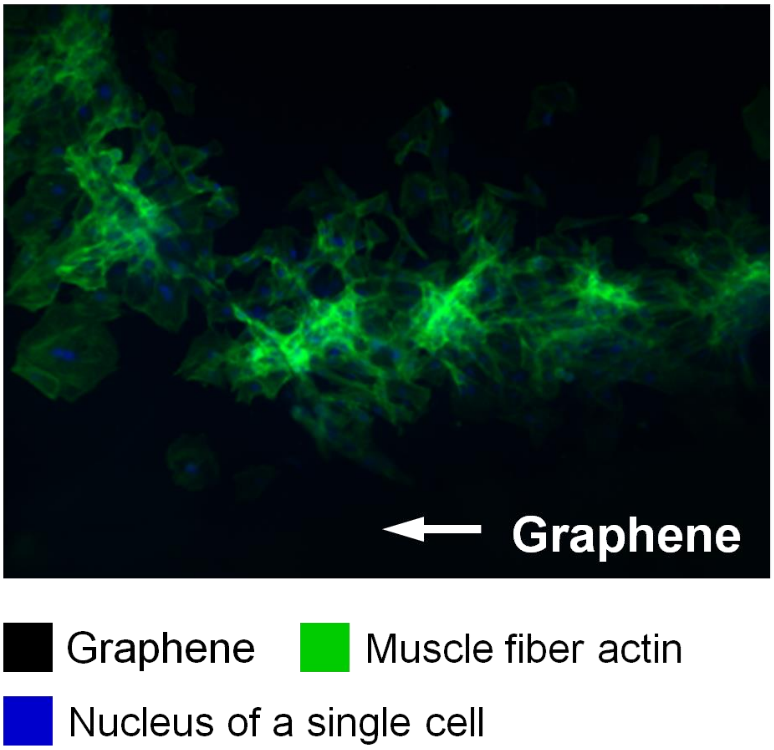

Figure 4.3 Florescent image of H9C1 cardiac muscle cells growing on graphene thin film CVD synthesized in our lab.

4.4 Graphene Based ISFET Sensing mechanism

Similar to conventional silicon based ISFET, our graphene based ion sensor operates based on the change in electrical conductance of graphene thin film with the

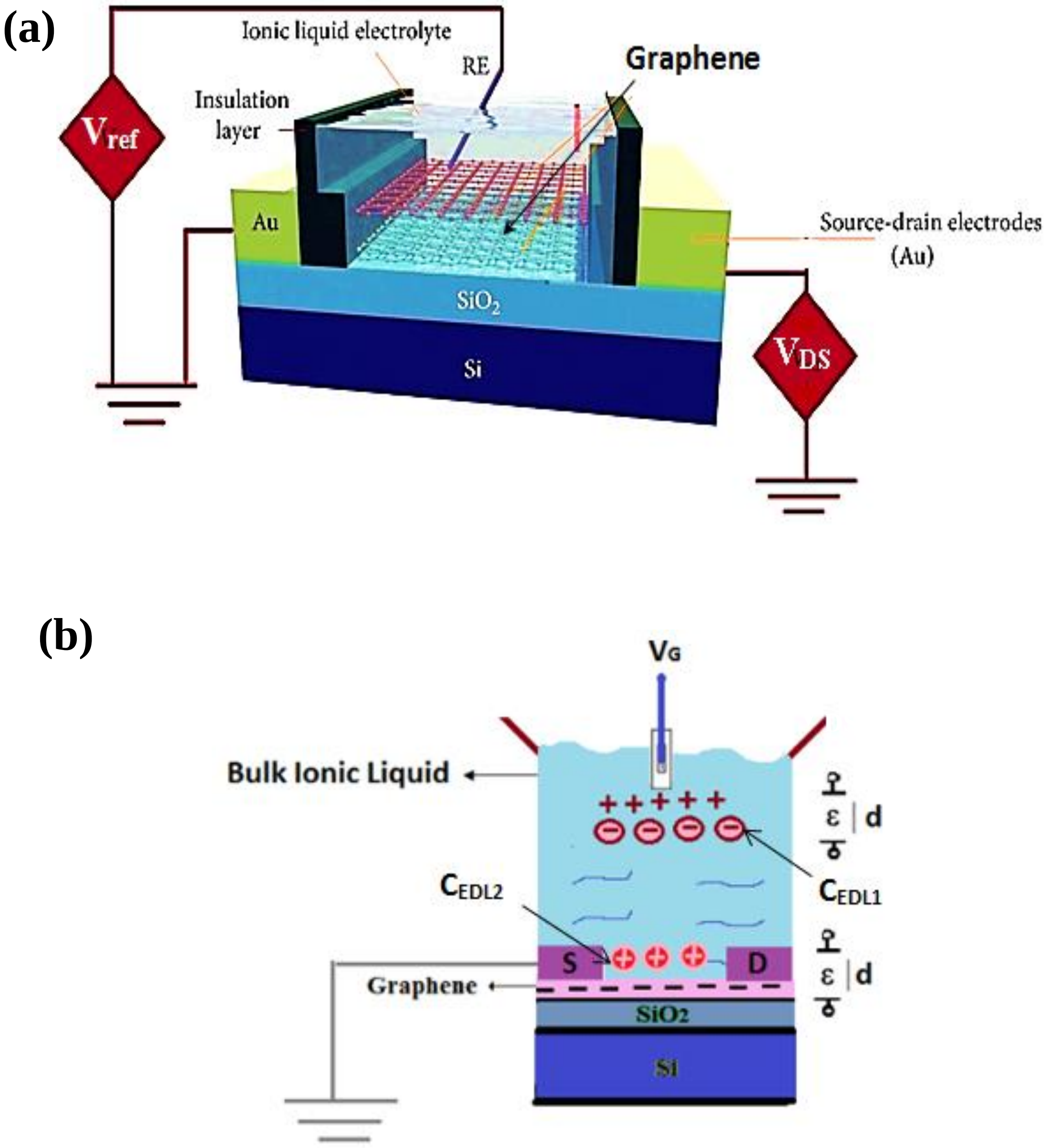

Figure 4.4 (a) Schematics of the proposed structure of the graphene based (ISFET) including its bias configuration used in the electrical measurements. The ion sensor is inserted in an electrolyte solution insulated by Epoxy in operating condition. (b) Cross section of graphene based ISFET showing an electrical double layer forming at the graphene/solution interface.[91]

change in surrounding ion concentration. Figure 4.4 schematically illustrates the three dimensional sensor structure and its operation principle. When graphene interacts with electrolyte solution, [92]-[93] an electrical double layer will be formed at the graphene/solution interface **Figure 4.4**(b), which generates a potential drop between graphene and bulk solution. A change in surrounding ion concentration results in a change in the capacitance of the electrical double layer (C_{EDL}). Under a fixed bias configuration as shown in **Figure 4.4**(a), the capacitance change causes a subsequent change in the surface potential of graphene thin film, which induces a detectable current change in the conducting channel between drain and source electrodes .Thus the transduction from an analog signal as a ion concentration change to an electrical signal as current change is achieved.

4.5 Device fabrication and Encapsulation using Epoxy

In our sensor development, chemical vapor deposition (CVD) synthesized graphene on copper foil samples [94] were used to fabricate the graphene based ISFETs. The fabrication procedure is schematically illustrated in the flow chart of Figure 4.5, which involves three major steps: a) CVD synthesis of graphene; (b) graphene transfer; (c) Metal deposition and (d) Encapsulation of electrode using epoxy. CVD synthesis of graphene, graphene transfer and metal deposition performed using same procedure as described in section 0 and 3.2 using **Figure 3.1** and **Figure 3.2** respectively. ISFET encapsulation using epoxy process detail discussed below using **Figure 4.5**.

To fabricate ISFET, Cr (`~20/~50 nm) and Au (70 nm) metal was patterned on the graphene transferred on 300 nm SiO_2/Si substrate via either shadow mask or standard photolithography technique, defining the drain and source contact electrodes. For the

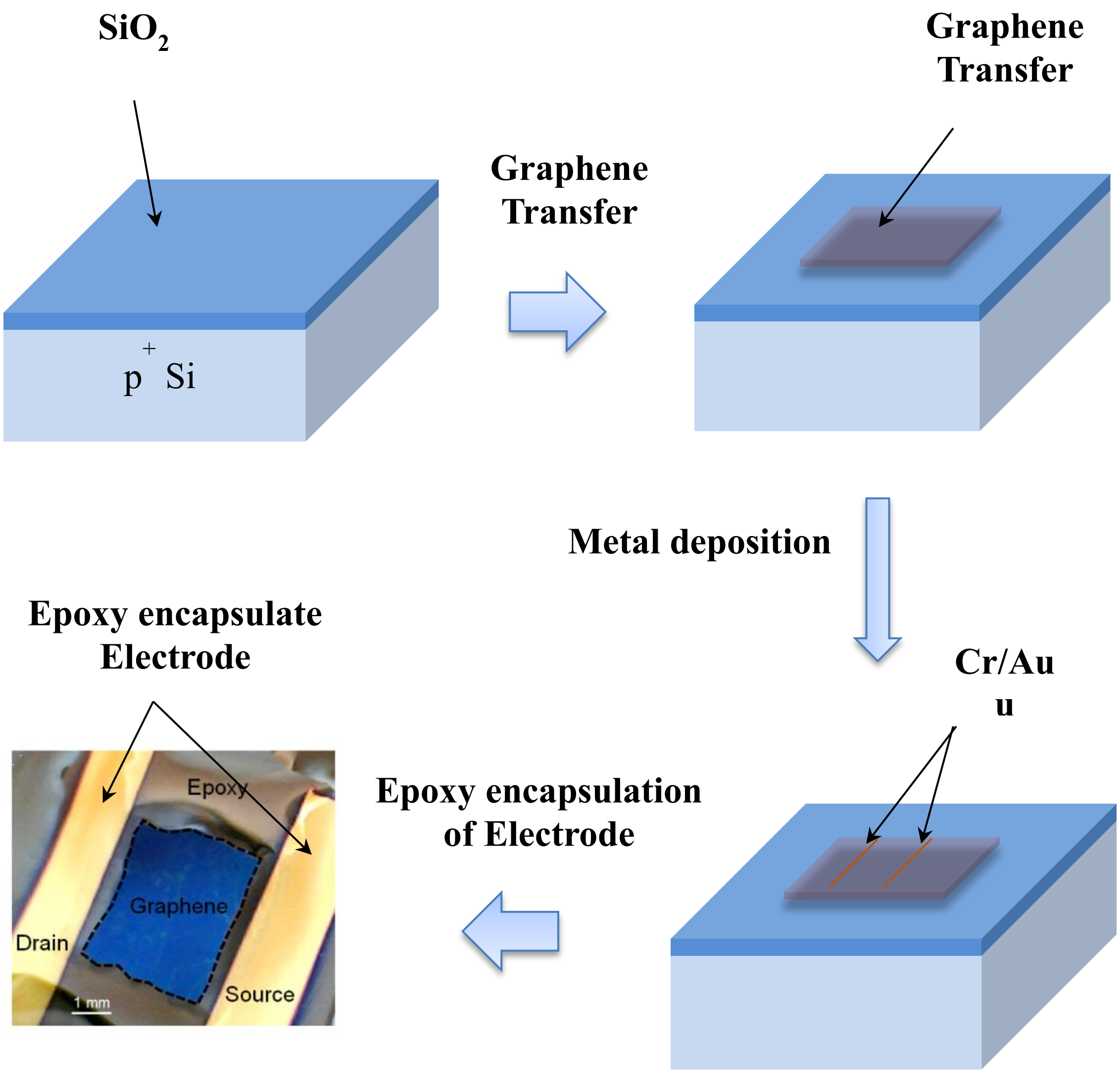

Figure 4.5 Fabrication process flow of the graphene based ISFET, which consist of Graphene transfer, shadow mask/photolithography followed by metal deposition using DC sputtering/E-beam evaporation. Final optical image of graphene based ion sensor electrodes encapsulated using biocompatible epoxy.

operation in an electrolyte environment, the wafer chip was mounted on a PCB board and wire bonded to ease measurement, biocompatible epoxy glue was deposited over the metal contact, SiO_2/Si chip and bonding wires, leaving an opening window on the graphene as the active sensing area to be in contact with electrolyte solution. The inset of **Figure 4.5** shows the optical image of a fabricated graphene based ISFET which encapsulated by epoxy while leaving active graphene region open for current channel.

4.6 I-V characteristics of graphene ISFET

With the fabricated prototype devices, we systematically studied their I-V and C-V characteristics respectively in electrolyte solution. The experimental setup is schematically illustrated in **Figure 4.6**. In I-V measurement, DC bias of V_{ds} and V_{gs} were supplied by a precision source measurement unit of Agilent B2900A,while. Current flowing from source to drain I_{ds} and from gate to source I_{gs} were simultaneously measured. By varying the K^+ ion concentration from 0 μM to 1 mM in deionized water (DI), we obtained a series of left-shifted I-V curves from a representative epoxy coated graphene ISFET, as plotted in **Figure 4.7**(a). The I_{ds}-V_{tg} curves measured all show a “V” shaped p- to n-type transition and the dip in the “V” corresponds to a minimum conductivity of ~$4e^2/h$ at the Dirac point (ED).[106]. By comparing the slope of the transfer characteristics of the ISFET measured in air and electrolyte solution, we found the transconductance of the solution-gated graphene FET (~ 33 μS) is over 100-fold larger than that in air (~0.3 μS). The transconductance enhancement can be mainly

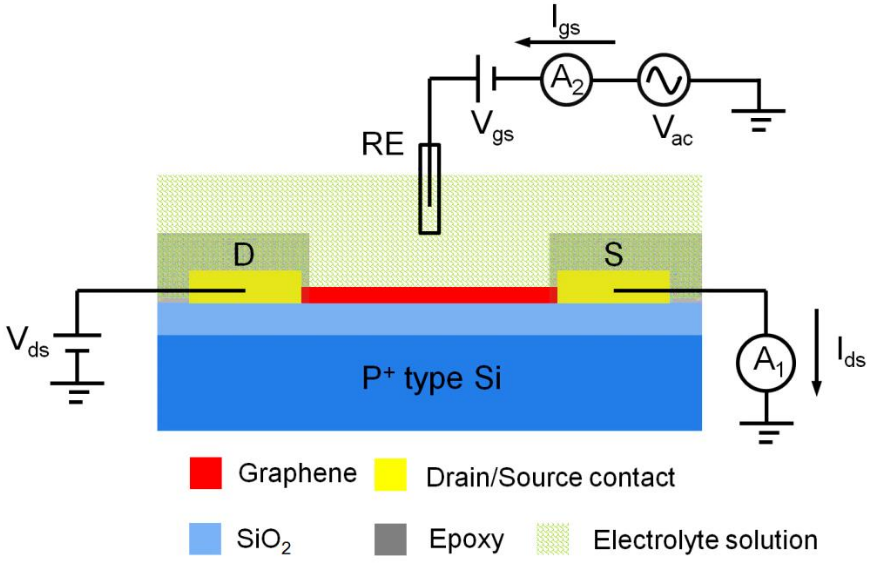

Figure 4.6 Schematic diagram of the experimental setup for sensor electrical (I-V and C-V) characterization

attributed to the high mobility of charge carriers in graphene and the large interfacial capacitance at the graphene/solution interface [107], which will be discussed later in the section.

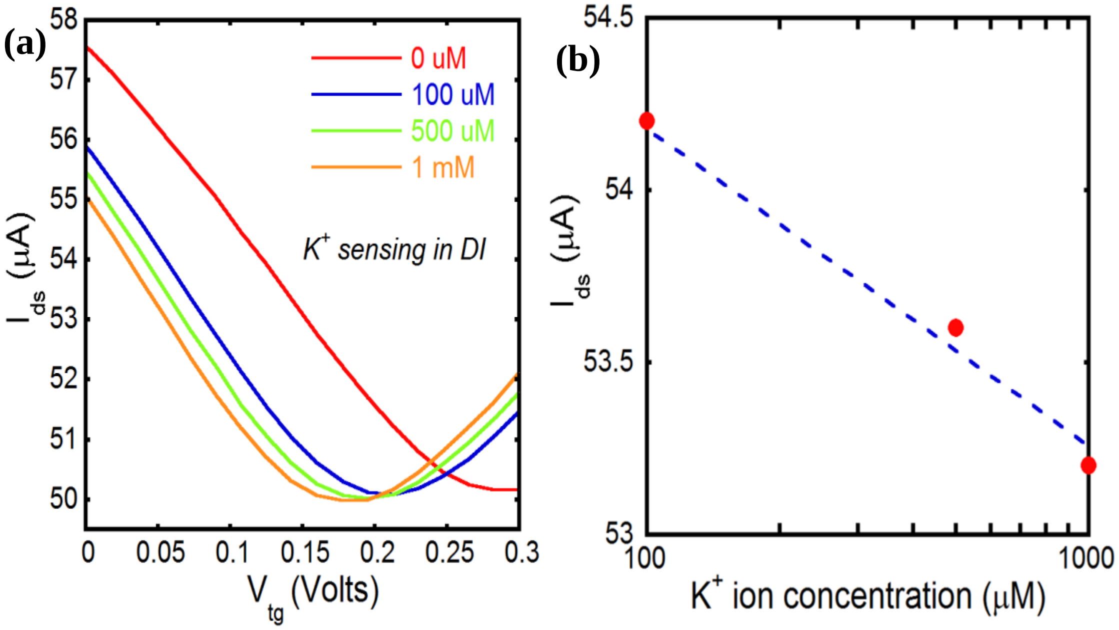

Figure 4.7 (a) I-V characteristics of an epoxy coated graphene ISFET in DI water with different K^+ ion concentration. In the measurement, V_{ds} was set to be constant 0.5 V and V_{tg} (solution-gated voltage) was swept from 0 to 0.3 V via a Ag/AgCl reference electrode (Bioanalytical System, Inc.) immersed in the solution. (b) Drain-source current I_{ds} as a function of K^+ ion concentration, at V_{tg} = 0.05 V.

In addition, **Figure 4.7** (a) shows a clear K ion concentration dependence of the ISFET transfer characteristics. The transfer curves shifted toward the negative direction of the electrolyte-gate voltage (V_{tg}) with increasing K^+ ion concentration, indicating that the prototype graphene ISFET detected K^+ ion in DI water. By biasing the device at a fixed V_{tg}, we extracted the corresponding I_{ds} with different K^+ ion concentration and plotted in **Figure 4.7** (b). As expected, the drain-source current I_{ds} has a linear relationship with the K^+ ion concentration on a semi logarithmic scale. The sensitivity of the sensor was estimated to be 1 μA/decade from the slope of the linear fit.

4.7 C-V characteristics of graphene ISFET

In addition to I-V characterization, we also performed device C-V characterization in electrolyte solution. In C-V measurement, an ac signal with excitation amplitude of 50 mV at a frequency of 500 Hz was superimposed to the DC bias V_{tg}. The drain and source electrodes was shorted to ground. The capacitance was measured by the out-of-phase components of detected current. By sweeping V_{tg} from -0.8 to +0.8 V, we obtained a series of up shifted C-V curves with different K^+ ion concentration as showed in **Figure 4.8** (a). Similar to the I-V measurement, by biasing the device at a fixed V_{tg} at 0.6 V, we obtained the measured capacitance values with different K^+ ion concentration and plotted in **Figure 4.8**(b). Interestingly, the measured capacitance of the ISFET shows a linear dependence on K^+ ion concentration like what was observed for the measured current, I_{ds}.

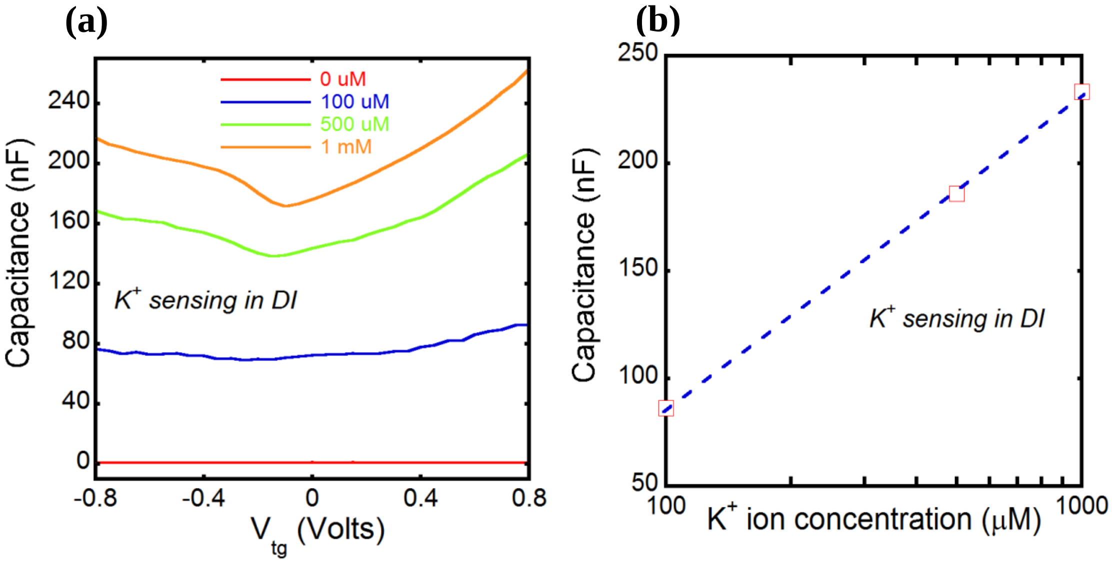

Figure 4.8 (a) Device C-V characteristics in DI water with different KCl concentration. (b) Measured capacitance as a function of K^+ ion concentration, at V_{tg} = 0.6 Volts.

To demonstrate our graphene based ISFET has the capability of real-time detecting K+ concentration change in electrolyte solution, we operated the ISFET in its capacitive-mode at a fixed DC operating point, i.e. V_{ds} = 0.5 V and V_{tg} = 0.6 V. By sequentially introducing different volume of concentrated KCl solution into DI water, we were able to alter the K^+ ion concentration in the testing solution. **Figure 4.9**(a) shows the time dependent sensor response to K^+ ion concentration change from 0 µM to 1 mM. As expected, the measured capacitance increased with higher K^+ concentration. Moreover, the ISFET sensor also shows very good sensing repeatability in multiple measurement cycles with different steps in K^+ concentration change. To determine the sensor resolution, we also did a control test by introducing K^+ free control solvent as a DI water into the testing solution. The results plotted in **Figure 4.9**(b)) clearly indicate our ISFET sensor is able to detect K^+ ion concentration change down to 5 µM in DI water.

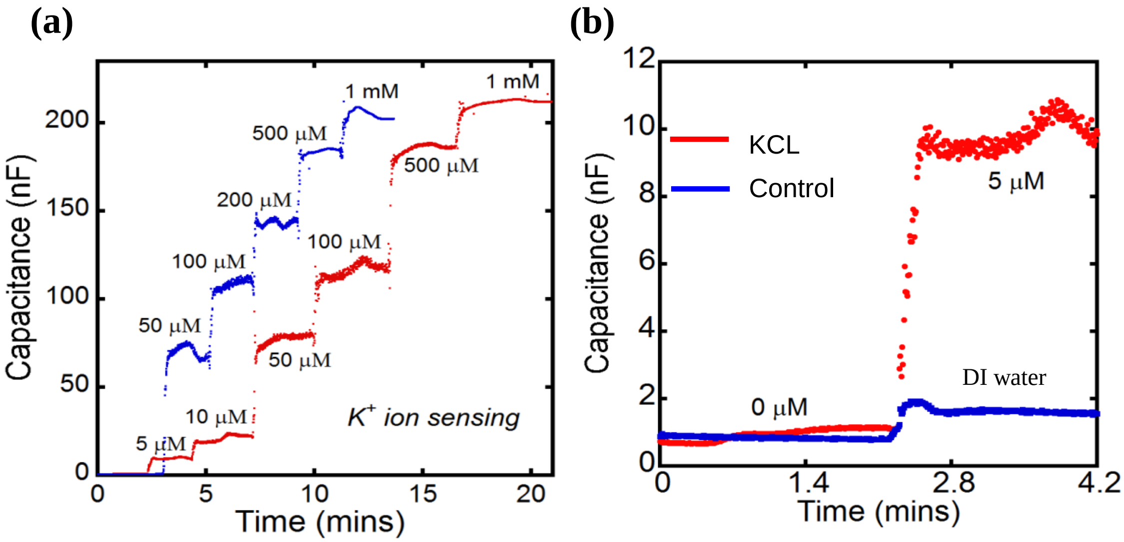

Figure 4.9 (a) Time dependent capacitance measurements with varying K+ concentration from 0 µM to 1 mM in DI water. Two measurement cycles were performed with different steps in K+ concentration change. (b): Sensor response to 5 uM KCl (red curve) along with a control test without KCl (blue curve).

To further identify the measured capacitive components in the device C-V characterization discussed above, we analyzed the equivalent electrical circuit involved in the measurement. As illustrated in **Figure 4.10**, at a fixed electrolyte solution-gate voltage V_{tg}, two electrical double layers are formed at the interface between reference electrode/solution and graphene/solution, respectively.[92]-[93]. In addition to these two capacitive components, the quantum capacitance of graphene also exists in the circuit and is in series connection with the two double layer capacitances. Along with the capacitive components, there are also resistive components contributed by the bulk solution and graphene. Since LCR meter measures the out of phase components of detected current, the measured impedance only consists of the capacitive components of C_{EDL1}, C_{EDL2} and C_Q, respectively. The two series connected capacitance C_{EDL2} and C_Q

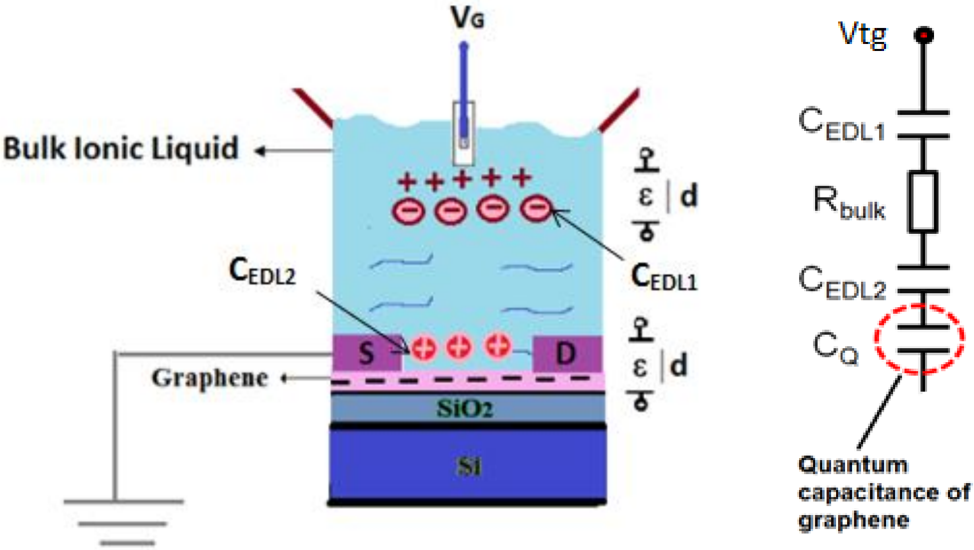

Figure 4.10 Schematic diagram of a graphene ISFET under C-V characterization in KCl electrolyte together with the equivalent electrical circuit describing its operation [92]-[93]· In the circuit, C_{EDL1} and C_{EDL2} represent electrical double layer capacitance formed at reference electrode (RE)/electrolyte and graphene/electrolyte interfaces, respectively. R_{BULK} and R_{gr} correspond to the electrical resistance of bulk salt solution and graphene thin film, respectively.

constitutes the so called solution/graphene interfacial capacitance ($C_{interfacial}$), which acts as the gate capacitance of the graphene ISFET.

4.8 Doping Effect of Epoxy on ISFET

The epoxy used to encapsulate ISFET was a biocompatible adhesive specially designed for medical electronics including USP Class VI and/or ISO-10993 compliance [95]. For biological sensing application, we assessed the epoxy encapsulated ISFET sensors by electrical measurements and presented the results below

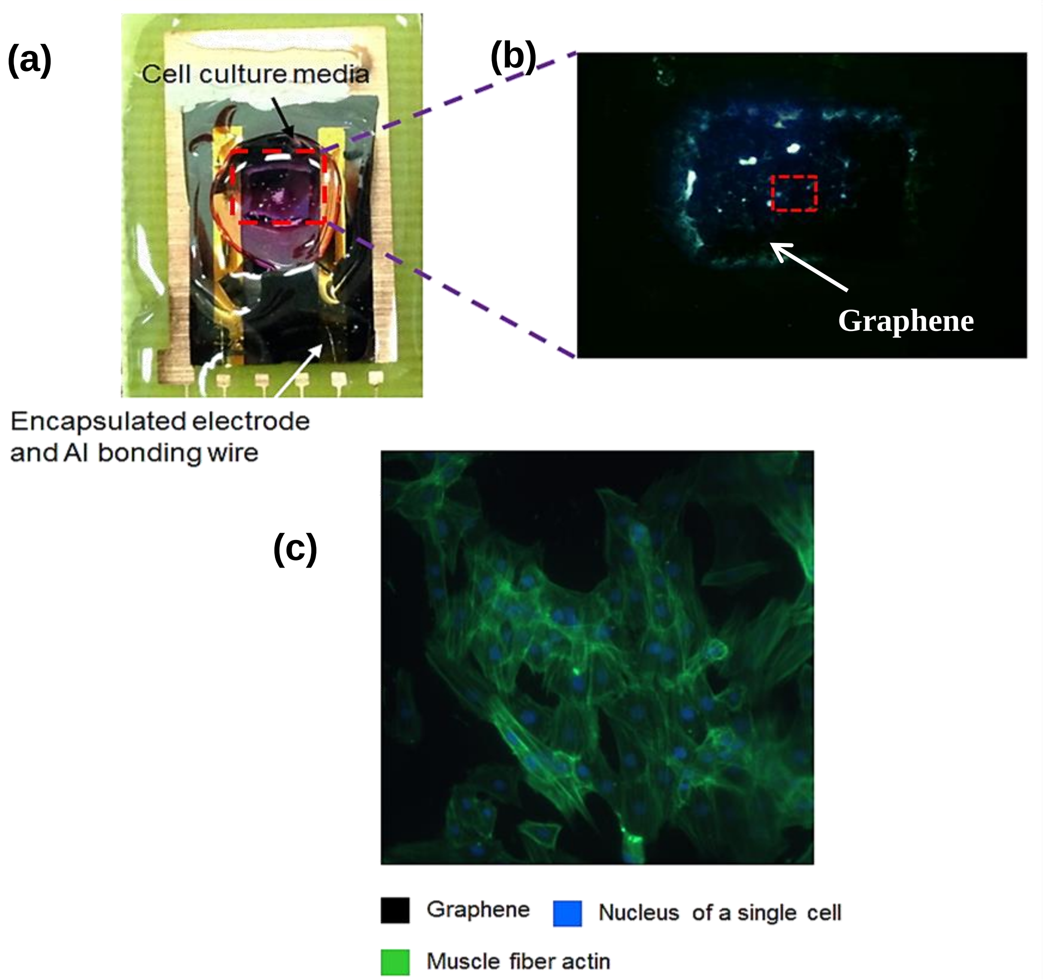

Figure 4.11 (a) Optical image of an epoxy coated graphene ISFET with H9C1 cardiac muscle cells directly plated and cultured on its active sensing area in red box. (b) Enlarge view of the active sensing area defined by the epoxy. (c) Florescent image of the H9C1 cells growing on the graphene thin film

We studied the biocompatible of the epoxy coated ISFET. By plating and culturing living cells (H9C1 cardiac muscle cells) directly on epoxy coated graphene epoxy. Florescent image of the H9C1 cells growing on the graphene film. as shown in Figure 4.11(c), we found cells are growing well not only on the graphene film **Figure 4.11**(b) but also at graphene and epoxy edges **Figure 4.11** (b), indicating excellent biocompatibility of both the CVD synthesized graphene and the epoxy.

4.8.1 Effect of epoxy on the electric transport properties of graphene

Apart from its good electrical insulation and excellent biocompatible, we noticed that the epoxy used for the ISFET sensor packaging seems to have a significant effect on the electrical properties of the sensing material, graphene. We conducted systematic investigation and reported our results below.

In the preliminary study, we examined the I-V characteristics of a back-gated graphene ISFET before and after epoxy encapsulation in air. **Figure 4.12**(a) illustrates the device structure with its DC biasing for electrical measurement. In contrast to top gate configuration discussed in Section 4.4, under back gate configuration [94], the channel conductance of graphene ISFET is modulated by the gate bias applied via a heavily doped Si substrate and SiO_2 layer serves as the gate dielectric layer in between graphene film and the substrate. The measured transfer characteristics are given in **Figure 4.12**(b). We observed Dirac point shift of over 20 Volts towards negative direction in I-V characteristics as shown in **Figure 4.12** (c).The shift in Dirac point indicates carrier concentration change in graphene film. Noticing the recent investigations reported on organic molecule doping of graphene [100]-[101], we inferred that the carrier concentration change in graphene could be raised from the chemical doping from epoxy vapor to graphene film during epoxy curing process. However, as shown in the inset of **Figure 4.12**, the interaction of epoxy with graphene not only occurs in ISFET conducting channel but might also at graphene/metal contact interfaces. To further investigate the effect of epoxy on the modulation of carrier concentration in graphene, we conducted separate experiments on epoxy free graphene FET devices as discussed below.

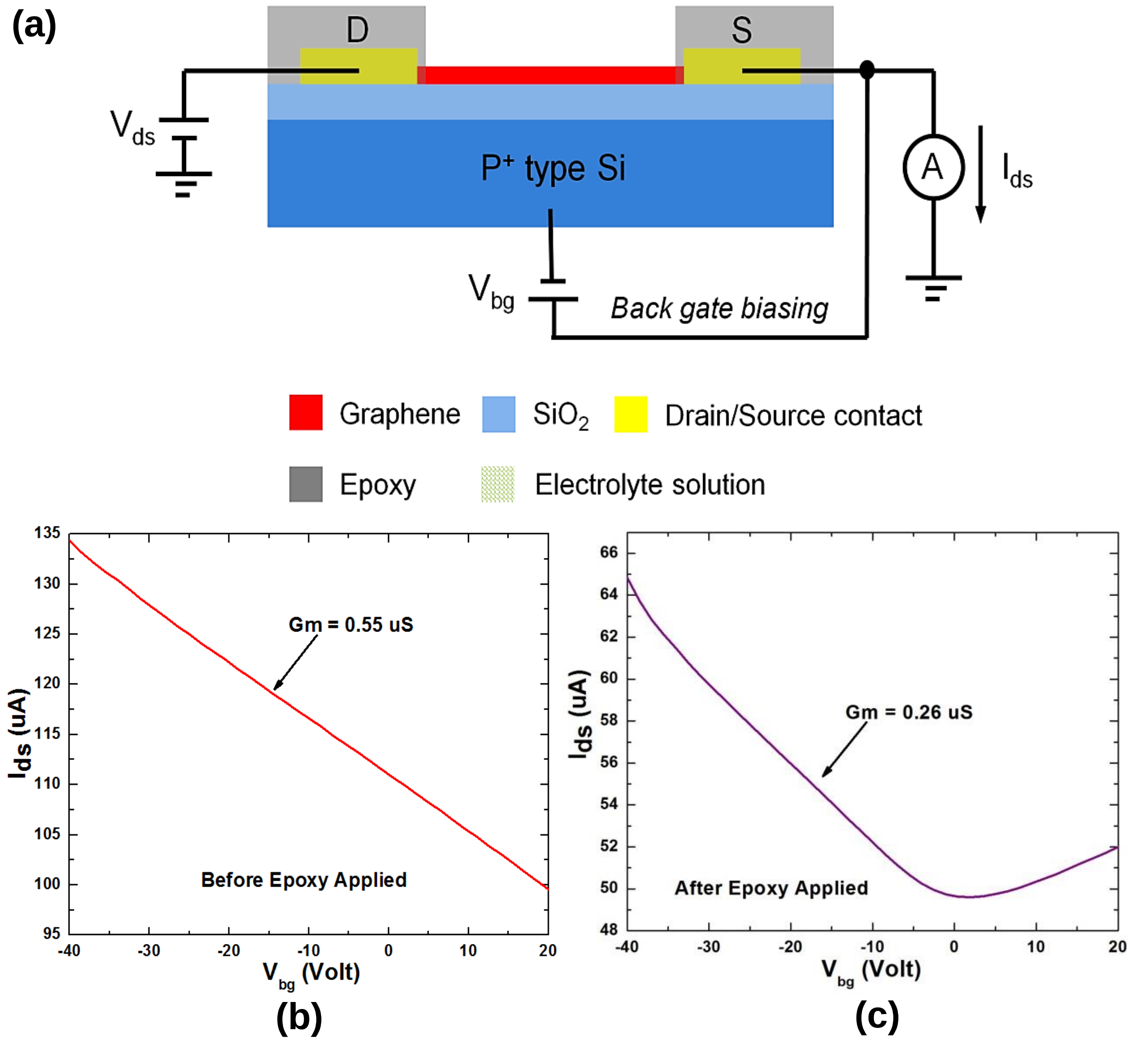

Figure 4.12 (a) Electrical biasing scheme of a back gate configured graphene ISFET. (b) Device transfer characteristics before epoxy applied (C) Device transfer characteristics after epoxy applied .

Figure 4.13(a) shows the experiment setup. CVD derived graphene on Cu sample was transferred to a SiO_2/Si wafer chip of 300 nm/ 500 µm by the wet-etching method as described in detail section 3.1. Standard photolithography method was used to define the drain and source electrodes of the graphene FET. The chip was later mounted on a home built PCB board and using Al wire it was wire bonded for electrical connection. Conductive silver paste from SPI Supplies, Inc. was used to make electrical connection

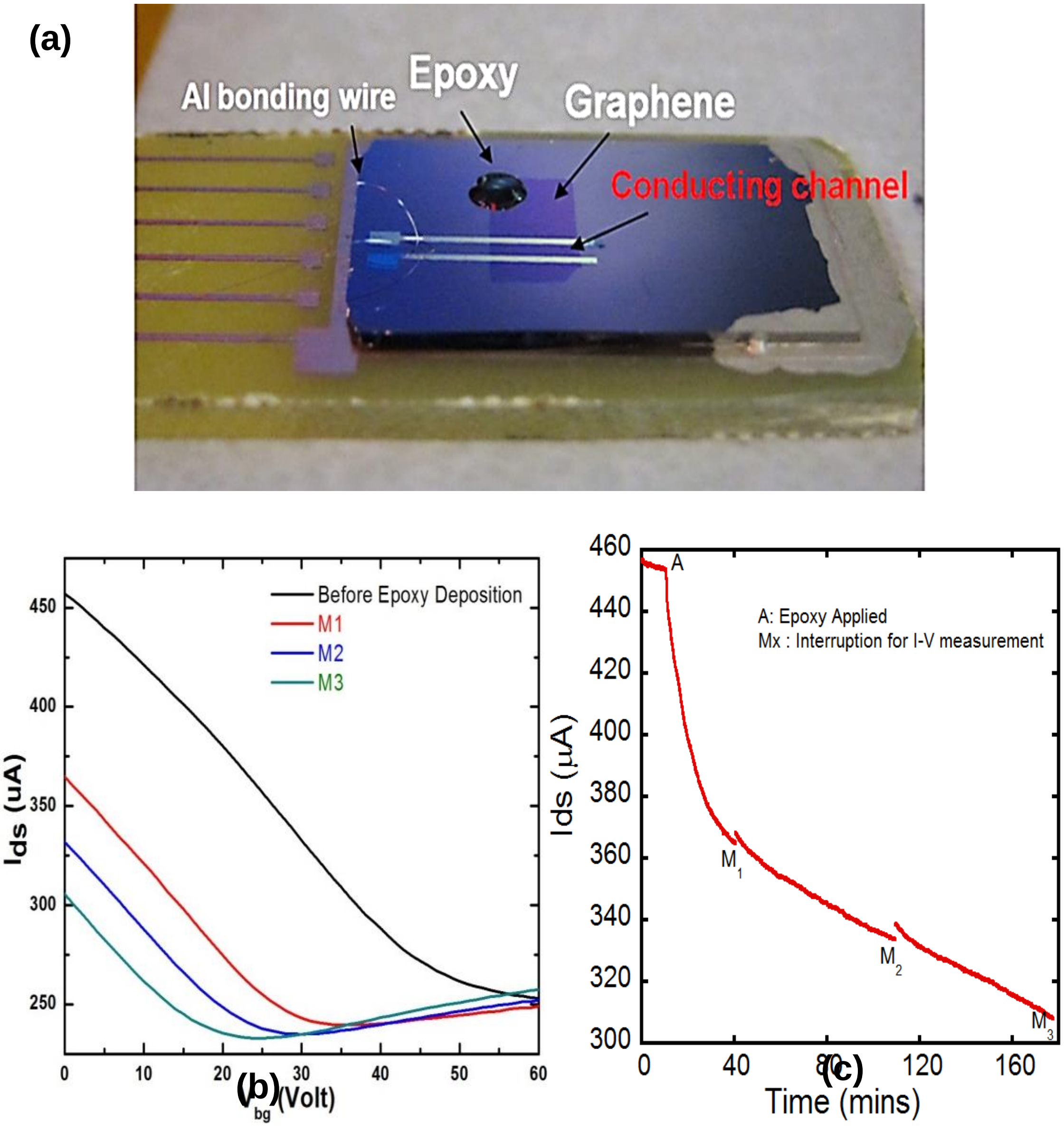

Figure 4.13 (a) Optical image of the device setup for the epoxy effect study. A droplet of uncured epoxy was deposited on the graphene 2~3 mm away from the conducting channel of a back gated graphene FET. (b): Time dependent current change upon epoxy deposition. Inset shows the device I-V characteristics taken at different time instants. (c) Real time current measurement from point A epoxy applied and till it was cured.

between the Si substrate and the Cu pad underneath the chip, which serves as the gate electrode here. To begin with, we grounded both gate and source electrodes and applied a constant DC bias ~1 V across the drain and source electrodes. After a relative stable current level (I_{ds}) was reached, we deposit a small droplet of the epoxy on the graphene film but 2 ~ 3 mm away from the conducting channel (L = 1 mm and W = 4.5 mm) as shown in **Figure 4.13** (a). Upon the epoxy deposition, we observed a significant time-dependent current decrease as shown in **Figure 4.13** (b). In addition, from the device I-V characteristics seen in **Figure 4.13** (c) current measured at different time points during the experiment, we found that the I-V curves were left shifted over time. Interestingly, the slope of the transfer characteristics of the graphene FET, which indicates the carrier mobility [94], seemed not being affected much by the epoxy deposition. To further understand, the time dependent effect of epoxy on the electric transport properties of graphene. We calculated the channel conductance (G), carrier mobility (μ_{FET}) and concentration (p) based on the measured transfer characteristics (at V_{ds} = 1 V and V_{bg} = 0 V) and listed them in **Table 4.1.** We found upon epoxy deposition, the field effect mobility of hole carriers increased, but its concentration decreased over time, which indicates n-type doping occurring in the graphene film. Since both the carrier mobility and concentration enter linearly into the graphene conductance. The current change

Table 4.1 Electric transport parameters of graphene under the influence of epoxy

Time (mins)	**Current I_{ds} (μA)**	**Dirac Point (volts)**	**Conductance G (μs)**	**Carrier Mobility (Cm^2/vs)**	**Carrier concentration n(p) (10^{13} cm^{-2})**
0	457	>60	457	75	1.07
30	365	34	365	111	0.58
100	332	29	332	111	0.53
170	306	24	306	116	0.46

observed from the time dependent measurement was dominated by the modulation of carrier concentration under the effect of epoxy.

From the material safety data sheet (MSDS) [102] of the epoxy released by Epoxy technology, Inc., we noticed that the curing agent consists of several organic ingredients including 2,2,4-Trimethyl, 6-hexanediamine ($C_9H_{22}N_2$).

Based on the investigation conducted so far, we concluded that the epoxy used for ISFET encapsulation here has a strong n-type doing effect on graphene, which might be result from the organic ingredients (e.g. $C_9H_{22}N_2$) in its curing agent. The experiment findings might lead to a new approach of organic molecule doping of graphene. On the other hand, epoxy might also change the contact resistance between graphene and metal electrodes, which results in transconductance degradation of the epoxy coated ISFETs as observed in **Figure 4.12**

4.9 ISFET encapsulation using photoresist

As the encapsulation material for our ISFET sensor, epoxy has been proved to be a good electrical passivation material with properties of good chemical stability and excellent biocompatibility. However, electrical measurements conducted with epoxy encapsulated graphene ISFET have revealed that epoxy has significant effect on the electrical transport properties of graphene and more importantly the transconductance of the ISFET. Transconductance directly related to the sensitivity of the ion sensor, which degrades during sensor encapsulation using epoxy effect. On the other side, because of scalability issue with graphene [103], further device miniaturization on graphene ISFET is needed for better electronic performance which leads to increase in carrier mobility, thus optimized sensor performance. Smaller device dimension will also allow us to realize high pixel integration of an array of ISFETs on a single wafer chip to detect different ions in biological system or use the ISFET sensor in other biomedical applications including bio-implantable devices. Because of its intrinsic material property, epoxy is not process-compatible with the state-of-art of lithography techniques. With the epoxy, we are not able to pattern the active area in graphene with well controlled dimensions. Thus we considered to use alternative material for the sensor encapsulation.

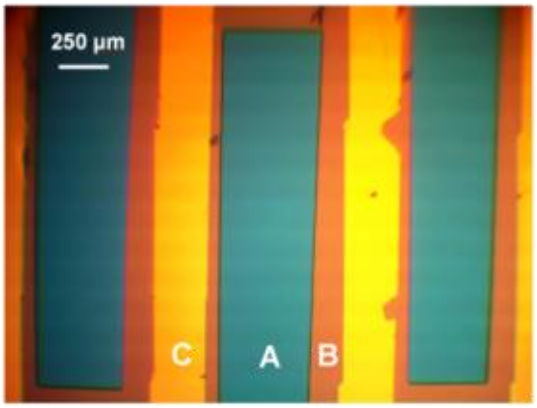

A: Graphene
B: PR S1811
C: Cr/Au metal contacts

Figure 4.14 Optical image of an array of three ISFETs fabricated on a single graphene film. Photoresist, S1811 was used to passivate the drain/source electrodes. The channel L ~ 0.45 mm and W ~ 2 mm were defined by standard photolithography.

As a biocompatible material for sensor packaging applications, epoxy based photoresist, e.g. SU-8 [104]-[105], has emerged as the material of choice for biosensor development due to its well-known biocompatibility, high stability to chemical and radiation damage, easy to process wafer-level capability and low cost. To prove the feasibility of using photoresist for our ISFET packaging, we used positive photoresist S1811 as an alternative encapsulation material to the commercial epoxy in the preliminary study. Figure 4.14 shows the optical image of three parallel ISFETs fabricated on a single graphene film using photoresist for the sensor encapsulation.

CHAPTER 5

CONCLUSION

This thesis explored the best possible process parameters to grow low defect monolayer graphene in a home-build chemical vapor deposition unit. The optimized parameters were obtained by a series of growth and characterization steps which involved learning from day to day growth, and understanding growth mechanism from most recent publications and incorporating these knowledge into improving the CVD of graphene. Graphene transfer process was developed to fabricate devices on any desired substrates. The graphene based device processing was developed and optimized. Graphene based devices such as GFETs, and ISFET were fabricated along with various test structures such as small channel and long channel devices. Various characterizations was performed, on graphene and devices, such as Raman spectroscopy, AFM, mobility, Temperature effect and Bias stressing, I-V, C-V characterization. Graphene based ISFET sensor development was pursued thereafter. Graphene ISFETs were used to tune sensitivity and selectivity for K+ ion in electrolyte solution.

5.1 Summary

Amongst many amazing properties of graphene the one that makes it very promising sensing material is the ability to change the carrier concentration of graphene by electrical, chemical and optical means. In order to fabricate devices out of graphene of good quality, large area graphene is needed. In chapter 2 such a reliable method of producing good quality, large area graphene for practical device application has been investigate by chemical vapor deposition technique. The CVD reactor was built by assembling different components such as quartz tube chamber, horizontal split furnace, mechanical pump, MFCs and pressure gauges. The optimized process parameter were obtained by understanding growth mechanism and by performing series of growth on different types of substrates and under different growth conditions. Cu foils were found to be ideal substrate to grow monolayer graphene. Due to very low solubility of C in Cu the graphene growth is surface mediated and essentially self-limited resulting in monolayer graphene which is also independent of the cooling rate as against Ni based growth. Therefore sophisticated hardware for controlling the cooling rate is not essential for growth on copper. The good quality, low defect, large area, monolayer graphene was successfully grown in routine basis using optimized process parameters as suggested from low ID/IG (0.1-0.2) and high I2D/IG (3 to 4) and small 2D FWHM (<30 cm-1) of Raman spectrum of as-grown graphene.

After fabricating Graphene based small channel GFET device and its characterization using Raman spectroscopy, Mobility measurement, temperature effect and bias stressing experiment has been described in chapter 3.

Chapter 4 In the development of biocompatible ion sensor, we designed, fabricated and characterized a novel graphene based ion sensitive field effect transistor . To prove biocompatibility of graphene we planted cell culture on graphene and grow cell on it.(ISFET) for real-time K^+ efflux measurement in electrolyte solution. I-V and C-V characteristics of the ISFET sensor have been extensively studied in both electrolyte and DI solutions. From the C-V measurement, we identified and calculated the interfacial capacitance at the graphene/solution interface, which consists of the electrical double layer capacitance (C_{EDL}) at the interface and the quantum capacitance of graphene (C_Q)

In the fabrication of graphene ISFET, we found the epoxy glue used for the sensor encapsulation had significant effect on the electric transport properties of graphene including conductivity, carrier concentration and field effect mobility. N-type doping effect of the epoxy on graphene has been carefully identified and confirmed by systematic experiments, which is promising for new alternative approach to dope graphene.

REFERENCES

[1] K. S. Novoselov, A. K. Geim, S. V. Morozov, D. Jiang, M. I. Katsnelson, I. V. Grigorieva, S. V. Dubonos, and A. Firsov, “A Two-dimensional gas of massless Dirac fermions in grapheme,” *Nature* **438**, 197 (2005).

[2] A. K. Geim and K. S. Novoselov, "The rise of graphene," *Nat. Mat.* **6,** 183 (2007).

[3] I. W. Frank, D. M. Tanenbaum, A. M. Van der Zande, and P. L. McEuen, "Mechanical properties of suspended graphene sheets," *J. Vac. Sci. Technol. B* **25,** 2558 (2007).

[4] S. Ghosh, I. Calizo, D. Teweldebrhan, E. P. Pokatilov, D. L. Nika, A. A. Balandin,W. Bao, F. Miao, and C. N. Lau, " Extremely high thermal conductivity of graphene: Prospects for thermal management applications in nanoelectronic circuits," *Appl. Phys. Lett.* **92,** 151911 (2008).

[5] K. S. Novoselov, A. K. Geim, S. V. Morozov, D. Jiang, M. I. Katsnelson, I. V. Grigorieva, S. V. Dubonos, and A. Firsov, “A Two-dimensional gas of massless Dirac fermions in grapheme,” *Nature* **438**, 197 (2005).

[6] W. Andreoni, *The physics of fullerene-based and fullerene-related materials* vol. 23:Springer, 2000.

[7] R. Saito, G. Dresselhaus, and M. S. Dresselhaus, *Physical properties of carbon nanotubes* vol. 4: World Scientific, 1998.

[8] Y. B. Zhang, Y. W. Tan, H. L. Stormer, and P. Kim, “Experimental observation of the quantum Hall effect and Berry’s phase in graphene,” *Nature* **438,** 201 (2005).

[9] K. S. Novoselov, D. *J*iang, F. Schedin, T. J. Booth, V. V. Khotkevich, S. V. Morozov, and A. K. Geim, “Two dimensional atomic crystals,” *Proc. Natl Acad. Sci. USA* **102**, 10451 (2005).

[10] K. S. Novoselov, Z. Jiang, Y. Zhang, S. V. Morozov, H. L. Stormer, U. Zeitler, J. C. Maan, G. S. Boebinger, P. Kim, and A.K. Geim, “Room-temperature quantum Hall effect in grapheme,” *Science* **315**, 1379 (2007)

[11] J. S. Bunch, A. M. van der Zande, S. S. Verbridge, I. W. Frank, D. M. Tanenbaum, J. M. Parpia, H. G. Craighead, and P. L. McEuenBunch, " Electromechanical Resonators from Graphene Sheets," *Science* **315,** 490 (2007).

[12] T. J. Bunch, S. S. Verbridge, J. S. Alden, A. M. van derZande, J. M. Parpia, H. G. Craighead, and Paul L. McEuen, "Impermeable Atomic Membranes from Graphene sheets," *Nano Lett.* **8**, 2458 (2008).

[13] F. Rana, "Graphene Terahertz Plasmon Oscillators," *IEEE Trans. Nanotechnol.* **7,** 91 (2008).

[14] G. Liang, N. Neophytou, D.E. Nikonov, and M.S. Lundstropm, "Performance Projections for Ballistic Graphene Nanoribbon Field-Effect Transistors," *IEEE Trans. Electron Dev.* **54,** 657 (2007).

[15] J.R. Williams, L. Di Carlo, and C.M. Marcus, "Quantum Hall Effect in a Gate-Controlled p-n Junction of Graphene," *Science* **317,** 638 (2007).

[16] M.C. Lemme, T.J. Echtermeyer, M. Baus, and H. Kurz, " A Graphene Field-Effect Device," *IEEE Trans. Elect. Dev. Lett.* **28,** 284 (2007).

[17] F. Schedin, A. K. Geim, S. V. Morozov, E. W. Hill, P. Blake, M. I. Katsnelson, and K. S. Novoselov, "Detection of individual gas molecules adsorbed on graphene," *Nat. Mater.* **6,** 652 (2007).

[18] G. W. Semenoff, "Condensed-Matter Simulation of a Three-Dimensional Anomaly," *Phys. Rev. Lett.* **53,** 5449 (1984).

[19] P. Avouris, Z. Chen, and V. Perebeinos, "Carbon-based electronics," *Nat. Nano.* **2,** 605 (2007).

[20] J.-C. Charlier, P.C. Eklund, J. Zhu, and A.C. Ferrari, "Electron and Phonon Properties of Graphene: Their Relationship with Carbon Nanotubes," from Carbon Nanotubes: Advanced Topics in the Synthesis, Structure, Properties and Applications, Ed. A. Jorio, G. Dresselhaus, and M.S. Dresselhaus. Berlin/Heidelberg: Springer-Verlag (2008).

[21] S. V. Morozov, K. S. Novoselov, M. I. Katsnelson, F. Schedin, D. C. Elias, J. A. Jaszczak, and A. K. Geim, "Giant Intrinsic Carrier Mobilities in Graphene and Its Bilayer," *Phys. Rev. Lett.* **100,** 016602 (2008).

[22] J. H. Chen, C. Jang, S. Xiao, M. Ishigami, and M. S. Fuhrer, "Intrinsic and Extrinsic Performance Limits of Graphene Devices on SiO_2," *Nat. Nano.* **3,** 206 (2008).

[23] A. Akturk and N. Goldsman, "Electron transport and full-band electron-phonon interactions in graphene," *J. of Appl . Phys.* **103,** 053702 (2008).

[24] http://3dprint.guru/graphene-bio-ink-and-3d-printing/

[25] https://www.alliedmarketresearch.com/graphene-market

[26] J. H. Chen, C. Jang, S. Adam, M. S. Fuhrer, E. D. Williams, and M. Ishigami, "Charged Impurity Scattering in Graphene," *Nature Physics* **4,** 377 (2008).

[27] S. Adam, E. H. Hwang, V. M. Galitski, and S.D. Sarma, "A self-consistent theory for graphene transport," *Proc. Nat. Acad. Sci. USA* **104,** 18392 (2007).

[28] A. B. Kuzmenko, E. van Heumen, F. Carbone, and D. van der Marel, " Universal Optical Conductance of Graphite," *Phys. Rev. Lett.* 100, 117401 (2008).

[29] R. R. Nair, P. Blake, A. N. Grigorenko, K. S. Novoselov, T. J. Booth, T. Stauber, N. M. R. Peres, and A. K. Geim, "Fine Structure Constant Defines Visual Transparency of Graphene," *Science* 320, 1308 (2008).

[30] Y. Hao, M. Bharathi, L. Wang, Y. Liu, H. Chen, S. Nie, et al., "The role of surface oxygen in the growth of large single-crystal graphene on copper," Science, vol. 342, pp. 720-723,2013.

[31] J. Baringhaus, M. Ruan, F. Edler, A. Tejeda, M. Sicot, A. Taleb-Ibrahimi, et al., "Exceptional ballistic transport in epitaxial graphene nanoribbons," Nature, vol. 506, pp. 349-354, 2014

[32] J.-U. Lee, D. Yoon, and H. Cheong, "Estimation of Young's modulus of graphene by Raman spectroscopy," Nano letters, vol. 12, pp. 4444-4448, 2012.

[33] A. A. Balandin, "Low-frequency 1/f noise in graphene devices," Nature nanotechnology,vol. 8, pp. 549-555, 2013.

[34] A. A. Balandin, S. Ghosh, W. Bao, I. Calizo, D. Teweldebrhan, F. Miao, and C. N. Lau," Superior Thermal Conductivity of Single-Layer Graphene," *Nano Lett.* 8, 902 (2008).

[35] N. Mingo and D. A. Broido, " Carbon Nanotube Ballistic Thermal Conductance and Its Limits," *Phys. Rev. Lett.* 95, 096105 (2005).

[36] C. Lee, X. Wei, J.W. Kysar, and J. Hone, "Measurement of the Elastic Properties and Intrinsic Strength of Monolayer Graphene," *Science* 321, 385 (2008).

[37] K. I. Bolotin, K. J. Sikes, J. Hone, H. L. Stormer, and P. Kim, "Temperature-dependent transport in suspended graphene," *Phys. Rev. Lett.* **101,** 096802 (2008).

[38] K. Novoselov, D. Jiang, F. Schedin, T. Booth, V. Khotkevich, S. Morozov, *et al.*, "Twodimensional atomic crystals," *Proceedings of the National Academy of Sciences of the United States of America,* vol. 102, pp. 10451-10453, 2005.

[39] C. Soldano, A. Mahmood, and E. Dujardin, "Production, properties and potential of graphene," *Carbon,* vol. 48, pp. 2127-2150, 2010.

[40] Y. Hernandez, V. Nicolosi, M. Lotya, F. M. Blighe, Z. Sun, S. De, *et al.*, "High-yield production of graphene by liquid-phase exfoliation of graphite," *Nature Nanotechnology,* vol. 3, pp. 563-568, 2008.

[41] D. A. Dikin, S. Stankovich, E. J. Zimney, R. D. Piner, G. H. Dommett, G. Evmenenko, *et al.*, "Preparation and characterization of graphene oxide paper," *Nature,* vol. 448, pp. 457-460, 2007.

[42] E. Rollings, G. H. Gweon, S. Y. Zhou, B. S. Mun, J. L. McChesney, B. S. Hussain, *et al.*, "Synthesis and characterization of atomically thin graphite films on a silicon carbide substrate," *Journal of Physics and Chemistry of Solids,* vol. 67, pp. 2172-2177, 9// 2006.

[43] W. A. de Heer, C. Berger, M. Ruan, M. Sprinkle, X. Li, Y. Hu, *et al.*, "Large area and structured epitaxial graphene produced by confinement controlled sublimation of silicon carbide," *Proceedings of the National Academy of Sciences,* September 29, 2011 2011.

[44] C. Berger, Z. Song, T. Li, X. Li, A. Y. Ogbazghi, R. Feng, *et al.*, "Ultrathin Epitaxial Graphite: 2D Electron Gas Properties and a Route toward Graphene-based Nanoelectronics," *The Journal of Physical Chemistry B,* vol. 108, pp. 19912-19916, 2004/12/01 2004.

[45] S. Shivaraman, M. V. S. Chandrashekhar, J. Boeckl, and M. Spencer, "Thickness Estimation of Epitaxial Graphene on SiC Using Attenuation of Substrate Raman Intensity," *Journal of Electronic Materials,* vol. 38, pp. 725-730, 2009/06/01 2009.

[46] Y. Wu, P. Ye, M. A. Capano, Y. Xuan, Y. Sui, M. Qi, *et al.*, "Top-gated graphene fieldeffect- transistors formed by decomposition of SiC," *Applied Physics Letters,* vol. 92, pp. 092102-092102-3, 2008.

[47] K. V. Emtsev, A. Bostwick, K. Horn, J. Jobst, G. L. Kellogg, L. Ley, *et al.*, "Towards wafer-size graphene layers by atmospheric pressure graphitization of silicon carbide," *Nat Mater,* vol. 8, pp. 203-207, 03//print 2009.

[48] S. Park and R. S. Ruoff, "Chemical methods for the production of graphenes," *Nature nanotechnology,* vol. 4, pp. 217-224, 2009.

[49] R. Muñoz and C. Gómez-Aleixandre, "Review of CVD Synthesis of Graphene," *Chemical Vapor Deposition,* vol. 19, pp. 297-322, 2013.

[50] C. Mattevi, H. Kim, and M. Chhowalla, "A review of chemical vapour deposition of graphene on copper," *Journal of Materials Chemistry,* vol. 21, pp. 3324-3334, 2011.

[51] X. Li, W. Cai, L. Colombo, and R. S. Ruoff, "Evolution of Graphene Growth on Ni and Cu by Carbon Isotope Labeling," *Nano Letters,* vol. 9, pp. 4268-4272, 2009/12/09 2009.

[52] D. K. Schroder, *Semiconductor material and device characterization*: John Wiley & Sons, 2006.127

[53] J. W. Kuehn and S. O. Konorov, "Raman Spectroscopy – a powerful tool in gem identification," presented at the The 3rd International Gem & Jewelry Conference (GIT2012), Bangkok Thailand and Pailin Cambodia, 2012.

[54] M. S. Dresselhaus, A. Jorio, M. Hofmann, G. Dresselhaus, and R. Saito, "Perspectives on carbon nanotubes and graphene Raman spectroscopy," *Nano letters,* vol. 10, pp. 751-758, 2010.

[55] A. Ferrari, J. Meyer, V. Scardaci, C. Casiraghi, M. Lazzeri, F. Mauri, *et al.*, "Raman spectrum of graphene and graphene layers," *Physical review letters,* vol. 97, p. 187401, 2006.

[56] A. K. Singh, M. A. Uddin, J. T. Tolson, H. Maire-Afeli, N. Sbrockey, G. S. Tompa, *et al.*, "Electrically tunable molecular doping of graphene," *Applied Physics Letters,* vol. 102, pp. 043101-5, 01/28/ 2013.

[57] A. K. Geim and K. S. Novoselov, “The rise of graphene,” *Nat. Mater.*, vol. 6, no. 3, pp. 183–191, Mar. 2007.

[58] Y. Zhang, Y. W. Tan, H. L. Stormer, and P. Kim, “Experimental observation of the quantum Hall effect and Berry’s phase in graphene,” *Nature*, vol. 438, no. 7065, pp. 201–204, Nov. 2005.

[59] F. Schwierz, “Graphene transistors,” *Nature Nanotechnol.*, vol. 5, no. 7, pp. 487–496, May 2010.

[60] Y.-M. Lin, C. Dimitrakopoulos, K. A. Jenkins, D. B. Farmer, H.-Y. Chiu, A. Grill, and P. Avouris, “100-GHz transistors from wafer-scale epitaxial graphene,” *Science*, vol. 327, no. 5966, p. 662, Feb. 2010.

[61] K. S. Novoselov, A. K. Geim, S. V. Morozov, D. Jiang, Y. Zhang, S. V. Dubonos, I. V. Grigorieva, and A. A. Firsov, “Electric field effect in atomically thin carbon films,” *Science*, vol. 306, no. 5696, pp. 666–669, Oct. 2004.

[62] M. C. Lemme, T. J. Echtermeyer, M. Baus, and H. Kurz, “A graphene field-effect device,” *IEEE Electron Device Lett.*, vol. 28, no. 4, pp. 282– 284, Apr. 2007.

[63] C. Choi, C. S. Kang, C. Y. Kang, S. J. Rhee, M. S. Akbar, S. Krishnan, M. Zhang, and J. C. Lee, “Positive bias temperature instability effects of Hf-based nMOSFETs with various nitrogen and silicon profiles,” *IEEE Electron Device Lett.*, vol. 26, no. 1, pp. 32–34, Jan. 2005.

[64] J. F. Zhang and W. Eccleston, “Positive bias temperature instability in MOSFETs,” *IEEE Trans. Electron Devices*, vol. 45, no. 1, pp. 116–124, Jan. 1998.

[65] S. Zafar, A. Callegari, E. Gusev, and M. V. Fischetti, “Charge trapping related threshold voltage instabilities in high permittivity gate dielectric stacks,” *J. Appl. Phys.*, vol. 93, no. 11, pp. 9298–9303, Jun. 2003.

[66] K. Zhao, J. Stathis, A. Kerber, and E. Cartier, “PBTI relaxation dynamics after ac VS. DC stress in high-K/metal gate stacks,” in *Proc. Int. Rel. Phys. Symp.*, 2010, pp. 50–54.

[67] B. Liu, M. Yang, C. Zhan, Y. Yang, and Y.-C. Yeo, “Bias Temperature Instability (BTI) characteristics of graphene field-effect transistors,” in *Proc. VLSI-TSA*, 2011, pp. 1–2.

[68] B. Huard, N. Stander, J. A. Silpizio, and D. Goldhaber-Gordon, “Evidence of the role of contacts on the observed electron-hole asymmetry in graphene,” *Phys. Rev. B, Condens. Matter*, vol. 78, no. 12, p. 121 402, Sep. 2008.

[69] S. V. Morozov, K. S. Novoselov, M. Katsnelson, F. Schedin, D. C. Elias, J. A. Jaszczak, and A. K. Geim, “Giant intrinsic carrier mobilities in graphene and its bilayer,” *Phys.Rev.Lett.*, vol. 100, no. 1, p. 016602, Jan. 2008.

[70] Z. H. Ni, H. M. Wang, Z. Q. Luo, Y. Y. Wang, T. Yua, Y. H. Wu, and Z. X. Shen, “The effect of vacuum annealing on graphene,” *J. Raman Spectrosc.*, vol. 41, no. 5, pp. 479–483, Apr. 2009.

[71] Cecilia Jienez, Andrey Bratov, Natalia Abramova and Antoni Baldi, “ISFET based sensors: Fundamentals and Applications,” Encyclopedia of Sensors, vol. **5**, pp. 151-196, 2006.

[72] P. Bergveld, “Development of an ion-sensitive solid-state device for Neurophysiological measurements,” *IEEE Transaction on Biomedical Engineering*, vol. **BME-17**, pp. 70-71, 1970.

[73] P. Bergveld, “Development, operation, and application of the ion-sensitive field effect transistor as a tool for electrophysiology,” *IEEE Transactions on Biomedical Engineering*, vol. **BME-19**, pp. 342-351, 1972.

[74] W.H. Baumann, M. Lehmann, A. Schwinde, R. Ehret, M. Brischwein and B. Wolf, “Microelectronic sensor system for microphysiological application on living cells,” *Sensors and Actuators B*, vol. **55**, pp. 77-89, 1999.

[75] Wen H. Ko, Jacques Mugica and Alain Ripart, *Implantable sensors for closed-loop prosthetic systems* pp. 89-114: Futura Publishing Company, 1985.

[76] Steve D. Cara, Danuta Petelenz and Jiří Janata, “pH-based enzyme potentiometric sensors. Part 2. Glucose-sensitive field effect transistor,” *Analytical Chemistry*, vol. **57**, pp. 1920-1923, 1985.

[77] P. Arquint, M. Koudelka-Hep, B.H. Van der Schoot, P. Van der Wal and N.F. de Rooij, “Micromachined analyzers on a silicon chip,” *Clin. Chem.*, vol. **40**, pp. 1805-1809, 1994.

[78] C. Colapicchioni, A. Barbaro, F. Porcelli and I. Giannini, “Immunoenzymatic assay using CHEMFET devices,” *Sensors and Actuators B*, vol. **4**, pp. 245-250, 1991.

[79] Nikos Chaniotakis and Nikoletta Sofikiti, “Novel semiconductor materials for the development of chemical sensors and biosensors: A review,” *Anayltica Chimica Acta*, vol. **615**, pp. 1-9, 2008.

[80] A. Bratov, N. Abramova and A. Ipatov, “Recent trends in potentiometric sensor arrays: A review,” *Anayltica Chimica Acta*, vol. **678**, pp. 149-159, 2010.

[81] L Bousse, N. F. de Rooij, and P. Bergveld, “The influence of counter-ion adsorption on the ψ_0/pH characteristics of insulator surfaces,” *Surface Sci.*, vol. **135**, pp. 479-496, 1983.

[82] M. Esashi and T. Matsuo, “Integrated micro multi ion sensor using field effect of semiconductor,” *IEEE Trans Biomed Eng.*, vol. **BME-25**, pp. 184-191, 1978.

[83] S. D. Moss, J. Janata and C. C. Johnson, “Potassium ion-sensitive field effect transistor,” Analytical Chemistry, vol. 47, pp. 2238-2243, 1975.

[84] A. Bratov, N. Abramova, J. Munoz, C. Domínguez, S Alegret and J Bartrolí, “Ion sensor with photocurable polyurethane polymer membrane,” J. Electrochem. Soc., vol. 141, L111-112, 1994.

[85] Feng Yan, Pedro Estrela, Yang Mo, Piero Migliorato and Hiroshi Maeda, “Polycrystalline silicon ISFETs on glass substrate,” *Sensors*, vol. **5**, pp. 293-301, 2005.

[86] A.K. Geim and K. S. Novoselov, “The rise of graphene,” *Nature Materials*, vol. **6**, pp. 183-191, 2007.

[87] K. S. Novoselov, A. K. Geim, S. V. Morozov, D. Jiang, Y. Zhang, S. V. Dubonos et al., “Electric field effect in atomically thin carbon films,” *Science*, vol. **306**, pp. 666-669, 2004.

[88] Christoph Sprossler, Morgan Denyer, Steve Britland, Wolfgang Knoll and Andreas Offenhausser, "Electrical recordings from rat cardiac muscle cells using field effect transistors," *Physical Review E*, vol. **60**, pp. 2171-2176, 1999.

[89] C. Schmidt, "Bioelectronics: The bionic material," *Nature*, vol. **483**, p. S43, 2012.

[90] Lucas H. Hess, Michael Jansen, Vanessa Maybeck, Moritz V. Hauf, Max Seifert and Martin Stutzmann *et al.*, "Graphene transistors arrays for recording action potentials from electrogenic cells," *Advanced Materials*, vol. **23**, pp. 5045-5049, 2011.

[91] Hediyeh Karimi, Rubiyah Yusof, Mohammad Taghi Ahmadi, et al., "Capacitance Variation of Electrolyte-Gated Bilayer Graphene Based Transistors," Journal of Nanomaterials, vol. 2013, Article ID 836315, 5 pages, 2013. doi:10.1155/2013/836315

[92] Jianting Ye, Monica F. Craciun, Mikito Koshino, Saverio Russo, Seiji Inoue, Hongtao Yuan *et al.*, "Accessing the transport properties of graphene and its multilayers at high carrier density", *PNAS.*, vol. **108**, pp. 13002-13006, 2010.

[93] Eri Uesugi, Hidenori Goto, Ritsuko Eguchi, Akihiko Fujiwara and Yoshihiro Kubozono *et al.*, "Electric double-layer capacitance between and ionic liquid and few-layer graphene," *Nature Scientific Report*, vol. **3**, pp. 1595-1595-5, 2013.

[94] A.K. Singh, M. A. Uddin, J. T. Tolson, H. Maire-Afeli, N. Sbrockey, G. S. Tompa et al., "Electrically tunable molecular doping of graphene," *Appl. Phys. Lett.*, vol. **102**, pp. 043101-043101-5, 2013.

[95] http://www.epotek.com/site/files/brochures/pdfs/medical_brochure.pdf

[96] A.K.M. Newaz, Yevgeniy S. Puzyrev, Bin Wang, Sokrates T. Pantelides and Kirill I. Bolotin, Probing charge scattering mechanisms in suspended graphene by varying its dielectric environment," *Nature Communication*, vol. 3, 2011.

[97] Si Chen, Zhi-Bin Zhang, Laipeng Ma, Patrik Ahlberg, Xindong Gao and Zhijun Qiu, "A graphene field-effect capacitor sensor in electrolyte," *Appl. Phys. Lett.*, vol. **101**, pp. 154106-154106-5, 2012.

[98] Xiaochen Dong, Yumeng Shi, Wei Huang, Peng Chen and Lain-Jong Li, "Electrical detection of DNA hybridization with single-base specificity using transistors based on CVD-grown graphene sheets," *Advance Materials*, vol. **12**, pp. 1-5, 2012.

[99] Yasuhide Ohno, Kenzo Maehashi, Yusuke Yamashiro and Kazuhiko Matsumoto, "Electrolyte-gated graphene field –effect transistors for detecting pH and protein adsorption," *Nano Letter*, vol. **9**, pp. 3318-3322, 2009.

[100] Xiaochen Dong, Dongliang Fu, Wenjing Fang, Yumeng Shi, Peng Chen and Lain-Jong Li, “Doping single-layer graphene with aromatic molecules,” *Small*, vol. **5**, pp. 1422-1426, 2009.

[101] Xiaomu Wang, Jian-Bin Xu, Weiguang Xie and Jun Du, “Quantitative analysis of graphene doping by organic molecular charge transfer,” *Journal of Physical Chemistry C*, vol. **115**, pp. 7596-7602, 2011.

[102] http://oldwww.epotek.com/SSCDocs/MSDS/301_msds.PDF

[103] Justin C. Koepke, Joshua D. Wood, David Estrada, Zhun-Yong Ong, Kevin T. He, Eric Pop et al., “ Atomic-scale evidence for potential barriers and strong carrier scattering at graphene grain boundaries: a scanning tunneling microscopy study,” *ACS Nano*, vol. **7**, pp. 75-86, 2013.

[104] P.A. Hammond and D.R.S. Cumming, “Encapsulation of a liquid-sensing microchip using SU-8 photoresist,” *Microelectronic Engineering*, vol. **73-74**, pp. 893-897, 2004.

[105] Ewan H Conradie and David F Moore, “SU-8 thick photoresist processing as a functional material for MEMS applications,” *J. Micromech. Microeng.*, vol. **12**, pp. 368-374, 2002.

[106] Priscilla Kailian Ang, Wei Chen, Andrew Thye Shen Wee, and Kian Ping Loh, “Solution-gated epitaxial graphene as pH sensor,” JACS., vol. **130**, pp. 14392-14393, 2008.

[107] L.H Hess, M. V. Hauf, M. Seifert, F. Speck, T. Seyller, M. Stutzmann *et al.*, “High-transconductance graphene solution-gated field effect transistors,” *Applied Physics Letters*, vol. **99**, 033503-033503-3, 2011

APPENDIX A : DEVICE FABRICATION PROCESS FLOW

A detail of Graphene Growth and device fabrication is described in Chapter 2 and Chapter 3. This appendix gives more detail about process flow, steps required and

Table A: Photolithography process for GFETs fabrication

Graphene Growth	Chemical vapor deposition Process Cu foil: 1×1.5 inch, Thickness: 25 um Gas 1: Ar 900 SCCM, Gas 2: H_2 100 SCCM, Gas 3 : CH_4 35 SCCM Process time:-~5 hours
RIE Etching	Equipment: Plasma RIE Graphene Etching on back side of Cu foil Spin coat PMMA twice on top at 3000 rpm for 40 sec Gas 1: O_2 50 SCCM, Power: 150 W, Pressure: 300 mT, Time: 180 sec
Graphene Transfer	Cu foil/Graphene/PMMA kept in Cu etchant Cu etchant:- kept foil on $FeCl_3/(NH_4)_2S_2O_8$ for overnight Rinse with DI multiple times and HCL once Scoop Graphene/PMMA on 300 nm Si/Sio_2 Remove wrinkles of PMMA: Back sample at 220 ˚C for 5 min Remove PMMA:- soak in aceton for 1~2 hours
Lithography	Substrate: 300 nm SiO_2/Si wafer with graphene film transferred on Photoresist: Microposit S1811 Spin coating: 4000 rpm for 30 secs (thickness: ~ 1 µm) Softbake: 110 ˚C for 1 mins on hotplate Exposure: λ = 436 nm, UV density = 150 mJ/cm^2 Post Exposure Bake: 100 ˚C for 1 min on hotplate Develop: MF 351 for 20~22 secs
Metal deposition	Equipment: Denton DV-502 E-beam metal evaporator Deposition of following metal stack at pressure below 2×10^{-6} torr Chromium (Cr): 20/50 nm Gold (Au): 70 nm
Metal liftoff	Dipped in acetone for overnight and spray by syringe Rinse with Acetone, IPA and DI Blow dry by N_2

associated parameters. First part will detail about Graphene growth and graphene transferred and the second part will give the description about Lithography, Metal deposition and metal lift off.

For ISFET device, Two types of graphene based ISFET sensors were fabricated using two different encapsulation materials, biocompatible epoxy (EPO-TEK 301, Epoxy Technology, Inc.) and positive photoresist (S1811, Shipley company). The fabrication process for ISFET consists of same as above explained for GFETs followed by sensor packaging as described in detail below.

A.1 Sensor packaging

For operation in electrolyte solution, fabricated graphene ISFETs were encapsulated by two different types of encapsulation materials, the epoxy glue (EPO-TEK 301) and photoresist (PR) S1811. In the epoxy encapsulation process, the wafer chip with the graphene ISFET fabricated on was first mounted on a homemade PCB board and wire-bonded. Epoxy glue was prepared by mixing the epoxy base (EPO-TEK 301-A) with its curing agent (301-B) under the weight ratio of 4:1. After properly mixing the epoxy/curing agent mixture, under 60 °C in air, we encapsulated the ISFET sensor by sequentially applying the mixture to cover the drain/source electrodes, four edges of the graphene film, Al bonding wires and the rest area of the wafer chip. After the epoxy was completely cured within ~ 2 hours, an opening window (i.e. the active sensing area of the ISFET) was defined in the graphene film. Inset of Fig. 4.7 shows a representative graphene ISFET encapsulated using the epoxy. Last, the epoxy coated ISFET sensor was brought back to room temperature and stored in a vacuum sample box for future study.

The fabrication process of PR encapsulated graphene ISFET is illustrated in **Figure A.1.** Adopting the same procedures discussed in sections i and ii above, CVD graphene was transferred on a 300 nm SiO_2/Si wafer chip (Step 1) and then drain/source metal contacts deposited (Step 2). Afterwards, a layer of PR S1811 (~ 1 µm in thickness) was spin-coated on the entire wafer chip covering both the graphene film and metal electrodes (Step 3). In Step 4, a 2nd round photolithography was performed, opening a window on top of the graphene film in between the electrodes and exposing the metal contact pads for wire bonding. The PR encapsulated ISFET chip was then mounted on a

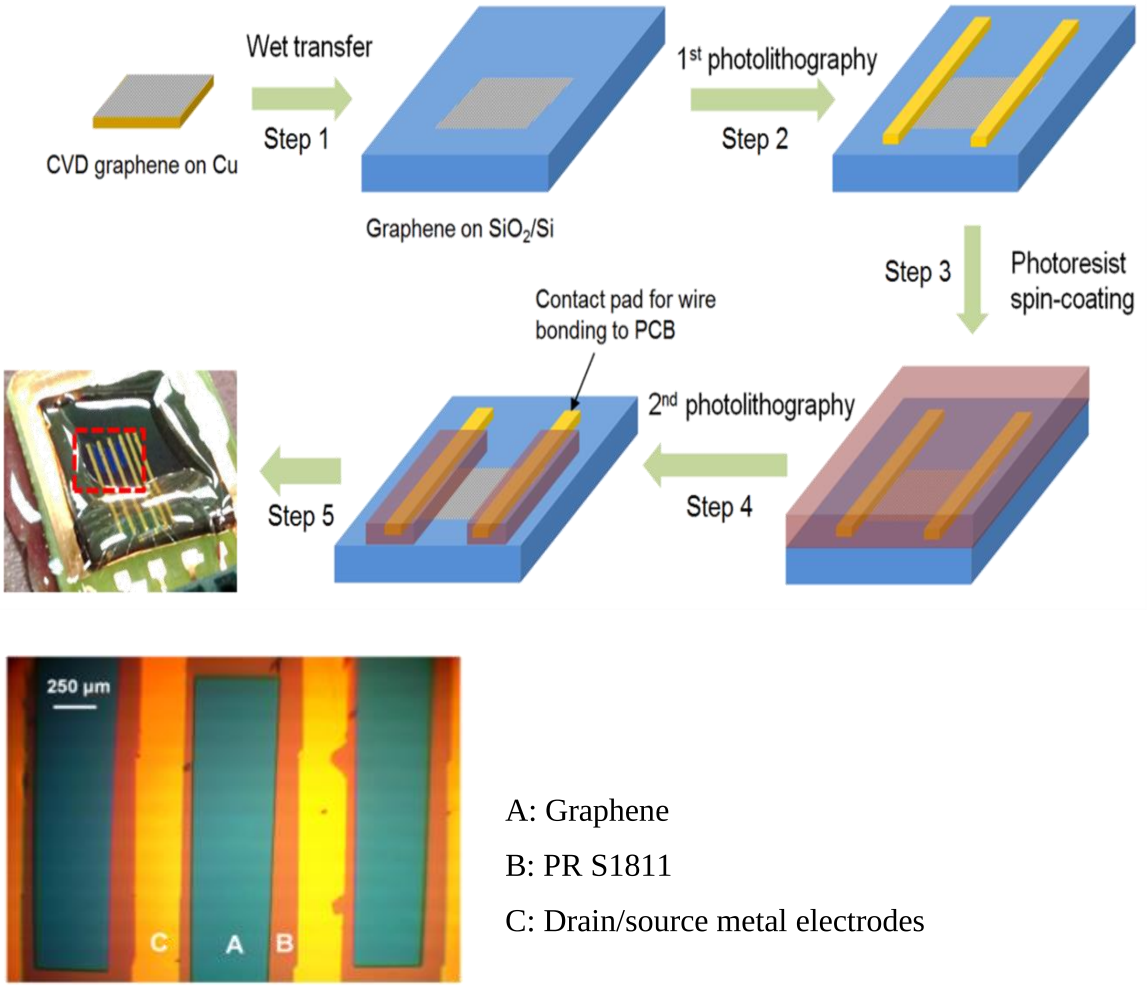

A: Graphene

B: PR S1811

C: Drain/source metal electrodes

Figure A.1: Fabrication process flow chart of the PR encapsulated graphene ISFET. After 2nd photolithography (Step 4), the wafer chip is covered with a layer of PR S1811. Only the center area of the graphene thin film (the active sensing area of the ISFET) and the metal contact pads are exposed. For illustration simplicity, here only the photoresist encapsulating the metal electrodes are shown in the figure. Inset of the figure shows the optical image of an array of three ISFETs fabricated on a single graphene film.

PCB board and wire-bonded (Step 5). The epoxy glue was used to encapsulate the Al bonding wires and the peripheral edges of the wafer chip. The optical image at the end of the process flow shows a representative graphene ISFET sensor encapsulated using the photoresist.